Tribology and Surface Engineering for Lubricious Dry-Sliding Contacts of MoS2 Based Coatings

Zachary Thompson

Submitted in accordance with the requirements for the degree of

Doctor of Philosophy

The University of Leeds

Institute of Functional Surfaces

School of Mechanical Engineering

August 2022

The candidate confirms that the work submitted is his/her own, except where work which has formed part of jointly-authored publications has been included. The contribution of the candidate and the other authors to this work has been explicitly indicated below. The candidate confirms that appropriate credit has been given within the thesis where reference has been made to the work of others.

Acknowledgements

Firstly, I would like to thank my primary academic supervisor, Professor Mike Bryant, with whom it has been a pleasure to work with during my studies. His attentiveness during meetings and when reviewing results, presentations and a thesis is truly appreciated. Without his continuous support, encouragement and advice throughout my studies, it would not have been possible.

Secondly, I would like to thank Dr Rob Beadling, particularly for his guidance and support towards the end of my PhD. I would also like to mention and thank Professor Anne Neville, who provided invaluable guidance and enthusiasm at the beginning of my PhD.

Finally, I would like to thank my wife Kirsty, whose continued encouragement and patience has been invaluable during my studies.

Abstract

Molybdenum disulphide (MoS_2) is a well-known solid lubricant with excellent lubricious and low wearing qualities when utilised in inert and high vacuum environments. However, the lubricity of MoS_2 during room temperature sliding is drastically reduced in humid, terrestrial atmospheres. The reason behind this degradation is not fully understood, with multiple conflicting arguments as to why this may be the case. One leading hypothesis suggests that adsorbed water restricts easy lamellar shear and thus leads to higher coefficients of friction, with oxygen playing no part. An opposing hypothesis suggests that oxidation caused by water and oxygen in the atmosphere leads to a degradation of the coating – a theory which is often disputed, as it is claimed that the threshold temperature for oxidation of MoS_2 is not reached. The purpose of this study was to elucidate the impact that water and oxygen have on the tribological and chemical degradation of MoS_2 coatings. Friction tests of both aged and unaged MoS2 coatings were carried out using a micro-tribometer. The unaged coatings were tested in dry, 25% and 50% relative humidity (RH) air or nitrogen. Aged samples were aged in the same environment but returned to an ideal dry nitrogen environment for friction testing. Surface analysis techniques, such as Raman spectroscopy, Scanning Electron Microscopy and Energy-Dispersive X-Ray Spectroscopy

were used to analyse the chemical changes caused by ageing and friction testing. Results show that both air and water in the sliding environment lead to higher coefficients of friction of unaged MoS_2. This is in line with the established literature. Higher coefficients of friction were also observed in air aged (N_2 + O_2) MoS_2 compared to nitrogen (N_2) aged MoS_2. Raman spectra showed oxidation of air aged MoS_2 in the wear scars at all humidity levels. Conversely, samples aged in nitrogen showed no oxidation at any humidity level, neither before nor after sliding. It was concluded that oxidation does not occur in MoS_2 aged at room temperature when no sliding has occurred. However, samples aged in air displayed MoO_2 and MoO_3 in the wear scar after sliding, leading to the theory that gaseous oxygen is needed for the oxidation of MoS_2 during sliding.

Table of Contents

List of Tables

List of Figures

Nomenclature

Terms	Definition	Units
A	Contact Area	m^2
b	Half contact width	m
E	Young's Modulus	$N \cdot m^{-2}$
F	Force	N
F_N	Normal Force	N
F_T	Transverse Force	N
K	Thermal conductivity	$W \cdot mK^{-1}$
L	Length of cylindrical contact	m
P_{max}	Maximum Hertzian contact pressure	Pa
Q	Work done by friction force	J

r	Radius	m
$T_{f_{max}}$	Max flash temperature	K
v_{rel}	Relative velocity between contacting surfaces	$m \cdot s^{-1}$
W	Normal applied load	N
a	Radius of spherical contact	m
μ	Coefficient of friction	-
v	Poisson Ratio	-
χ	Thermal diffusivity	$m^2 \cdot s^{-1}$

Abbreviations

Abbreviations	Definition
AST	Activated State Theory
MEMS	Micro-Electro-Mechanical System
MoS_2	Molybdenum Disulphide
PVD	Physical Vapour Deposited
RH	Relative Humidity
TMDs	Transition metal dichalcogenides
TST	Transition State Theory

1. Chapter One Introduction

Tribology is the study of interacting surfaces in relative motion, and it encompasses the science of friction, wear and lubrication [1]. Tribology, however, has a relatively short history as a distinct field of science, with the word 'tribology' first being coined in the Jost report in 1966 [2]. However, there is some suggestion that the Egyptians understood the importance of maintenance and function of mechanical systems, and that lubrication was used to aid the movement of large objects during construction [3]. The interactions between solids in relative motion are of fundamental importance in almost all engineering applications. This is in no small part due to wear; a prime cause for material wastage and reduction in mechanical performance. Jost et al. predicted that approximately £515 million (1:36 % of gross national product) could be saved if new lubricants were introduced into existing equipment throughout the country [4]; this amounts to over £9 billion in 2017, as outlined in Figure 1.1. Globally, Holmberg et al. [5] estimated that tribological contact accounts for ~23% of global energy consumption. It is, therefore, evident that huge environmental and economic benefits can be gained through the advancement of tribological knowledge.

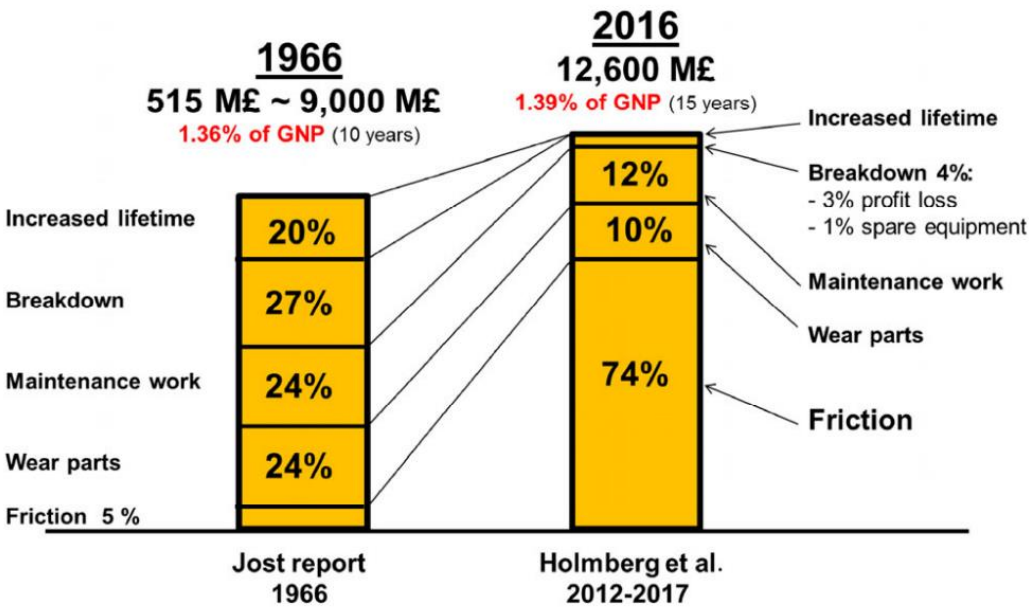

Figure 1.1 Potential savings in the UK 1966 and 2016 by implementing new tribology in machines and equipment, 515 million UK pounds converts to £9bn of 2017 value. From [5].

With the emergence of space travel and technologies, new environments have arisen, within which the use of lubricants is paramount. This has led to exciting research areas in lubricity in extreme environments. Due to the inability of liquid or oil-based lubricants to provide lubricity in the vacuum of space [6, 7], many solid lubricants have been proposed for use in these environments, with the most prominent being molybdenum disulphide (MoS_2). However, the exact mechanisms of their lubricity and wear in different environments are not fully understood and are widely disputed. MoS_2,

when utilised as a solid lubricant, is known to have a low coefficient of friction and high wear endurance in inert or vacuum conditions [8-10]. Therefore, making it ideal for use in long term space applications. MoS_2 is also used in industrial machining processes, presses and anti-adhesion coatings.

1.1 Motivation for research

When one thinks of lubrication, likely the first thing that comes to mind is typical liquid, oil based lubrication or common household or garage sprays such as WD-40. However, there are times, when for some reason or other liquid lubricants cannot be used. For example, in high vacuum conditions, at high temperatures or when the presence of a liquid lubricant could cause contamination to delicate parts. For such applications, a less common class of lubricants called dry, or solid lubricants can be used. Just as with liquid lubricants, the goal of solid lubrication remains the same; to separate interfaces, reduce friction and prevent wear of critical components. The employment of solid lubricants is usually between two metal interfaces, such as bearings or gears. However, solid lubricants are not without their own drawbacks; these materials' lubricity lies partly due to tribochemical reactions, and the materials often tend to be sensitive to their operating and storage environments [1, 7, 11-16]. For example,

Molybdenum disulphide had to be utilised under dry or vacuum conditions; therefore, its use in everyday equipment and machinery is often not possible. Furthermore, gaps in the knowledge of fundamental mechanisms of friction make the durability and friction of surfaces challenging to quantify. In addition, the vast majority of the research into direct tribology and storage conditions of solid lubricants are extreme, and the role of seemingly benign conditions such as ambient air storage has not been well explored.

Due to its excellent lubrication properties, MoS_2 has garnered interest for use as a solid lubricant in micro-electro-mechanical systems (MEMS). Which, over the past two decades, have seen substantial growth in usage from applications in automotive, aerospace and medical instrumentation[17-19]. However, due to the decreased contact areas in these devices, roughness may play a more significant role in the sliding behaviour and tribological performance [20].

1.2 Research aim

This study focuses on the lubricious performance of molybdenum disulphide (MoS_2) solid coatings undergoing small-scale sliding. MoS_2 is a lamellar solid which belongs to the transition metal

dichalcogenides (TMDs) group of materials, which confers low coefficients of friction due to the weak Van der Waals forces between lamellae, allowing them to slide easily over one another. The aim of this thesis was to better understand how 'benign' environmental conditions affect the friction mechanisms of MoS_2 coatings; both directly and due to storage. Elucidating the impact that the environment may have on solid MoS_2 coatings and understanding the reasons why environmental conditions reduce performance will lead to a framework for best practice use of this lubricious coating, both in storage and operation.

1.3 Research objectives

In order to meet the aims of this project, the following objectives were set:

- To conduct and complete a state-of-the-art literature review on friction, wear and MoS_2 as a lubricious coating.

- To understand how oxygen and water in the sliding environment effect the coefficient of friction of MoS_2 coatings and explore any structural or chemical changes that they may cause.

- To understand how introducing water and oxygen into the storage environment may affect the chemical composition of MoS_2 coatings, and how that impacts the coefficient of friction during sliding once they are returned to operation in an ideal, inert environment.
- To elucidate the mechanisms of how water and oxygen cause performance reductions in lubricious qualities of MoS_2 coatings.

1.4 Thesis outline

This thesis aims to elucidate the impact that water and oxygen have on the lubricous qualities of MoS_2 coatings. Starting with fundamental theory and a literature review to outline the state of the art and the gaps in knowledge. The literature review then informed the experimental methodology and results chapters to address the outline gaps in the current literature. The results chapters presented detach the impact that water and oxygen have during sliding and in the storage environment so that an understanding of the mechanisms behind the reduction in lubricious performance could be developed. The results presented were then drawn together and linked both with

each other and the literature presented within and drawn to a close with conclusions and future work.

- **Chapter Two**: Fundamental theory of friction wear and lubrication regimes, exploring real contact and focusing on dry sliding, and a Comprehensive literature review of lubricity and wear lifetime of MoS_2 in different environments.

- **Chapter Three**: Experimental methodology of tribological and material characterisation tests.

- **Chapter Four**: Explores and outlines water and oxygen's effects on the lubricity of MoS_2 coatings. This chapter will outline the tribological, chemical and material characteristics of molybdenum disulphide, and show the impact that water and oxygen can have when introduced to the sliding environment.

- **Chapter Five**: Explores and outlines the effects of water and oxygen contamination of MoS_2 coatings in the storage environment. This chapter will characterise tribological and chemical changes of MoS_2 in sliding as a result of the introduction of water and oxygen in the storage environment.

- **Chapter Six**: Overall discussion tying together the results presented in this thesis, and explaining the significance of the findings.

- **Chapter Seven:** Conclusions and future work.

2. Chapter Two Theory and Literature Review

2.1 Introduction

The main aim of this study was to elucidate the effect that water and oxygen have on the performance of MoS_2 coatings for use as a solid lubricant coating. Exploring both the impact that oxygen and water have in the sliding environment and how the introduction of these species in the storage environment may affect the performance of the coating.

This chapter details the fundamentals of tribology – lubrication, friction and wear. Starting with real surfaces, contact between solids, friction and wear mechanisms and then moving on to lubrication regimes, lubrication by solids, and lamella solids. Following this is an extensive review of the use of molybdenum disulphide as a solid lubricant in both terrestrial and ideal atmospheres. Starting with a history of MoS_2 use and a breakdown of known literature on chemical and structural changes brought about by water and oxygen on MoS_2.

2.2 Tribology

The word tribology stems back to Greek origin, with the prefix linking to the word 'tribos' meaning 'to rub', and the suffix 'ology' meaning 'the study of'. Thus, translating to the study of things that rub [11]. Tribology brings together the subjects of friction, wear and lubrication. The first recorded use of the word tribology was in a 1966 Jost report by the Department of Education and Science, where it was defined as 'The science and technology of interacting surfaces in relative motion' [21]. However, the scientific basis for the modern understanding of friction lubrication and wear came far earlier and was established by scientists like Hertz, Reynolds and Bowen and Tabor [22]. Improving the performance and lifetime of industrial components is often a key goal of tribological research. Components are tested under varying operating conditions, failure modes are analysed, and historical data is collected to determine current component performance. By scaling down contact geometry and simplifying the contact area for lab testing, researchers have better control over ranges of variables and can create more reliable, predictive models of failure probability and lifetime. This can be accomplished by combining new materials with the development of new monitoring methods that allow for a better understanding of how components operate in real-world situations [23]. As well as ensuring

major tribological factors such as materials, surfaces, lubricant and operating conditions are taken into consideration. Looking at tribology as a whole instead of more specific topics, such as friction wear and lubrication separately, encourages a problem-centred approach [24], as outlined in Figure 2.1. Although there has been extensive research in the field of tribology, there are still fundamental unanswered questions, such as the relationship between friction and wear, and how they can be controlled in practice [25].

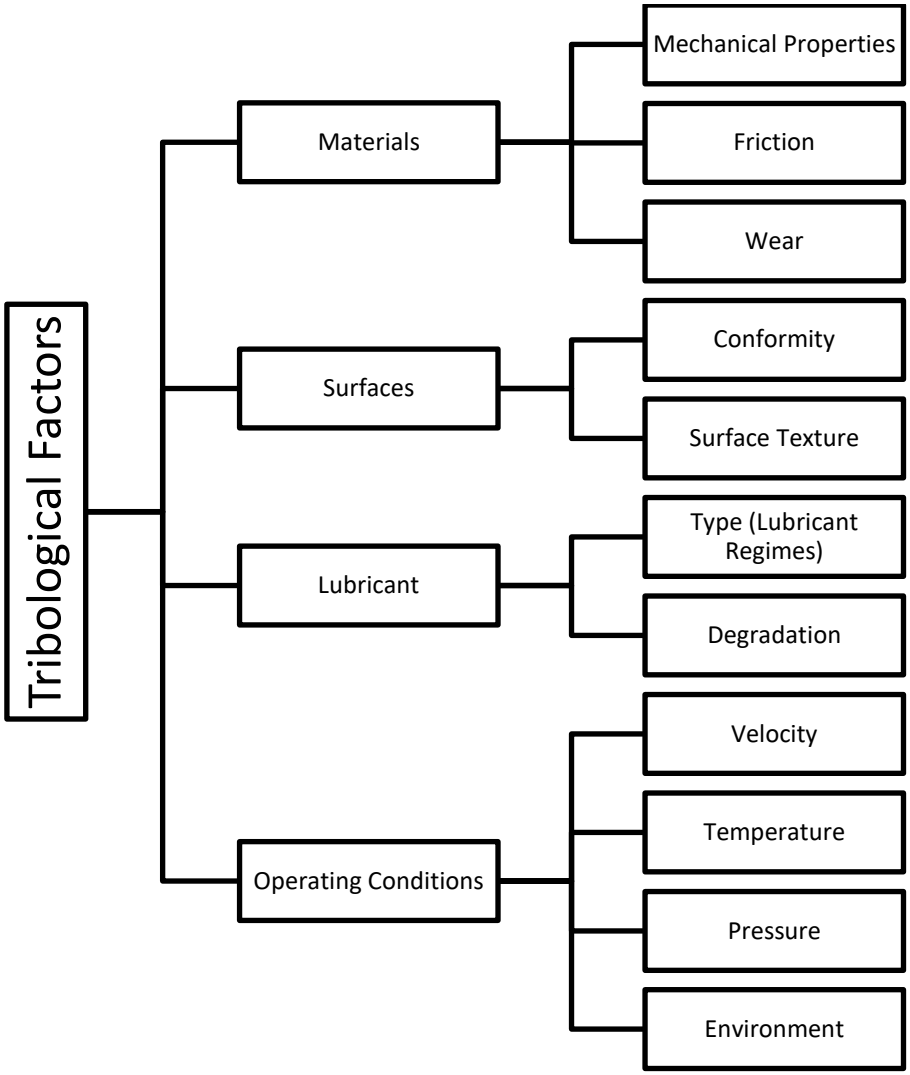

Figure 2.1 Tribological factors to consider when optimising a mechanical system redrawn from [24]

2.3 Contact between surfaces

2.3.1 True contact area

Solid surfaces, especially those found on metallic components, can look very smooth on a macroscopic scale. However, this is usually not the case; on a microscopic scale, even many mirror shined materials have protuberant features called asperities. These asperities cause a precipitous peak and trough array across the surface of a material. If one was to think of two contacting surfaces, for example, a brake pad on a disc, it is perceived that the contact area between the two objects would be the macroscopic area of the brake pad. Conversely, the true area of contact is far smaller. True contact only occurs when the high points of the asperities of adjacent surfaces touch, as shown in Figure 2.2. In addition, as stated in [26], the true contact area 'is proportional to the total normal load and therefore independent of the apparent contact area'. This is due to the deformation of the asperities when a load is applied. When these asperities deform under load, they generate an increased true contact area.

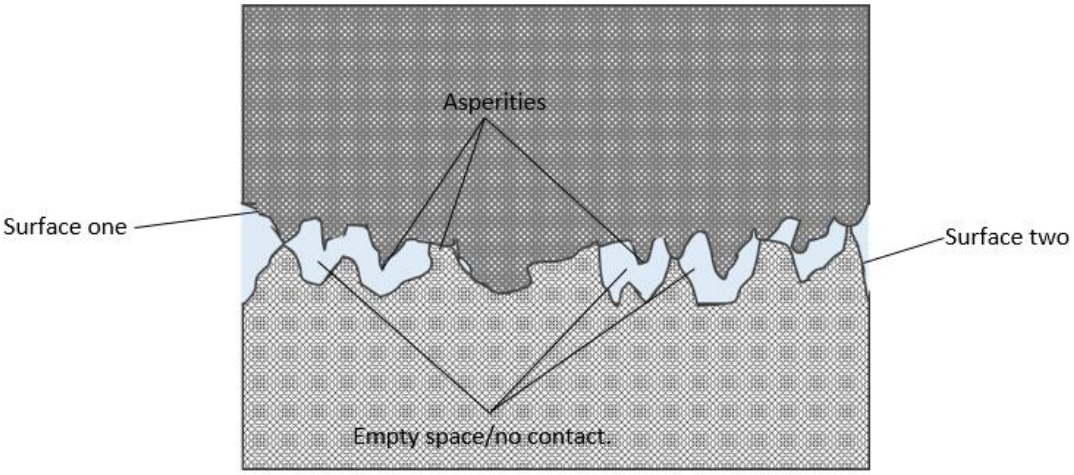

Figure 2.2 Example of real surface asperity contact in dry contact

The stresses of contacting asperities are reliant on the shape of the asperity and its elastic and plastic properties [1, 27]. The elastic properties between contacting bodies can be described by their elastic modulus, E, and Poisson's ratio $,v.$ The combined elastic modulus, E', of multiple contacting bodies is defined in Equation 2-1:

Equation 2-1

$$\frac{1}{E'} = \frac{1 - v_1^2}{E_1} + \frac{1 - v_2^2}{E_2} + \cdots \frac{1 - v_n^2}{E_n}$$

Plastic properties can be described by their hardness [27] where hardness is described as the expression of material strength during indentation at the full plasticity regime [28], and is defined in Equation 2-2. This equation can be well utilised for materials with rigid-plastic behaviour, however, determining the constraint factor for non-metallic or brittle materials can prove to be difficult[28]:

Equation 2-2

$$H \approx C\sigma_y$$

Where, C, is the constraint factor, and, σ_y, is the yield stress.

2.3.2 Hertzian contact

When a load is applied to bodies in contact, the bodies will deform; either elastically or plastically. Plastic deformation at the contact only occurs with extremely high stresses that exceed the elastic limit of the materials; this causes irreversible damage to the body. On the other hand, Applied loads that lead to stresses below the elastic limit will lead to elastic deformation, which is reversed when the load is removed. Equations developed by Hertz define the contact of surfaces with low conformity, for example, spherical or cylindrical contacts. However, Hertz's equations assume ideal smooth contacts and must be

given some boundary conditions due to assigning a shape to the surfaces in contact, thus leading to some limitations [29]. These are:

- The displacements and stresses must satisfy the differential equations of equilibrium for elastic bodies, and the stress must vanish at a great distance from the contact surface – meaning the stresses must therefore be localised.

- The bodies are in frictionless contact.

- At the surface of the bodies, the normal pressure is zero outside and equal and opposite inside the circle of the contact.

- The distance between the surfaces of the two bodies is zero inside and greater than zero outside the contact circle.

Examples of spherical contacts are outlined in Figure 2.3

Where :

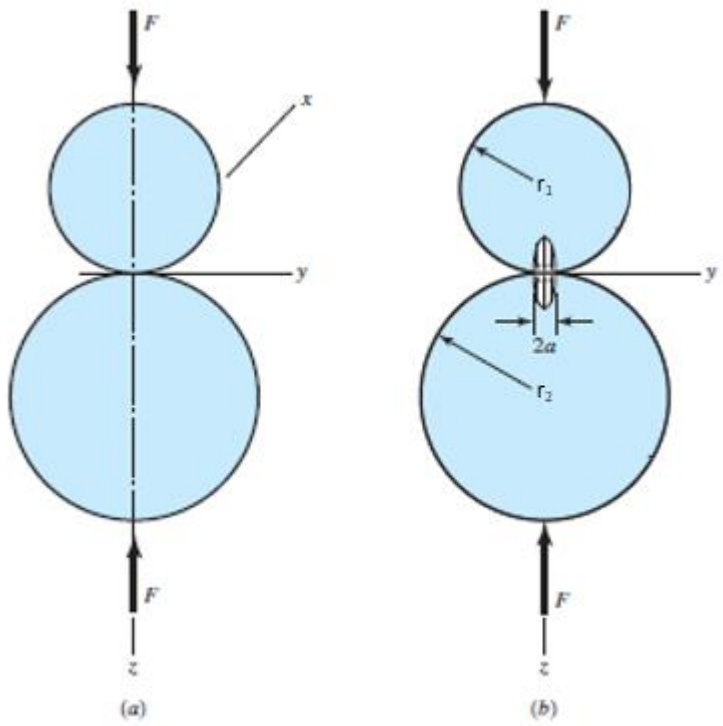

Figure 2.3 Hertzian contact schematic spherical contact [30].

F = Force

v = Poisson's ratio

E = Elastic/Young's Modulus

r = Radius

Equation 2-3

$$a = \sqrt[3]{\frac{3F\left[\frac{1-v_1^2}{E_1}+\frac{1-v_2^2}{E_2}\right]}{4\left(\frac{1}{r_1}+\frac{1}{r_2}\right)}}$$

Therefore, the maximum contact pressure is defined as:

Equation 2-4

$$P_{max} = \frac{3F}{2\pi a^2}$$

2.4 Friction

Friction is the resistance to motion that transpires when contacting surfaces are moved tangentially over one another. This resistive force is due to contacting asperities interacting in dry contact. There are three fundamental laws of friction, the first two were developed thanks to the studies of Leonardo Da Vinci and Amontons, and the third being derived from Coulomb's works [1, 11, 26, 31]. The three fundamental laws of friction are:

1. The friction force, F, is directly proportional to the applied load, W.
2. The friction force, F, is independent of the apparent area of contact, A.
3. The friction force, F, is independent of the sliding velocity

Despite the impact Da Vinci had with his work on friction, these laws are often referred to as the Amonton-Coulomb laws [32]. These laws however, are generally only true under ideal conditions.

F_T is approximately proportional to the true contact area and is therefore proportional to the normal load F_N. Where μ denotes the coefficient of friction and v_{rel} is the relative velocity between the contacting surfaces [26] outlined in Figure 2.4.

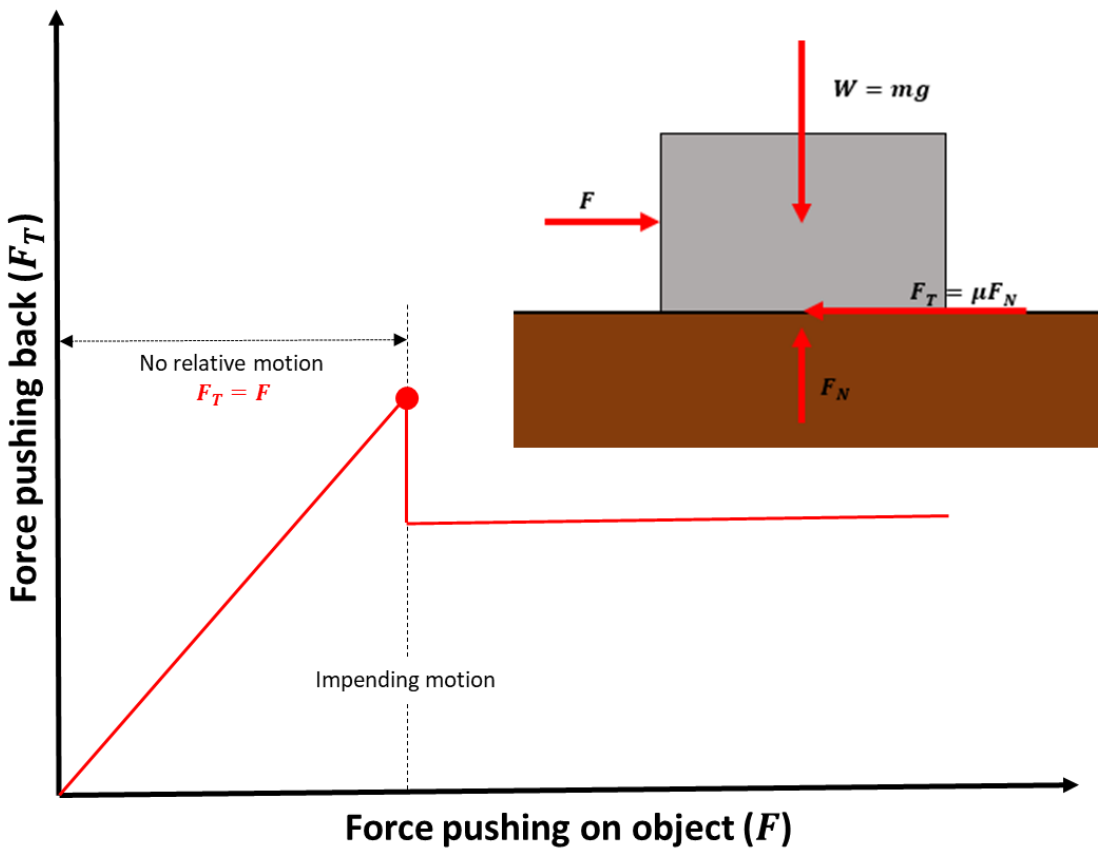

Figure 2.4 Static to kinetic friction

Equation 2-5

$$|F_T| = \mu F_N \quad v_{rel} \neq 0$$

As previously stated in the above Hertzian contact models, a smooth surface is assumed. However, true surfaces have peaks and troughs of asperities. These asperities are sheared when moved tangentially over one another; the shear force required for this is friction.

As well as not having perfect surfaces, there are also many other factors that affect the coefficient of friction in a tribological system. Such as environmental conditions like humidity, temperature or gaseous composition or contact pressure, sliding velocity and material couples (expanded on in chapter 2.7 and chapter 2.9).

2.5 Wear

Wear can be defined as a progressive material loss on a body's surface. Often as a result of relative motion to another body. Rates of wear can be affected by environment, material properties, the formation of chemical layers and working conditions [33]. Therefore, differing types of wear will manifest depending on the parameters of the particular system. The types of wear can be described as follows:

2.5.1 Melt wear

Melt wear is caused by frictional heating at the interface between contacting surfaces and has been evidenced on like metal pairing of

steel at sliding speeds as low as 1 $m \cdot s^{-1}$. Melt wear can lead to lower coefficients of friction during testing, due to the boundary lubricating effects of the liquid metal at the interface. As a film is generated at the interface, it acts in the same way as a hydrodynamic lubricating film [1]. However, although the coefficient of friction is low, the wear rate is high as the heat continues to melt more material.

2.5.2 Mechanical wear

In steel contacts sliding velocities less than 0.1ms-1 lead to negligible surface heating. Deformation of the material surface at these sliding speeds is principally due to frictional forces leading to shearing of asperities in the direction of sliding and ultimately leading to the removal of surface material; often in the form of small particles and wear debris [1]. After an initial running in period, mechanical wear displays a steady state wear rate. Running in is defined by a period where conformity, topography and frictional compatibility are optimised [1]. During the running in phase, the friction coefficient and wear rate is usually quite high; however, the most prominent asperities are sheared, and surfaces become smoother, they lower and reach steady state values.

2.5.3 Adhesive wear

Adhesive wear occurs when touching asperities from adjacent surfaces adhere together, and during tangential motion, the softer asperity is broken off, thus leaving it adhered to the harder surface. These asperity tips can then become detached, leading to wear particles. Severe adhesive wear can lead to macroscopic chunks of material being torn from the surface of a substrate; this is otherwise known as galling [1]. This wear mechanism is particularly prominent in like metal sliding pairs, especially during dry sliding at high velocities.

2.5.4 Fretting wear

Fretting wear can occur when adjacent contacting surfaces have small oscillatory motion of only a few tens of microns [1]. One defining characteristic of fretting wear in ferrous metals is the appearance of iron oxide particles which are reddish-brown in colour; these particles are harder than the bulk material and act as grinding material between surfaces. Thus producing highly polished patches on the fretted contact [1]. Fretting can lead to both abrasive and adhesive wear.

2.6 Tribochemistry

Tribochemistry is a sub-branch of chemistry known as mechanochemistry. Mechanochemistry refers to the study of chemical

and physical matter changes, brought about by the application of mechanical force through macroscopic motion [34]. Tribochemistry focuses on mechanochemical changes in tribological contact where chemical reactions at the tribo-contact are activated by shear stress, friction and wear processes.

Tribochemistry is vitally important in boundary and solid lubrication regimes. This is due to asperity-asperity contact arising due to the lack of fluid lubricant between contacting surfaces. The contacting asperities under mechanical load and macroscopic motion can lead to two tribochemical mechanisms; thermally induced reactions and mechanically-induced reactions. Thermally induced reactions can occur even at low temperatures due to flash temperature increases at the asperity contact, which can be orders of magnitude higher than the macro temperature of the contacting bodies [35]. Mechanically induced reactions can be caused by the asperity shear at the tribological contact.

2.6.1 Thermally induced reactions

The reaction kinetics of thermally induced chemical reactions can be described by the transition state theory (TST), which is sometimes also referred to as the activated state theory (AST). This theory assumes that an activated state is formed via the activation of its

reactants, meaning that the collision between reactant molecules does not form the product of the reaction directly. Therefore, the active state is formed as a highly excited and unstable intermediate, which then decomposes to form the products of the reaction [36]. This can be described as:

Equation 2-6

$$A + B \rightleftarrows [AB]^{\ddagger} \rightarrow C$$

Where A and B are the reactants, $[AB]^{\ddagger}$ is the activated complex of the reactants A and B, and C is the product of the reaction.

The rate of reaction and formation of product C is defined by:

Equation 2-7

$$r = k_T[A][B]$$

Where $[A]$ and $[B]$ are the concentrations of the reactants A and B, respectively. k_T is the reaction constant and is defined by the Eyring equation, with the inclusion of the transmission constant as follows:

Equation 2-8

$$k_T = \kappa \frac{k_B T}{h} e^{-\left(\frac{\Delta H^{\ddagger}}{RT}\right)} e^{\left(\frac{\Delta S^{\ddagger}}{R}\right)} = \kappa \frac{k_B T}{h} e^{-\left(\frac{E_a}{RT}\right)}$$

Where κ is the transmission constant k_B is the Boltzmann constant, T is the absolute temperature, h is Plank's constant, $\Delta H^{\ddagger}$ is activation enthalpy, $\Delta S^{\ddagger}$ is the activation entropy, R is the gas constant and E_a is the activation energy. The transmission constant for most cases is considered close to unity ($\kappa \approx 1$) and is therefore often omitted.

Thermally activated reactions are dependent on the temperature and the concentration of the reactants. Therefore, generally faster reactions occur at higher temperatures. It is for this reason that reactions due to flash temperature increases at the asperity-asperity contact can occur in otherwise lower temperature applications.

Although the temperature increase is short lived due to the very large heatsink of the material body on a micro to macro scale, the temperature at the asperity contact can increase in orders of magnitude when compared to the bulk. Because of this, flash temperatures can strongly influence mechanical properties of the materials, as well as leading to localised oxidation, and alter bonding [37, 38]. The maximum flash temperature during sliding can be calculated by the following [39]:

Work done by friction force:

Equation 2-9

$$Q = \mu W v_{rel}$$

Where μ is the coefficient of friction, W is the normal applied load and v_{rel} is the sliding velocity.

Equation 2-10

$$T_{f_{max}} = \frac{2\dot{Q}}{KA}\sqrt{\frac{2\chi b}{\pi v_{rel}}}$$

Where K is the thermal conductivity, χ is the thermal diffusivity, A is the contact surface, and b is half contact width.

Being able to calculate these flash temperatures for a given application are important to understand if localised, rapid oxidation may occur due to activation energy for thermal reactions being met.

2.6.2 Mechanically induced reactions

The application of a mechanical force to a surface can modify the free-energy surface of chemical reactions, often enabling thermodynamically unfavoured reaction pathways [40]. Many models have been proposed for calculating the rates of reactions in tribological contacts. One widely accepted model for the reaction rate can be described by a modified Arrhenius equation, where:

Equation 2-11

$$k_{\mu} = \frac{k_B T}{h} e^{\left(\frac{\sigma V - \mathrm{E_a}}{k_B T}\right)}$$

Where k_B is the Boltzmann constant, T is the absolute temperature, h is Plank's constant, σ is the shear stress, V is the material constant and E_a is the activation energy.

2.7 Diffusion mechanisms

Diffusion can occur by two different mechanisms, interstitial diffusion and substitutional diffusion [41]. In substitutional diffusion atoms from a bulk are replaced impurities or other atoms sitting on the surface of the material. For example oxygen substitution in MoS_2:MoO_2 [42]. Or if an atom is small enough it can sit interstitially between a lattice for example water molecules sitting between MoS_2 lattice. One study by Kuznetsov et al. [43] used density function theory and diffusion mechanics simulations to investigate the diffusion coefficients of water on MoS_2 at room temperature to be $0.5 \pm 0.1 \times 10^{-8} m^2 \cdot s^{-1}$ and proposed that water would likely only diffuse around cracks, impurities or edge sites in the material. The other mechanism they proposed is the hydrogen 'hopping' from one oxygen to another, or to sulphur and back.

2.8 Lubrication

The application of a lubricant can substantially reduce the coefficient of friction; the lubrication creates a boundary layer between surfaces and allows many asperities to slide over one another without making contact. In recent years, significant progress has been made in the field of lubrication, including the attainability of superlubricity. Superlubricity is a relatively new area of research, which has gained significant interest, and is defined as near zero friction and wear rates, where the friction coefficient is less than 10^{-3} [44]. Lubricants often either come in liquid, oil-based form or solid form. Although oil-based lubrication is the most commonly used in everyday applications; solid lubrication has many benefits over its liquid counterpart. These include cleanliness, the ability to confer extremely high wear resistance on machine parts, and the ability to provide lubrication in extremely high or low temperatures, in a vacuum and in the presence of strong radioactivity. Below, in Figure 2.5, the regimes of lubrication are outlined in the form of a Neo-Stribeck curve. The Neo-Stribeck curve describes the expected friction coefficients in the different friction regimes; dry friction tends to mean no lubrication, and thus displays the highest coefficient of friction; boundary lubrication, here a thin film is present between the contacting surfaces, asperity contact still occurs just at a lesser rate; mixed

lubrication, here the lubricant film is thicker, with only few contacting asperities; Hydrodynamic lubrication, the lowest coefficients of friction are achievable here, up to a point, and then increases with increasing film thickness due to the rate of shear increasing [45].

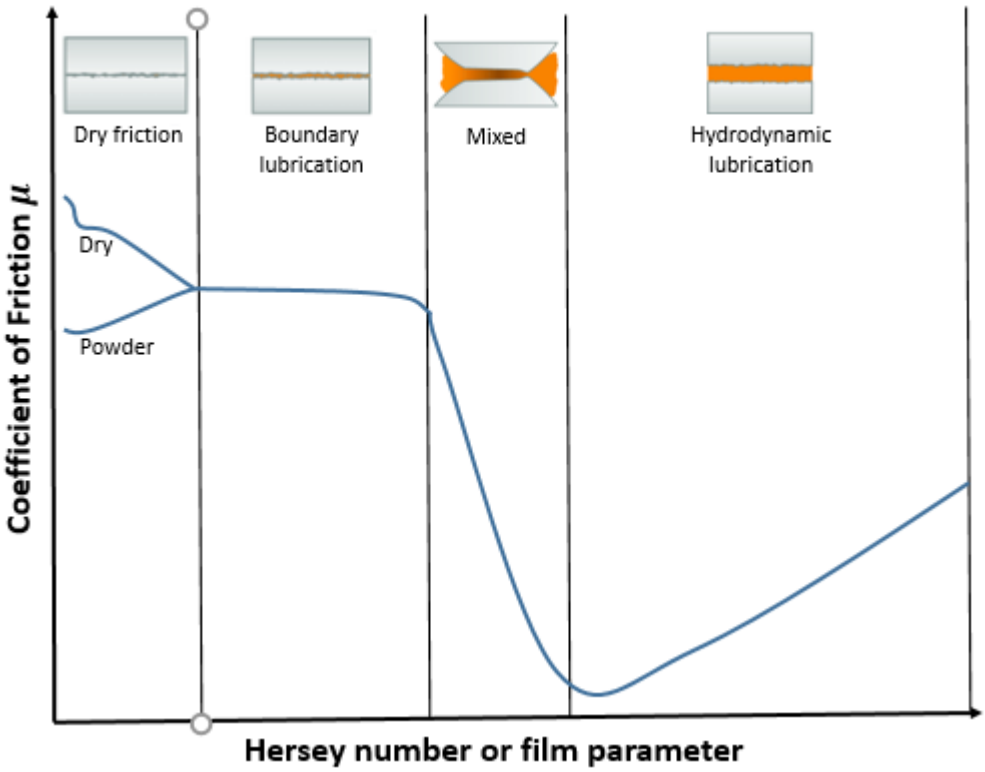

Figure 2.5 Neo-Stribeck curve, highlighting lubrication regimes

2.8.1 Solid lubrication

Solid lubricants can be utilised in situations where liquid lubricants are not applicable, such as the vacuum of space or elevated temperatures, which cause many liquid lubricants to volatilise and thus lead to failure of not only the lubricated component, but also unrelated components, if the vaporised liquids condense or react on their surfaces[7]. Furthermore, decomposition materials can build up at interfaces and restrict the easy sliding of adjacent surfaces [7]; this can be especially prevalent in long-life applications. With the use of solid lubricants, wear usually occurs through one or more of the following modes: abrasive wear, adhesive wear, and fatigue wear [46]. Like on many non-lubricating solids, wear rates of solid lubricants are often nonlinear. Examples of this can be seen in amorphous sputtered MoS_2 coatings, which can display rapid wear over initial cycles, but then can maintain extremely low wear rates for up to millions of cycles [7]

Solid lubricants fall into one of two categories; intrinsic lubricants, which have an atomic structure with easy shear at the surface, such as MoS_2, or, extrinsic lubricants, which require the influence of additives from their surroundings to activate an easy-shear mechanism, such as graphite, which needs water from the atmosphere to facilitate low

friction coefficients. Within these categories, there are two main types of solid lubrication used; these are soft metal film and lamellar lubricants. Soft metal films consist of materials such as silver, lead indium and copper. These metals are used on hard substrates, often in high load applications [11]. The mechanisms by which soft metal films work as lubricants is down to having shear properties less than the hard substrates to which they are applied. This means that their asperities will shear easier, thus reducing the coefficient of friction. Lubrication by soft metal films is particularly useful in high vacuum applications; this is due to the absence of oxygen facilitating repeated transferal of particles from the metallic film between the sliding surfaces [11]. However, they are not viable lubricants in low-temperature applications, where the soft metals can become brittle and be prone to flaking off of the worn substrate [11]. Soft metal films, however, do not offer friction coefficients as low as many of their lamellar counterparts.

Lamellar lubrication is the predominantly used form of solid lubrication, with the most common materials being graphite and molybdenum disulphide (MoS_2). Lamellar solids that are used for the purpose of lubrication exhibit anisotropy of mechanical properties [11], in the cases of MoS_2 and graphite weak bonding between layers of atoms causes the material to become self-lubricating and allows

lamellar to slide over one another with relatively low shear stress. The crystalline structure of graphite and MoS_2 are displayed below in Figure 2.6. As illustrated in this figure, strong bonding occurs in in-plane atoms, with weak bonding between layers. Of the two materials, MoS_2 shows significantly greater promise in the achievability of super-low friction coefficients and low wear rates.

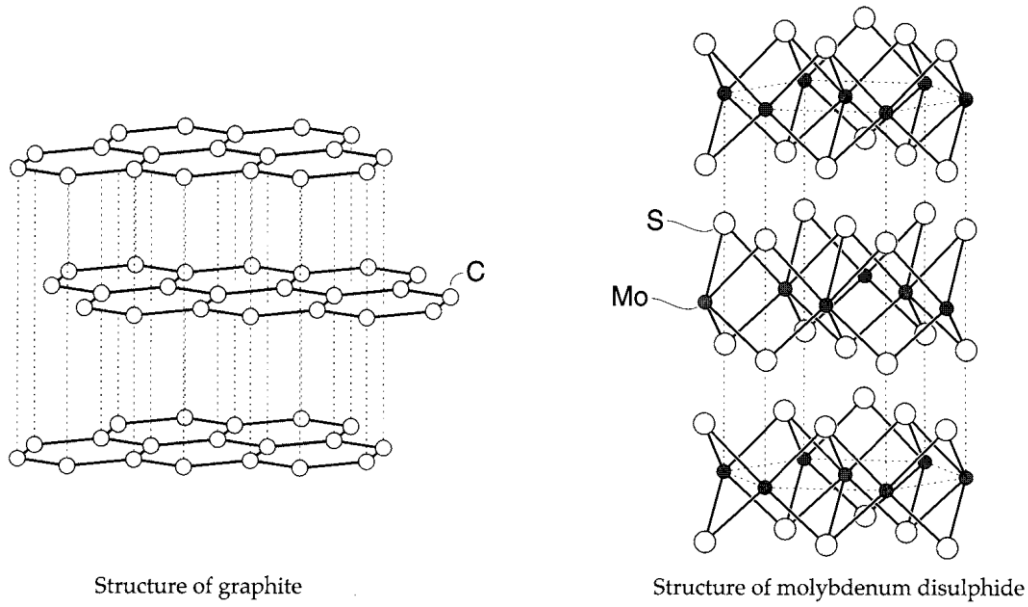

Figure 2.6 Crystal structures of graphite and molybdenum disulphide.

2.8.2 Graphite

Graphite works well as a solid lubricant due to its anisotropy of mechanical properties, which leads to failure at low shear stresses at

the interface [11]. Sliding between lamellae of graphite is facilitated by the presence of small amounts of oxygen and water, which limits bonding between layers [11]. For this reason, super low friction coefficients are not attainable in a vacuum, or when relative humidity is less than 1% [12]. Dienwiebel et al. in [12] explored the superlubricity of graphite. They carried out tests using an atomically sharp tungsten tip. Therefore only atomic scale friction was measured. Friction coefficients as low as 0.001 were observed in experiments in 10% humidity nitrogen streams.

2.8.3 Diamond like carbon

Another relatively new type of solid lubrication is diamond-like carbon or DLC films. DLC films offer vast potential for applications that require low friction and high wear resistance. DLCs fall into two main subcategories; films generated from hydrocarbon source gasses may contain high levels of hydrogen and are often referred to as hydrogenated DLCs (a-C:H), and films that are generated from solid carbon targets are virtually free of hydrogen, and thus are referred to as hydrogen free DLCs (a-C)[47]. The friction coefficients of DLCs are greatly affected by the hydrogen content and atmospheric conditions [48]; while hydrogenated DLCs attain the best results in dry inert

atmospheres, non-hydrogenated DLCs reduce their friction coefficient as humidity increases to a point [16]. Due to the nature of this project – that the intended environment is dry nitrogen, a-C:H DLC films are the focus in this section. Erdemir in [47] presents a-C:H DLC films with coefficients of friction as low as 0.001 in an inert gas, or vacuum conditions; this is due to the elimination of strong covalent bonds and better shielding of carbon atoms [48]. However, when oxygen and water molecules are added to the test chamber, the friction coefficient may increase to values higher than 0.1. Erdemir in [48] suggests this is due to the development of capillary forces around the real contact spots. Erdemir also states in [49] that highly hydrogenated DLCs (>40 at. % hydrogen) show extremely low wear rates and can endure more than 17 million cycles during sliding against 10mm balls in a dry nitrogen environment; this is shown below in Figure 2.7

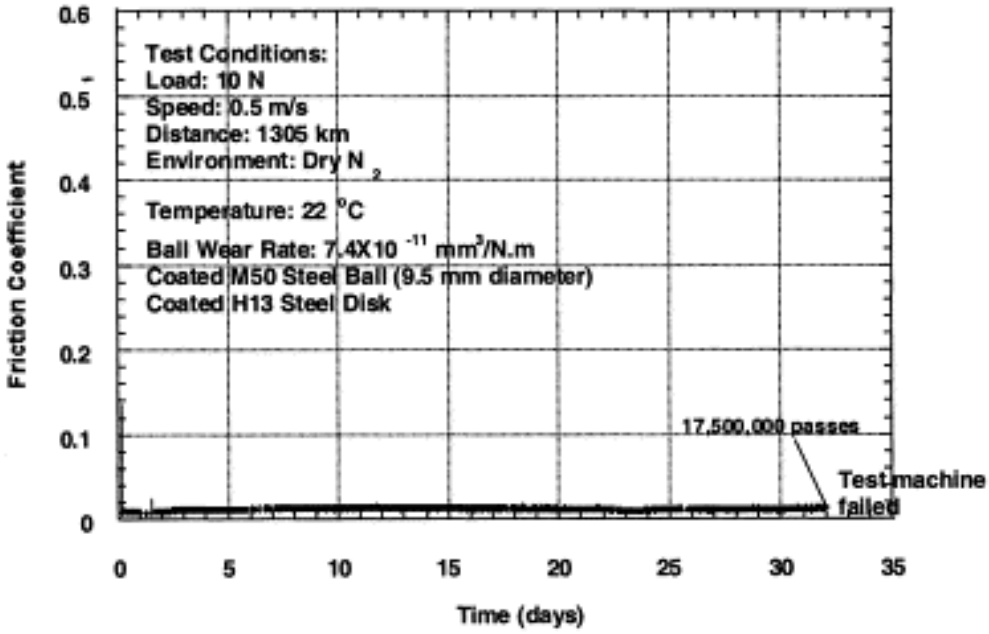

Figure 2.7 Long-duration friction and wear performance of DLC film derived from 25% CH_4+75% H_2 plasma. As taken from [49]

2.9 Physical vapour deposition

PVD is an excellent vacuum coating process for the improvement of wear and corrosion resistance. It is a highly versatile technique which can be used to coat many surface morphologies. PVD is a vaporisation coating technique that involves transfer of a material at an atomic level under vacuum conditions [50]. PVD entails the atomisation or vaporisation of a material from a solid source, often called the target,

using electron and/or ion beam bombardment. The vapours are then attracted to the substrate via a negative bias voltage onto an electrically conductive substrate, as outlined in Figure 2.8. PVD can produce very thin films ranging from tens of nanometres to several microns [51]. Typical PVD films are characterised by an initial phase of crystalline material formation, followed by an amorphous columnar growth throughout the remaining thickness of the coating.

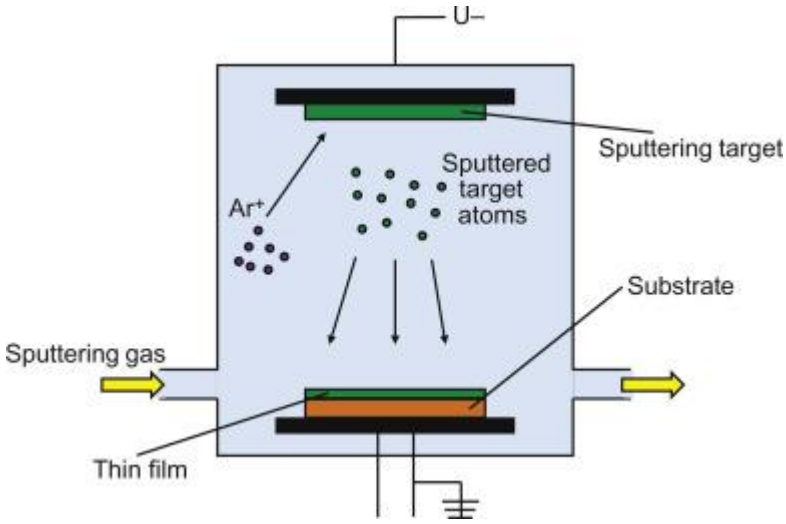

Figure 2.8 Schematic illustration of the physical vapour deposition process [52].

2.10 Molybdenum disulphide

The main aim of this study is to elucidate the effect that water and oxygen have on the performance of MoS_2 coatings for use as a solid lubricant coating. Exploring both the impact that oxygen and water have in the sliding environment and how the introduction of these species in the storage environment may affect the performance of the coating. Therefore, this chapter will consist of a comprehensive review of the use of molybdenum disulphide as a solid lubricant in both terrestrial and ideal atmospheres. Starting with a history of MoS_2 use and a breakdown of the known literature on chemical and structural changes brought about by water and oxygen on MoS_2.

2.10.1 History of MoS_2

Documented use of MoS_2 as a lubricant can be dated back to the early 20th century [53], although it was likely used far earlier and mistaken for graphite due to its similar appearance and material properties [13]. Initial uses and up until the late 1960s consisted of burnishing or rubbing MoS_2 powder onto a surface; however, due to the low shear nature of the material, resins and other organic substances were often needed to bind the lubricant to the surface [13, 54-56]. Although, producing coatings in this manner was relatively simplistic, obtaining repeatable results proved to be very difficult. Consistent thickness,

coating density and material adhesion were not easily achievable. Furthermore, with the advent of space travel, although MoS_2 coatings had favourable characteristics for use as a lubricant in extra-terrestrial travel; resins would outgas in the vacuum of space [13]. To overcome these issues, RF magnetron sputtering was used to deposit MoS_2 coatings. This allowed for far greater control of coating thickness, leading to denser coatings and purveyed superior substrate adhesion. Today coatings are most commonly produced using physical vapour deposition (PVD), by which far greater control of coating parameters can be enjoyed, such as thickness, density and texture. MoS_2 coatings produced by PVD tend to be amorphous in nature, but with an initial preferential basal orientation for the first few lamellar at the material interface.

2.10.2 An overview and structure

MoS_2 is a well-known solid lubricant, which has extensive use in industrial, automotive and aerospace applications. This is due to its ability to confer extremely low wear rates and near vanishing friction coefficients in dry and inert atmospheres [57]. It is well known that MoS_2 performs at its best in dry and inert atmospheres [14, 42, 46, 57-73]. However, its utilisation in terrestrial atmospheres, containing oxygen and water vapour, leads to a significant reduction in the

lubricity and wear life of the coating. One of the first observations on the environmental limitations of MoS_2 in sliding was in 1953 by Peterson and Johnson [74], who found that the coefficient of friction between MoS_2 lubricated metal surfaces increased with increasing relative humidity (RH) up to 65% RH, at which point it began to decrease. Following this, many studies have been carried out exploring the effects of water and oxygen on the lubricity and lifetime of MoS_2 as a solid lubricant [13-15, 42, 46, 57, 65-67, 71, 72, 75-90].

MoS_2 exhibits a lamellar structure and belongs to a family of materials known as transition metal dichalcogenides of the type MX_2 whereby a layer of metal atoms, such as molybdenum, Mo, or tungsten, W, are sandwiched between two chalcogen atom layers such as Sulphur, S, or Selenium, Se. Molybdenum disulphide, in particular, has a polycrystalline structure consisting of hexagonal layers of S-Mo-S crystals connected to adjacent covalently bonded by weak Van der Waals forces along the [002] plane, between the sulphur-sulphur faces (Figure 2.9). Due to the strong bonding in-plane and weak bonding out-of-plane, mechanical and other properties of MoS_2 are highly anisotropic [91]. It is widely accepted that the weak Van der Waals forces between MoS_2 layers lead to ultra-low coefficients of friction between lamellae, which allows preferential basal layer cleavage [9, 56, 66, 71, 89]. MoS_2 displays low sensitivity to stacking and a surface

energy of 47 mJ/m^2 = 0.025 eV per unit cell which is indicative of a low barrier to sliding and thus low coefficients of friction [92]. Deviations in MoS_2 from the ideal bulk crystal are commonplace. Komsa et al. calculated that the most favourable defect in MoS_2 are sulphur vacancies [93]. These sulphur defects may lead to a higher propensity for oxide formation to MoO_2 through oxygen substitution into sulphur vacant localities.

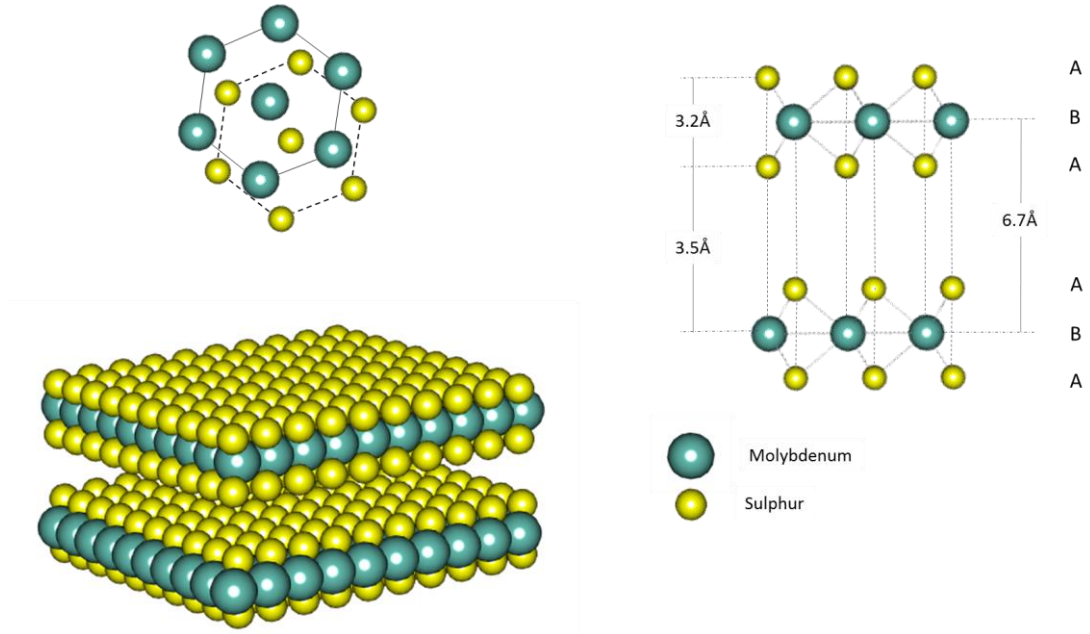

Figure 2.9 a) Top and b) 3D perspective view of hexagonal crystal structure of MoS_2 and c) orthogonal view of lamellar structure with lattice spacing dimensions

2.10.3 Coating architecture

The microstructure of the coating is another factor which can greatly affect the lifetime and friction coefficients of MoS_2 based coatings. The microstructure of the coating is controlled by the deposition method. Due to the run in period of MoS_2 where, as previously explained, columnar structures of MoS_2 must reorient parallel to the substrate surface and in the direction of sliding to allow easy lamellar shear; pre-oriented crystalline coatings from the point of deposition are highly sought after. Most PVD coatings have an amorphous structure [73, 94, 95], with only the first few layers displaying a preferential basal orientation, followed by columnar growth normal to the coating surface. Consistently producing PVD coatings with preferentially basally orientated layers presents significant challenges [63]. Temperature, argon flow, pressure and target materials all effect the growth of MoS_2 lamellae [96].

Curry et al. in [57] have explored the use of a new coating method which leads to a novel and interesting coating architecture. They compared friction coefficients of amorphous commercial MoS_2 coatings with basally oriented MoS_2, deposited via N_2 spray – a method not seen elsewhere in literature for the deposition of MoS_2 but has been utilised, although altered, in [97] where stainless steel coatings were produced, but only at temperatures exceeding 500°C. Curry stated that the N_2 spraying works similar to burnishing by shearing MoS_2 crystallites onto the substrate, but with basal orientation throughout the thickness of the coating; thus negating the crystallographic reorientation during the first few sliding cycles. However, no binding agents were used as is needed when burnishing MoS_2 onto a substrate. Therefore, the durability and adhesion to the substrate is questionable, especially with the deposition parameters outlined. To deposit the coating, MoS_2 powder was sprayed on to stainless steel substrates with a pressure of 0.6 ± 0.05 MPa positioned 50mm above substrate surface. Excess MoS_2 was then blown off. The average particle size of the powder was 3-4µm, yet coating thickness was only 100-300nm. The results obtained in tribometer testing showed to be very promising, with a significantly decreased environmental sensitivity, displayed below in Figure 2.10. The initial friction coefficient was lower in both dry nitrogen and humid air,

drastically so in the latter, and remained this way throughout the 100 cycles of the test.

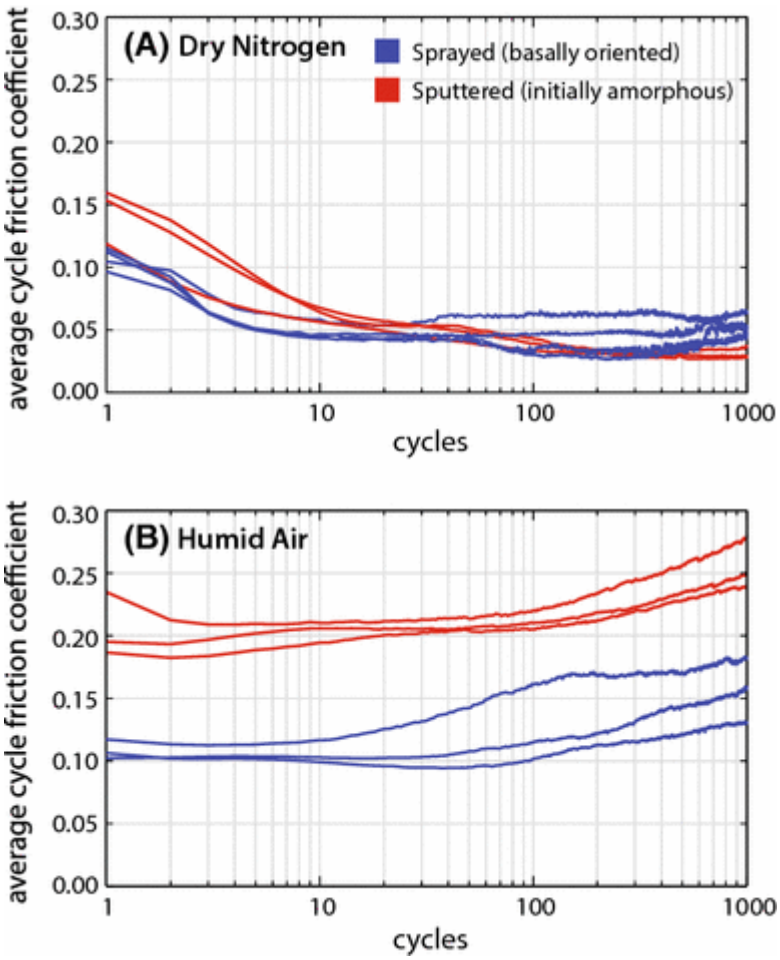

Figure 2.10 Comparing N_2 sprayed and PVD sputtered MoS_2 in air and dry N_2 [57]

2.10.4 Run-in of MoS_2 coatings and mechanisms of low friction

In sliding, MoS_2 nearly always undergoes a transition in friction performance during the initial cycles of sliding, this is known as the run in phase. During the run in phase, the coefficient of friction rapidly drops over the first few cycles, as highlighted in Figure 2.11. This is widely attributed to structural changes, by which, crystallographic reorientation of the coating occurs to produce preferential basal alignment of the lamellae, parallel to the sliding direction [73, 94] as outlined in Figure 2.12. The rapid drop in friction can also be attributed to surface oxide removal [65]. It is also stated in the literature that a transfer film formation on the counter interface is a requirement for achieving the low friction behaviour of MoS_2 films, and the ability of MoS_2 to transfer to counter interfaces is well documented [46, 73, 98].

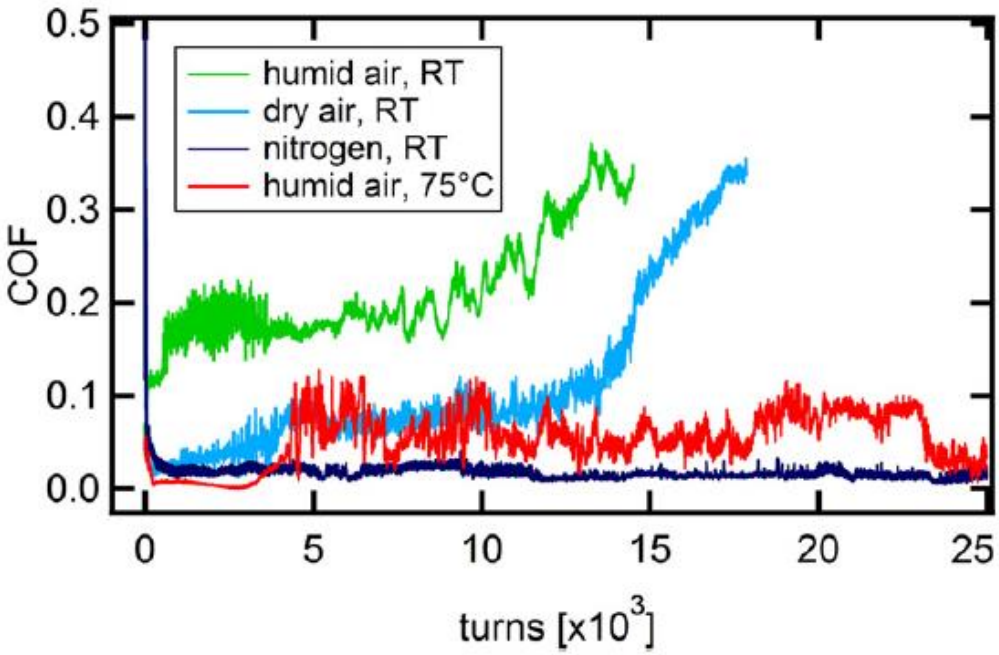

Figure 2.11 MoS_2 tested in different environments, highlighting the rapid drop of friction in the first few sliding cycles [79].

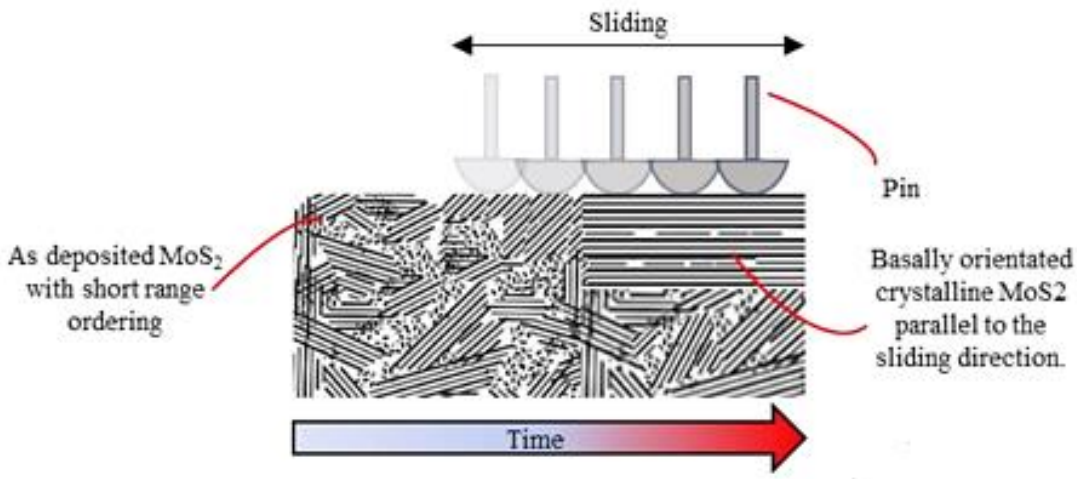

Figure 2.12 Run in process of MoS_2

Martin et al. [99, 100] aimed to elucidate the mechanisms that led to ultra-low friction – coined superlubricity - of MoS_2. Their findings showed the establishment of MoS_2 transfer film formation on the counter surface following sliding and a shear-induced orientation of MoS_2 basal planes aligned parallel to the sliding direction. Oviedo et al. [101] confirmed these findings by showing the formation of a transfer film during sliding using in situ sliding within a TEM, as outlined in Figure 2.13.

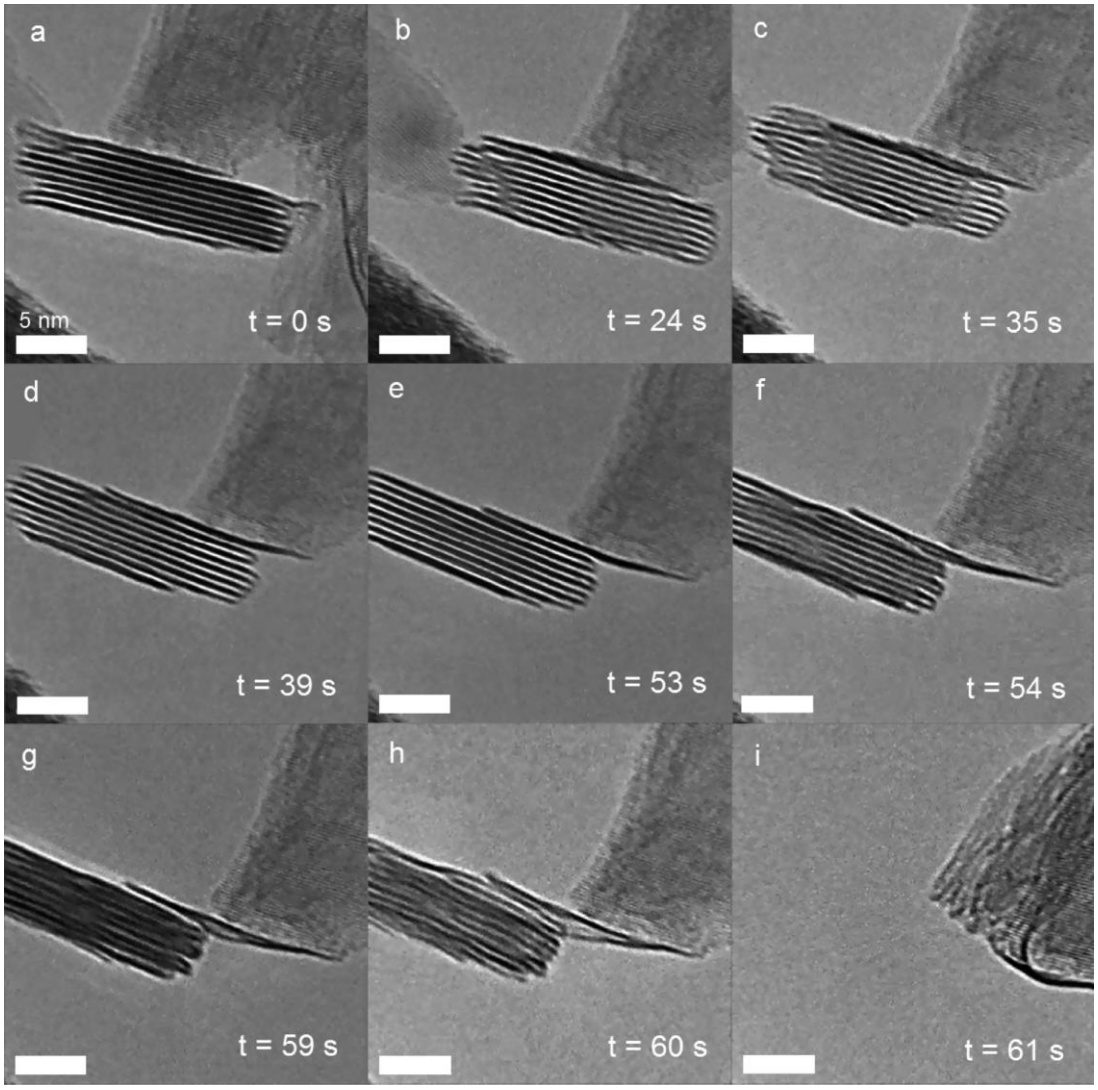

Figure 2.13 In situ TEM of MoS_2 sliding process and transfer film formation on oxidized tungsten tip. Courtesy of [101].

2.10.5 Environmental sensitivity of MoS_2 coatings.

It is well known that MoS_2 performs at its best in dry and inert atmospheres[14, 42, 46, 57-73]. However, despite this, there are discrepancies and contradictory results purported in the literature leading to a number of different hypotheses as to why this happens, which will be outlined in this section.

It is proposed that the lubricious lifetime of MoS_2 coatings in a vacuum is almost ten times that of coatings in atmospheric air [11]. The effect of adsorbed water and oxygen have been investigated and are believed to restrict the easy basal shear of the lamellae by situating themselves between MoS_2 layers [66, 76]. However, their effects are often studied individually. Therefore, data on the effects that both water and oxygen have together on the lubricious qualities of MoS_2 coating are limited.

The presence of molecular (O_2) and atomic (O) oxygen are thought to lead to surface limited oxidation of MoS_2 [14, 66]. This oxide layer leads to increased coefficients of friction during sliding, but are removed quickly during the run in phase [66]. This high friction, oxide removal required at run in can be particularly problematic in space or single to low cycle applications where oxidation may occur prior to assembly and testing of devices in terrestrial conditions. Oxidation is

also likely to occur in the presence of atomic oxygen, due to its extremely reactive nature, which is of particular concern when operating in low earth orbit [102]. Molecular oxygen was shown not to affect the lubricity of MoS_2 during room temperature sliding [65]. However, it does lead to oxidation at MoS_2 edge sites to MoO_3 and MoO_2, at temperatures over 350 °C, and this oxidation subsequently restricts the easy lamellar shear properties of MoS_2 [103]. The oxidation of MoS_2 is thought to start as physisorption of oxygen on the surface of the MoS_2 before reaction and becoming a molybdenum oxide (MoO_x).

Holinski and Ganshiemer [104] show that water adsorbs into the surface of MoS_2 due to the strong polarity of its sulphur terminated basal planes. Stating that water bonds simultaneously to two polarised sulphur atoms, thereby restricting the easy lamellar shear. However, there remains significant conflict in the proposed mechanisms behind reduced lubricity and wear life in humid, oxygen containing environments. The one constant in the literature is that MoS_2 displays poor lubricious qualities in humid air [13, 44, 56, 57, 73, 89, 94, 104, 105].

There are two dominant hypotheses regarding the degradation of lubricity in MoS_2 coatings in humid environments at room temperature; The first, and longest standing hypothesis, is that oxidation in the coatings restricts basal layer sliding between lamellae, thus leading to higher coefficients of friction [7, 64, 67, 83, 106-108]. Others refute this claim, stating that oxidation at room temperature is negligible and that water is the overriding component adversely affecting friction at room temperature [57, 63, 80]. These two hypotheses are outlined schematically in Figure 2.14.

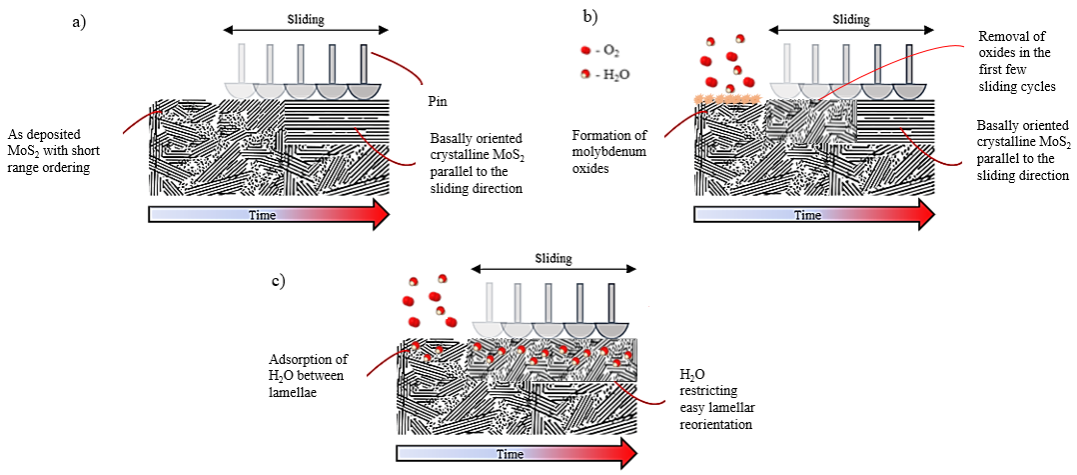

Figure 2.14 Schematic diagram illustrating inert sliding and the two main hypotheses of how the lubricity of MoS_2 is reduced in oxygen and water containing environments. a) Sliding in an inert environment. b) Oxidation and oxide removal during sliding in air leading to higher coefficients of friction in early sliding cycles. c) Adsorption of H2O in an air environment, and restriction of basal orientation and easy lamellar sliding.

Ross and Sussman [109] were one of the first to show a link between humidity and oxidation of MoS_2 at room temperature. Colorimetric determination of molybdic oxide along side gravimetric sulphate acidity was used to show that increased humidity led to an increase in molybdenum oxides. Haltner and Oliver [76] also showed that the coefficient of friction of MoS_2 increased with the introduction of humidity, and attributed this to oxidation, hypothesising that

frictional heating at the asperity contact facilitates oxidation at localised oxygen and water adsorption sites. Fleischauer et al. [83] claimed oxygen can be substituted for sulphur leading to MoO_2 at room temperature; these oxides would not be distinguishable from MoS_2 on XPS or Auger analysis due to the like-like oxidation states (4+) of the molybdenum in MoS_2 and MoO_2. More recently, Dudder et al. [110] showed that the MoS_2:MoO_3 ratio decreased during sliding in humid air – but not in dry oxygen, stating that aqueous species are most likely to lead to oxidation of the coating. Pető et al. [90] showed, using scanning tunnelling microscopy (STM), that substitution oxidation is present in MoS_2 aged for one month in ambient air. Oxidation by substitution to form $MoS_{2-x}O_x$ preserves the original crystal lattice of MoS_2 and can be accelerated by increasing thermal energy. Density functional theory calculations indicate that S removal by oxidation is thermodynamically favourable in MoS_2 [85, 90]. Substitutive oxidation occurring after deposition always had a negative effect on lubricating performance [83].

An interesting opposing statement by Khare et al. [66] claims that the room temperature friction response and lifetime is solely affected by physisorbed water, and thus, oxidation and oxygen plays no part. Stating that the friction coefficient was always at least 2x higher in humid environments (μ = 0.06-0.09) than in dry environments (0.02-

0.03). They showed that the surface of MoS_2 oxidises to MoO_3 in humid air. Using EDS and an in-situ tribometer, they demonstrated that oxidation is removed within 20 cycles of sliding when sliding in 45% RH air at room temperature and a normal load of one Newton, meaning that wear rate was faster than oxide formation, and thus, oxidation was negligible. Khare et al. [65] also compared the effects of accelerated ageing in humid and oxygen containing environments, and showed that water vapour does not impact coating composition via oxidation. Studies performed on MoS_2 oxidation via heating in an air stream for multiple hours have concluded that oxidation is not prevalent until around 350℃ [111-113]. Though, other studies have reported than the inclusion of water may reduce the temperature needed for oxidation of MoS_2; Ross and Sussman have reported that MoS_2 oxidation in the presence of water vapour may occur at temperatures below 100 °C according to the following reactions [109]:

Equation 2-12

$$2MoS_2 + 9O_2 + 4H_2O \rightarrow 2MoO_3 + 4H_2SO_4$$

Equation 2-13

$$MoS_2 + 2H_2O + 4O_2 \rightarrow MoO_2 + 2H_2SO_4$$

Equation 2-12 is also stated by Gao et al. [56]. Furthermore, due to the highly hygroscopic nature of H_2SO_4, the reaction will self-propel in water vapour due to local water condensation and adsorption [114]. However, the formation of sulphuric acid is disputed by Vierneusel et al. [67] who state that introduction of water leads to gaseous hydrogen disulphide formation:

Equation 2-14

$$2MoS_2 + 2H_2O + O_2 \rightarrow 2MoO_3 + 4H_2S$$

Although MoO_3 is the most stable oxide of MoS_2 [115], other molybdenum oxides may form. Walter et al. [116] highlight the synergy of water and oxygen, stating that The inclusion of water and oxygen in the reaction leads to a higher propensity for MoO_2, and results in faster oxidation rates at lower temperatures.

Serpini et al. [79] showed through their results of a dry N_2-O_2 alternating purge experiment with humid air, that there is negligible difference in the friction response of a PVD MoS_2 coating at room

temperature, in which the coefficient of friction in dry O_2 was comparable with dry N_2 as shown below in Figure 2.15. They state that the almost instantaneous drop in friction, when in transition from humid air to dry nitrogen, can only be explained if the water is only physisorbed in the first few layers. They also state that room temperature oxidation of MoS_2 is so slow it becomes a negligible output.

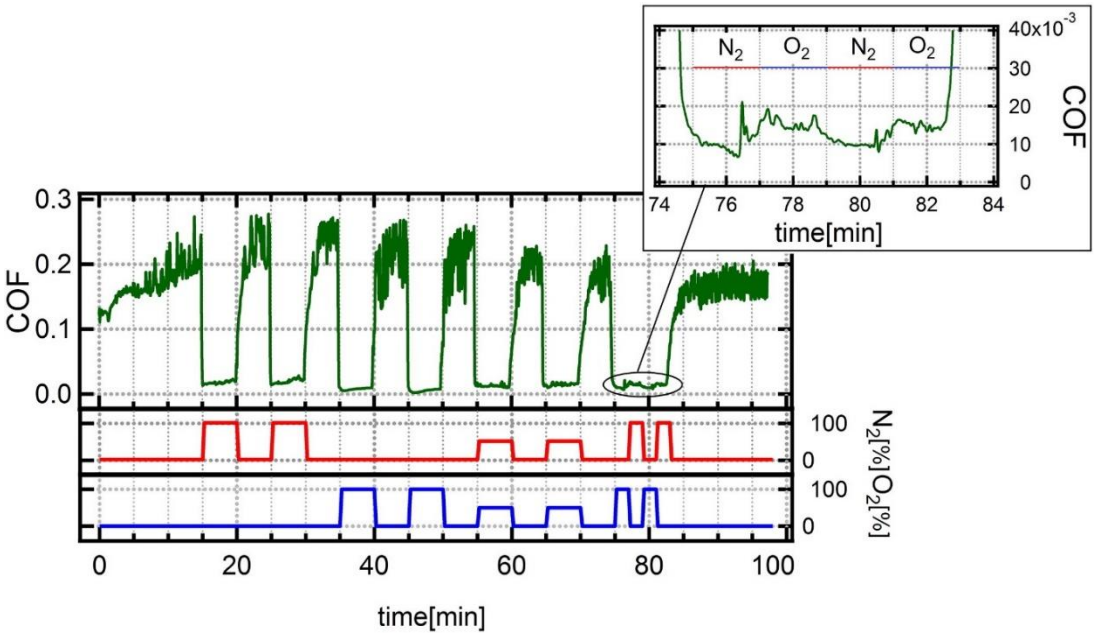

Figure 2.15 N_2-O_2 alternate pump and purge experiment with air to show the friction coefficient of MoS_2 at room temperature curtesy of [79]

However, one short sight of these experiments is the short testing duration, only amounting to around 50 minutes sliding in humid air, thus, giving very little time for water adsorption and substantial oxide formation. Furthermore, it does not state the role of oxide removal during sliding. When sliding in air the oxides may be being formed and removed simultaneously, therefore allowing for a rapid return to low coefficients of friction when purged with a dry environment. In addition to this, no surface characterisation was outlined in this study; therefore, claiming oxides did not play a role is not possible. The test is also comparing how oxygen affects most on its own when compared with nitrogen on its own, and does not explore the synergistic effect that water and oxygen may have on oxide formation.

Tests were also carried out in [79] in room temperature (RT) air, RT dry air, RT dry nitrogen and 75 °C humid air, as seen in Figure 2.11. They recorded the lowest friction coefficients in dry nitrogen; however, still achieved low friction coefficients in humid air at 75 °C; they attributed this to reduced water adsorption, but with a temperature low enough as not to oxidise the coating.

The low friction coefficients of MoS2 in differing environments have also been investigated by Donnet et al. in [71]. The tests were carried out with stoichiometric MoS2 applied using physical vapour

deposition (PVD) in an ultra-high vacuum to ensure the coating was free of oxygen and other contaminants. Friction tests were carried out using a pin on plate tribometer in; ultra-high vacuum (UHV: 5×10^{-8} Pa, 3.75×10^{-10} Torr), high vacuum (HV: 10^{-3} Pa, 7.5×10^{-6} Torr), dry nitrogen (10^5 Pa, 750 Torr) and ambient air (10^5 Pa, 750 Torr). The pin tip was hemi-spherical with 4 mm curvature radius and was made from AISI 52100 steel, sliding on MoS2 coated plate of the same material. 'Super-low' friction coefficients below 0.004 were obtained in both UHV and dry nitrogen, while still low friction coefficients of 0.013-0.015 were recorded in the HV, however, significantly higher friction coefficients in the range of 0.2 were recorded for ambient air as reported in [71] however not displayed on their results presented in Figure 2.16. This highlights the significant differences between dry atmospheres and humid, oxygen rich atmospheres. But goes no way into explaining the reason and mechanisms behind the higher friction coefficients. Furthermore, as the tests were only run over 100 cycles, wear rates and time to failure were not explored.

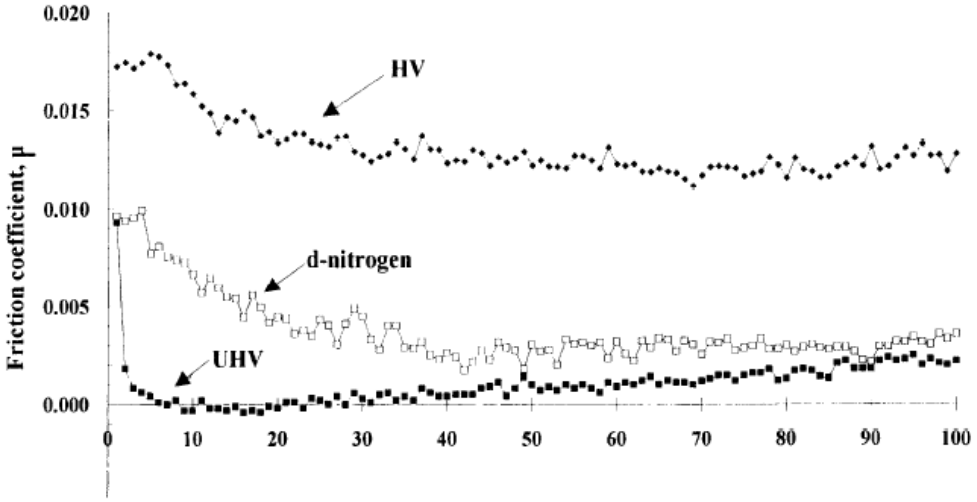

Figure 2.16 Coefficient of friction verses number of cycles in different testing environments [71].

Very few studies explore the effect that air and water have on MoS_2 over longer exposure times. Krantz et al. [117] investigated the effect of humid storage environments on the durability of MoS_2 coated gears when operated in a vacuum at a pressure of 3×10^{-7} Torr. Exposure to humid air was achieved by placing the gears in a closed chamber, on a perforated plate. The perforated plate stood over a saturated solution of water and sodium bromide. Samples were exposed to humid air for 10, 17, 28 and 77 days. They found that the samples exposed to 57% RH air for 77 days had, on average, a 35% reduced wear durability.

Lince et al. [118] also explored the effect of exposing nanocomposite sputter-deposited MoS_2 coatings to humid air for prolonged periods (over two years) of time for real-time (unaccelerated) ageing before pin on disc tribology testing in a dry N_2 environment. The nanocomposite coatings tested were; Ni-MoS_2, Au-Sb_2O_3-MoS_2 and Sb_2O_3-MoS_2 onto AISI 440C stainless steel disks to a nominal thickness of 400 ± 100 nm and then stored in an enclosed container that was humidity controlled to 59% RH by using a saturated solution of NaBr and samples were removed periodically for testing. Control samples were stored in a flowing dry N_2 environment where RH <0.08%. Tribology testing was carried out using uncoated 6 mm OD AISI 440C steel balls at a load of 3N and a sliding speed of 20cm/s. The average endurance of the coatings decreased with increasing storage time, by around 55% after 2.3 years for the Ni-MoS_2 coated sample, 27% after 2.3 years for the Au-Sb_2O_3-MoS_2 coating, and 27% after 1.1 years for the Sb_2O_3-MoS_2 coating. However, the steady state/minimum coefficient of friction remains very similar. This is likely due to any oxide formation being removed during the many sliding cycles. XPS was used to confirm oxide formation with MoO_3 peaks present in all aged samples. Even that of N_2 aged samples. This is due to the rapid onset of surface oxide formation of MoS_2 coatings when exposed to air. However, the MoO_3:MoS_2 ratio is higher in the air aged samples as outlined in Figure 2.17. However, as explained

previously, one significant drawback of using XPS to analyse oxidation in the overlap of the MoO_2 and MoS_2 peaks, due to the like-like oxidation states (4+) of the molybdenum in MoS_2 and MoO_2, meaning that quantification of MoO_2 is not possible using XPS [83].

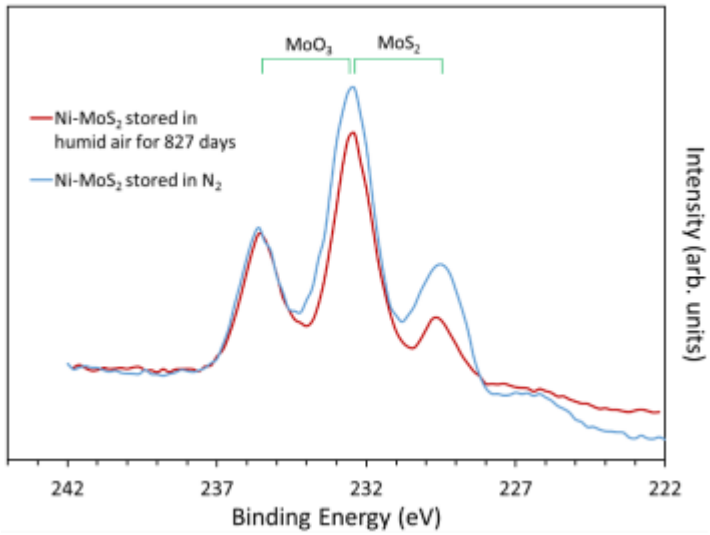

Figure 2.17 XPS spectra in the Mo 3d region for Hohman Plating Ni-MoS2 coatings stored in dry N_2 and stored in 59% RH air for 2.3 years. Courtesy of [118]

Extensive research has taken place on improving the tribological performance and reducing the environmental sensitivity of MoS_2 films by using dopants (often referred to as co-sputtering) such as titanium, nickel, lead, gold and silver [7, 20, 59, 119-126]. Dopants in MoS_2 can be located in the structure of MoS_2 films in several different ways.

Substitution can occur at either the Mo or the S site, with the latter having a higher affinity for substitution [127]. Atoms can become intercalated between the MoS_2 layers [128]. Alternatively, atoms can be adsorbed to the surface or edge sites. Savan et al. [8] theorised that dopants such as Au could saturate the edge sites, thus promoting preferential growth of MoS_2 crystallites parallel to the surface, and therefore reducing the coefficient of friction. This theory that Au inclusion in MoS_2 films would lead to lower coefficients of friction was backed up by Lince et al. [126], who studied the influence of contact stresses of doped MoS_2 coatings with varying levels of Au content. The coatings were sputtered on to Si wafers, and tribological tests were carried on a pin-on-disk tribometer in a dry N_2 environment. Their results showed that Au-doped MoS_2 coatings performed better than pure MoS_2 in both coefficient of friction and wear as outlined in Figure 2.18.

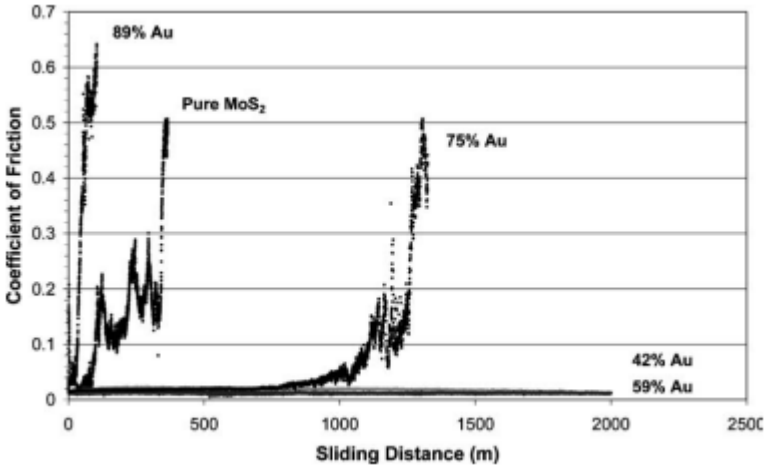

Figure 2.18 Coefficient of friction obtained at a contact stress of cosputtered MoS_2 coatings with 42, 59, 75, and 89 at.% Au courtesy of [126]

Savan's theory was further backed up in numerous studies [69, 129-131], which showed that Au-doped MoS_2 outperformed pure sputtered MoS_2 coatings in ambient conditions, with lower coefficients of friction and "higher frictional stability" [129] as outlined in Figure 2.19 where MoS_2 doped with 5 at.% of Au displayed lower coefficients of friction and fewer frictional fluctuations during sliding when compared with pure a pure MoS_2 coating.

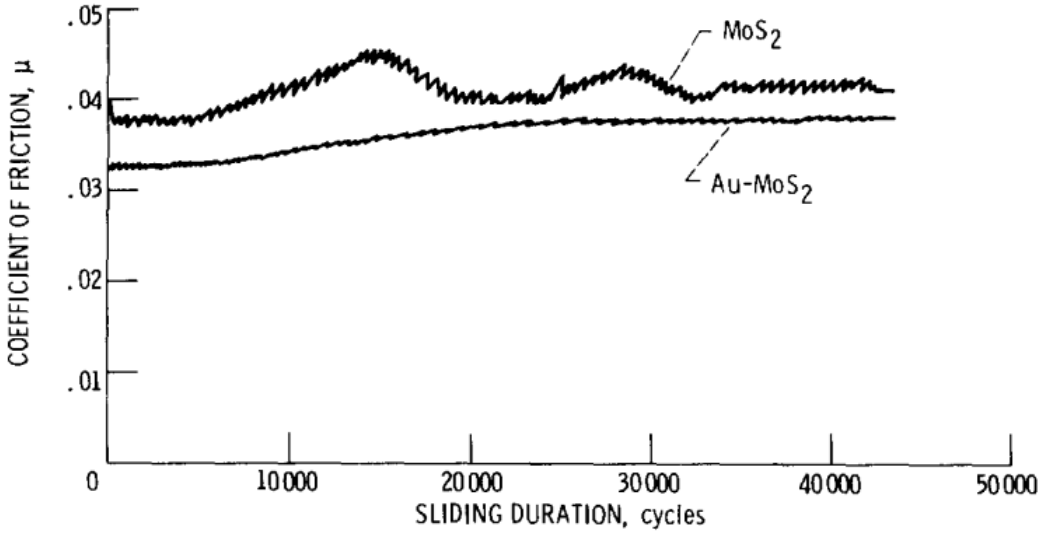

Figure 2.19 Coefficient of friction of 5 at% Au doped MoS_2 compared with pure MoS_2.

Zabinski et al. [130] explored how multiple dopants, including Fe, Ni, Au and Sb_2O_3, affected the chemistry, crystallinity and tribological performance of MoS_2 coatings. The results showed that dopants that led to increased tribological performance were due to increasing the crystallite size of the coating and increasing the coating density. The coefficient of friction results are presented in Table 2-1.

Table 2-1 Coefficient of Friction, μ, in dry N_2/air adapted from [130]

Coating ID	Coefficient of friction, μ in air/N_2
MoS_2	0.25/0.05
Ni	Fail/0.02
Fe	0.25/0.02
Au	0.12/0.02
Sb_2O_3	0.08/0.01
Sb_2O_3/Au	0.06/0.02

One dopant that shows particular promise for reducing the environmental sensitivity of MoS_2 coating is Ti. With significant bodies of research coming from Teer/MIBA UK on their trademarked material MoST^{TM} [123-125, 132-135]. The inclusion of titanium in the MoS_2 coating increases the hardness and wear resistance of the coatings; this is outlined in durability tests carried out by Bellido-González et al. [125], where MoST coatings were deposited onto AISI M42 tool steel and pin on disc tribometer tests were carried out between 30-40% RH.

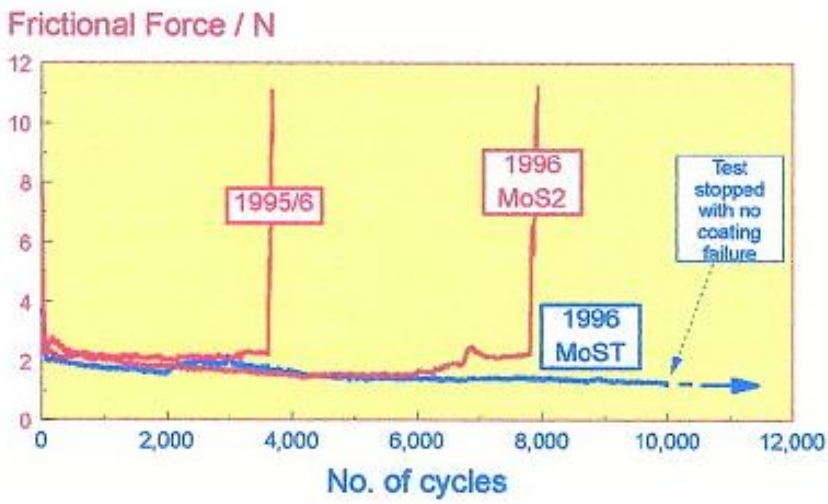

Figure 2.20 Tribological testing comparing durability of MoS_2 and MoST courtesy of [125]

Wang et al. [123] explored how differing Ti contents in the MoS_2 film affected the mechanical and tribological properties of the coating. MoSt Composite coatings were deposited using Teer's Close Field Unbalanced Magnetron Sputtering Ion Plating (CFUBMSIP) system [136] onto AISI M42 Tool Steel and Si substrates with Ti contents of 0 .at%, 15.3 at.% and 19.5 at.%. Using X-Ray diffraction (XRD), they showed that the coating became more crystalline with higher Ti content. Furthermore, the coatings' hardness increased with increasing Ti content, as highlighted in Figure 2.21 and the coefficient of friction, when tested in a humid environment, is also much lower, as shown in Figure 2.22.

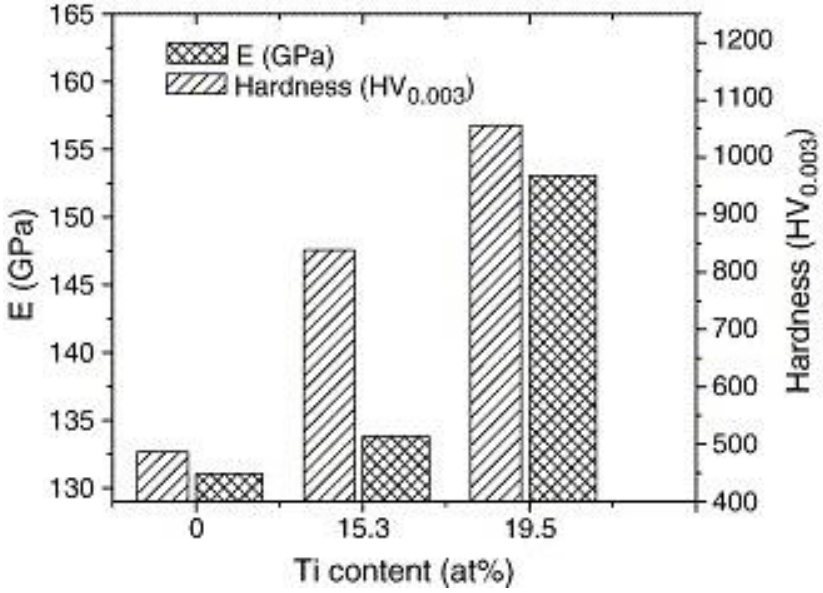

Figure 2.21 Hardness and elastic modulus of MoST coatings with different Ti content [123].

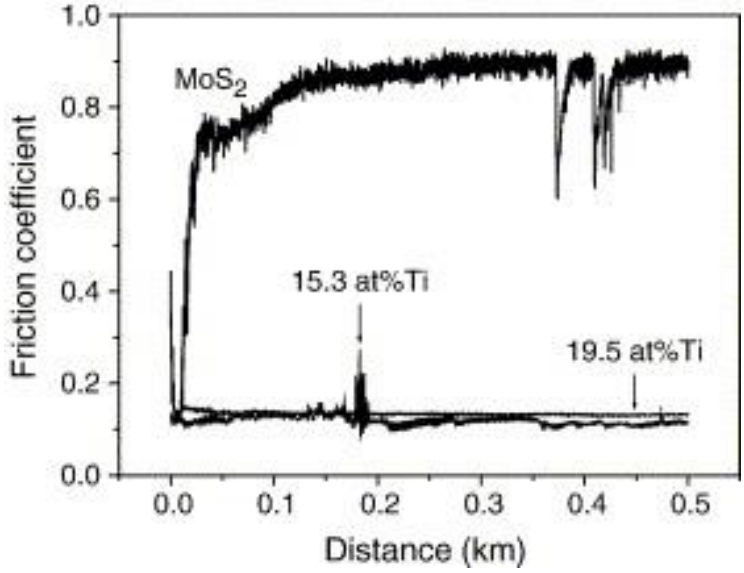

Figure 2.22 Tribological results for the MoST coatings with different titanium content at 10 N load, 25 °C and 38% humidity.

2.11 Raman spectroscopy for MoS_2, MoO_2 MoO_3 and MoS_xO_y

2.11.1 Raman spectroscopy of MoS2

When MoS_2 is stimulated with electromagnetic waves, under ambient conditions, the Mo and S atoms undergo both in plane and out of plane vibration leading to Raman scattering and a Raman Shift. The first order Raman modes are the; E_{2g}^2 with a peak position of ~34cm^{-1}, E_{1g}

at ~287 cm^{-1}, E_{2g}^{1} at ~383 cm^{-1} and A_{1g} at ~409 cm^{-1} [137]. The E_{2g}^{2} and E_{2g}^{1} modes involve vibrations of both the Mo and the S atoms. However, only the S Atom vibrates in the E_{1g} mode. In the A_{1g} mode, the S atoms vibrate away from the Mo atoms in the MoS_2 layer, and is therefore an out of plane vibration.

The in plane vibration of the E_{2g}^{2} adjacent to the MoS_2 layers has the lowest intensity of the first order vibrational modes. The E_{1g} mode also has a relatively low intensity vibration. However, it is susceptible to laser polarisation in the incident plane. If this happens, then it leads to a higher intensity vibration [138].

The two most prominent modes, with the highest peak intensities of the first order Raman modes, are the E_{2g}^{1} and A_{1g} modes. This is outlined in Figure 2.23. This figure also highlights the in plane and out of plane vibration of the two modes.

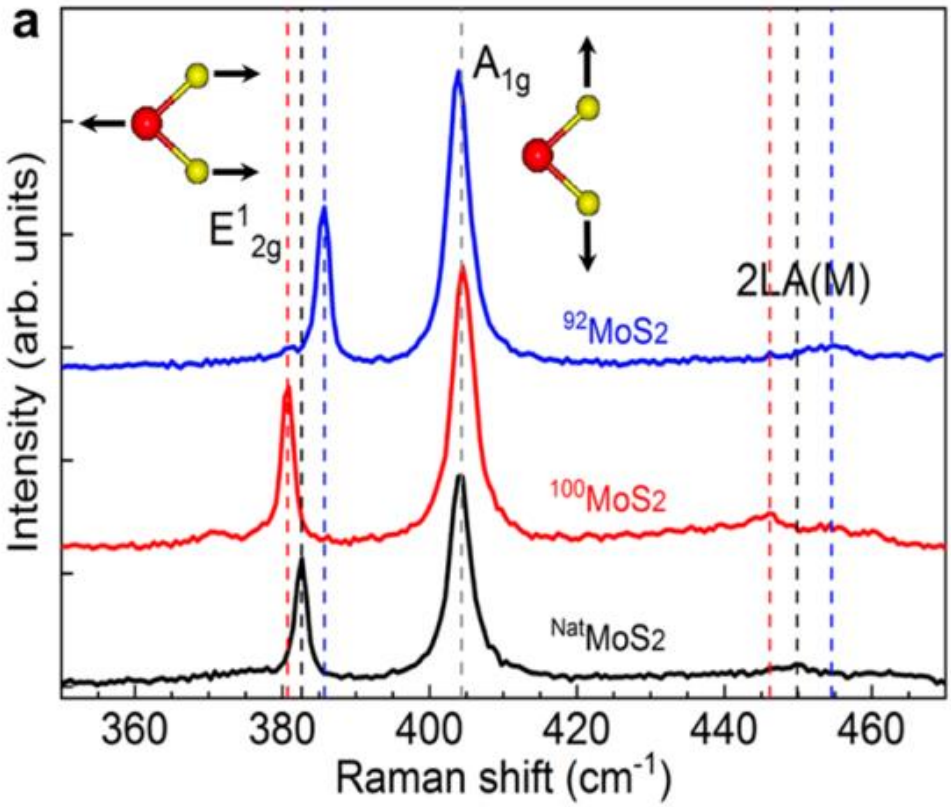

Figure 2.23 Representative example of an MoS_2 Raman spectra, highlighting the E^1_{2g} and A_{1g} peaks.

2.12 Summary

MoS2 coatings are known for their excellent performance in dry and inert atmospheres, but their lubricious qualities are affected when exposed to humid environments. The literature suggests that the presence of water and oxygen affects the easy basal shear of the

lamellae in MoS_2 coatings, leading to reduced lubricity and wear life. However, there are discrepancies and contradictory results in the literature regarding the exact mechanisms behind this degradation. Some studies propose that oxidation in the coatings restricts basal layer sliding, while others refute this claim, stating that water is the overriding component adversely affecting friction at room temperature. There are also limited data on the effects of water and oxygen together on the lubricious qualities of MoS_2 coatings. Overall, the literature shows that MoS_2 displays poor lubricious qualities in humid air, but there is no consensus on the mechanisms behind this. The gaps in the literature include the need for more studies on the effects of water and oxygen together, and the need for more conclusive evidence on the exact mechanisms behind the degradation of lubricity in MoS_2 coatings in humid environments.

3. Chapter Three Experimental Methodology

3.1 Introduction

This chapter outlines the main experimental procedures undertaken in this work and explains the function of the equipment used. Tribological analysis of MoS_2 in sliding was used to measure the lubricious performance, Raman spectroscopy measured changes to bonding and oxidation state and TEM and EDX were utilised to observe structural and chemical changes respectively. The tribological and chemical analysis in the project is split into three different testing protocols. The first testing protocol explores how changes in the testing environment affect the coating. The second testing protocol explores how differing ageing environments affect the coating. And the final protocol explores how the stop-start sliding characteristics of MoS_2 are affected in different environments. Preparation of samples, environmental conditions, tribological procedures, surface analysis techniques and material characterisation are all outlined in this chapter.

3.2 Experimental materials and sample preparation

In this study, all samples consisted of an AISI 440C stainless steel substrate discs with an outer diameter (OD) of 10 mm and were

polished to an average surface finish of R_a = 200 nm. The steel discs were deposited with a commercially obtained (Miba UK), high purity (>99%) MoS_2 coating was magnetron sputter deposited via PVD to a nominal thickness of 1 μm. Prior to deposition, samples were ultrasonically cleaned in a solvent solution, followed by surface ion bombardment, to ensure the absence of contamination, and to aid coating adhesion. The tribological counter sample used in all tests was an uncoated 3 mm AISI 440C stainless steel ball bearing (simply bearings, UK).

3.3 Environmental control

A custom-built gas humidifier outlined in Figure 3.1 was used to control the relative humidity in the tribological testing environment and in the ageing chambers. A dry gas source consisting of either N_2 or $N_2 + O_2$ was passed through a desiccant chamber, following this, the dry gas source was split into two branches, both containing flow meters. One of the branches passed through a gas bubbler, containing deionised water in order to humidify that branch of the gas source. The other branch remained dry, before re-joining the 'wet' branch and arriving in the environmental chamber. The humidity of the outlet gas into the chamber could be controlled by adjusting the flow meters, and

was measured using a hygrometer (Traceable Hygrometer, Fischer Scientific, UK).

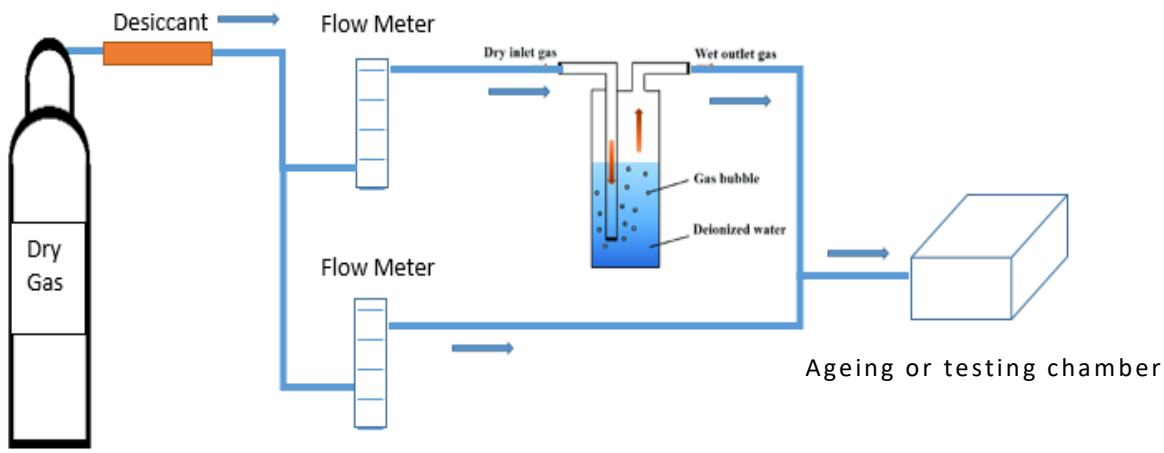

Figure 3.1 Gas humidifier.

During tribological testing, a continuous gas stream of the desired composition and humidity was passed over the sample to ensure a stable constant testing environment. In order to explore how the storage environment affected the coating, the MoS_2 coated samples were aged in six different environments of varying gas and humidity makeup. These environments were either nitrogen or air, and at 0, 25 and 50% RH in each gas outlined in Table 3-1.

Table 3-1 Ageing environments.

	GASEOUS ENVIRONMENT	
RELATIVE HUMIDITY	Air	Nitrogen
0	$O_2 + N_2$	N_2
25	$O_2 + N_2 + H_2O$	$N_2 + H_2O$
50	$O_2 + N_2 + H_2O$	$N_2 + H_2O$

To ensure the samples remained in the intended environment for the duration of the ageing period, they were placed into hermetically sealed chambers (Sure Seal hermetic chamber, WPI instruments, UK) shown in Figure 3.2. The chambers had gas inlet and outlet fittings to which gas lock off taps were fitted. The humidifier described above was used to achieve the desired humidity within the chamber. Both the inlet and outlet gas lock off taps were kept open while the chambers were purged, and the environment within the chamber was monitored using the probe arrangement listed above. Once the desired humidity

level was achieved, the chamber taps were then locked off simultaneously.

Figure 3.2 Ageing chamber with hermetical seal.

3.4 Tribological testing

Tribological testing consisting of reciprocal sliding of a ball contacting on a flat surface was carried out using a micro-tribometer (NTR_3, Anton Paar, CH) which has a normal force resolution of 0.003 μN, and a friction force resolution of 0.006 μN for highly accurate tribological measurements. The NTR_3 is a Linear reciprocating tribometer, which uses the displacement of stiff calibrated can cantilevers, measured via capacitance probes, to obtain friction forces (F_t) under a given normal load (F_n) via piezo controlled actuation (including sliding) outlined in Figure 3.3. The cantilevers used on the NTR3 are dual quad-beam force cantilevers, designed to minimise the error caused by torsional displacement. This is especially important in low load applications such as in this study, where normal spring cantilevers can easily be twisted out of shape by sample topography, which in turn would bring non-negligible errors in friction measurements. Quad beam cantilevers work by allowing elastic deformation in both normal and tangential directions, whilst preventing torsional deformation. The role of tribological testing was to measure the lubricious performance and coefficient of friction of MoS_2 coatings. Three repeats were performed each on different samples to ensure experimental variance did not affect the presented results. A representative example is displayed in the results presented

in this thesis. Error was calculated using maximum variance over the three tests. In a further effort to ensure repeatability of results, all testing was performed at 21± 2 °C. Steady state friction was defined as remaining within a ±5% range of COF for 100 cycles all samples display steady state friction over the final 300 cycles, therefore steady state values presented in the results are an average of the final 300 cycles of sliding.

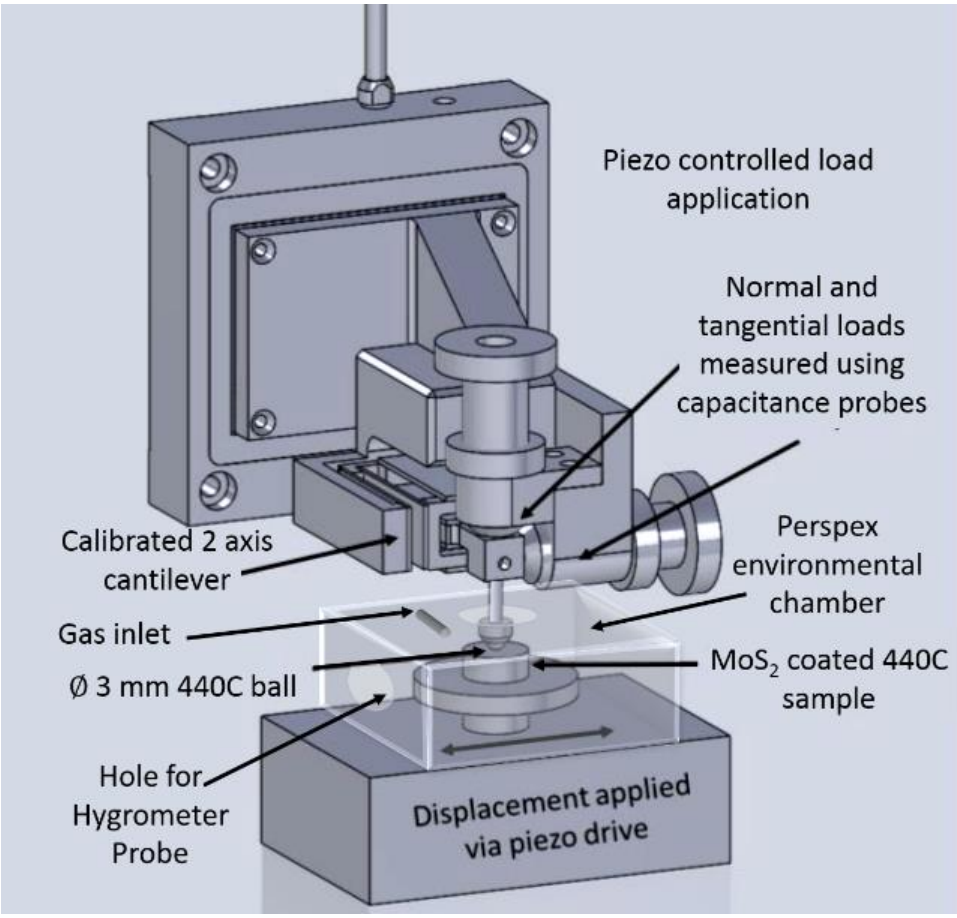

Figure 3.3 Schematic of Anton Paar NTR$_3$ Tribometer with custom local atmospheric chamber.

3.4.1 Tribological testing in different environments.

Coated samples returned from Miba, UK were vacuum packed with a desiccant to ensure no environmental degradation of the coatings took place. In addition to this, prior to tribological testing or aging, all samples were kept under vacuum with a desiccant in a vacuum chamber. Tribological testing was split into two testing streams: changing sliding environment, or changing storage environment. The same environments were used in both testing streams, outlined in Table 3-2, so that the impacts caused by the sliding environment, were clearly identifiable from the impact of the storage environment.

Table 3-2 Testing and storage environments.

	GASEOUS ENVIRONMENT	
RELATIVE HUMIDITY (%)	Air	Nitrogen
0	$O_2 + N_2$	N_2
25	$O_2 + N_2 + H_2O$	$N_2 + H_2O$
50	$O_2 + N_2 + H_2O$	$N_2 + H_2O$

For the aged samples all sliding was performed in a dry nitrogen environment. Tribological testing was carried out on aged samples at weekly time intervals after one, two and three weeks. Both the sliding and storage environments were established with a custom environmental cell with an integrated hygrometer as previously outlined. To ensure the environment is fully established and stable before the test, once the environment had met the required humidity, a period of five minutes was allotted with constant hygrometer monitoring before either sliding or sealing the storage environment. The hygrometer was then monitored every 60s during the sliding tests to ensure the humidity did not stray out of range of ± 1% RH for the duration of the test. The normal force applied was at F_n = 100 mN, with a stroke amplitude of 1 mm and a frequency of 0.5 Hz for a total of 1500 cycles. The data was captured at a rate of 400Hz and at each

point, total sliding distance, cycle number, X position, normal force, transitional force and coefficient of friction was recorded. The coefficient of friction per cycle, μ, was calculated by taking the taking an average of the forward and reverse friction forces within the middle 50% of each cycle. The testing protocol outlining the sliding and aging environments is outlined in Table 3-3. The aim of this testing was to establish the impact that water and oxygen had on the lubricious performance of MoS_2 coatings both in the sliding environment and in the storage environment.

Table 3-3 Tribology testing protocol

Test	Ageing environment	Ageing time (weeks)	Sliding environment
1	N/A	0	0% RH N_2
2	N/A	0	25% RH N_2
3	N/A	0	50% RH N_2
4	N/A	0	0% RH air
5	N/A	0	25% RH air
6	N/A	0	50% RH air
7	0% RH N_2	1	0% RH N_2
8	25% RH N_2	1	0% RH N_2
9	50% RH N_2	1	0% RH N_2
10	0% RH air	1	0% RH N_2
11	25% RH air	1	0% RH N_2
12	50% RH air	1	0% RH N_2

13	0% RH N_2	2	0% RH N_2
14	25% RH N_2	2	0% RH N_2
15	50% RH N_2	2	0% RH N_2
16	0% RH air	2	0% RH N_2
17	25% RH air	2	0% RH N_2
18	50% RH air	2	0% RH N_2
19	0% RH N_2	3	0% RH N_2
20	25% RH N_2	3	0% RH N_2
21	50% RH N_2	3	0% RH N_2
22	0% RH air	3	0% RH N_2
23	25% RH air	3	0% RH N_2
24	50% RH air	3	0% RH N_2

3.5 Raman spectroscopy

Raman spectroscopy was carried out using an InVia spectrometer (Renishaw, UK) to observe if any changes in the chemical composition had occurred. A Raman laser with a 488 nm wavelength and a low laser power of 1mW was used to ensure that no laser induced oxidation of the coating took place. Samples were analysed using a short distance 50x objective. This gave a laser spot size of 400 nm. Measurements were taken inside and outside of the wear scar on both aged and unaged samples so that the effects of ageing alone and ageing alongside tribology could be seen. Intensity data was normalised between 0 and 1 so spectra could be compared.

Table 3-4 Raman peak assignment

Raman Peak (cm^{-1})	Assignment
287, 383, 409	MoS_2
202, 227, 363, 489, 565, 728	MoO_2
197, 819	MoO_3

3.6 Scanning electron microscopy and energy dispersive X-Ray spectroscopy

Scanning Electron Microscopy with integrated Energy Dispersive Spectroscopy (SEM-EDS) on a Carl Zeiss EVOMA15: variable pressure SEM with an Oxford Instruments AZtecEnergy EDX System was used to observe the elemental changes on the coatings after ageing and tribology testing. The integrated EDS detector was then used to detect the atomic composition of the coating. The SEM-EDS analysis was focused around the wear scar to observe changes at the sliding interface. SEM scans were taken at an accelerating energy of 5 keV. The low electron energy was used to reduce bulk material interaction, as coatings were only 1 μm thick. The elemental composition of the coated surfaces was mapped, enabling the spatial distribution of elements to be resolved. Particular attention was drawn to the

presences of molybdenum, sulphur and oxygen. The sampling depth of the electron beam was calculated to be 0.2 m with [139]:

Equation 3-1

$$\boldsymbol{x(\mu m) = \frac{0.1E^{1.5}}{\rho}}$$

Where E is the accelerating voltage in keV and ρ is the density in $g \cdot m^{-3}$.

Figure 3.4 Carl Zeiss EVOMA15: variable pressure Scanning Electron Microscope with an Oxford Instruments Aztec Energy, Energy Dispersive X-ray spectroscopy System

3.7 Focused ion beam sample preparation

Focused Ion Beam (FIB) on an FEI Helios G4 CX DualBeam, was used to prepare wafer thin samples to be analysed on a transmission electron microscope (TEM). Samples were initially Ir coated to prevent charging during TEM wafer section collection. Following this a primary protective Pt layer (≈200–300 nm) was deposited over the area of sample collection using an electron beam. Then, a further Pt layer was deposited using a Ga+ ion beam. Next, material from either side of the protective Pt was milled away to an approximate depth of

10μm using an ion beam at 30 kV. Further thinning of this section was performed using the ion beam, before being partially cut free from the bulk material. The milled section was then removed using a Kleindiek micromanipulator, before being mounted inside the chamber of the microscope and attached to a Cu TEM grid by way of Pt deposition. Ga+ ions continued to be used to further thin the section to produce electron transparent sections see Figure 3.5. Two windows were milled on each sample. The first of which had a nominal thickness of 20-30 nm. The second window was thinned further to around 10-15 nm. The thicker window was produced as a precaution, in case the thinner of the windows failed, or collapsed during transportation between the FIB and the TEM.

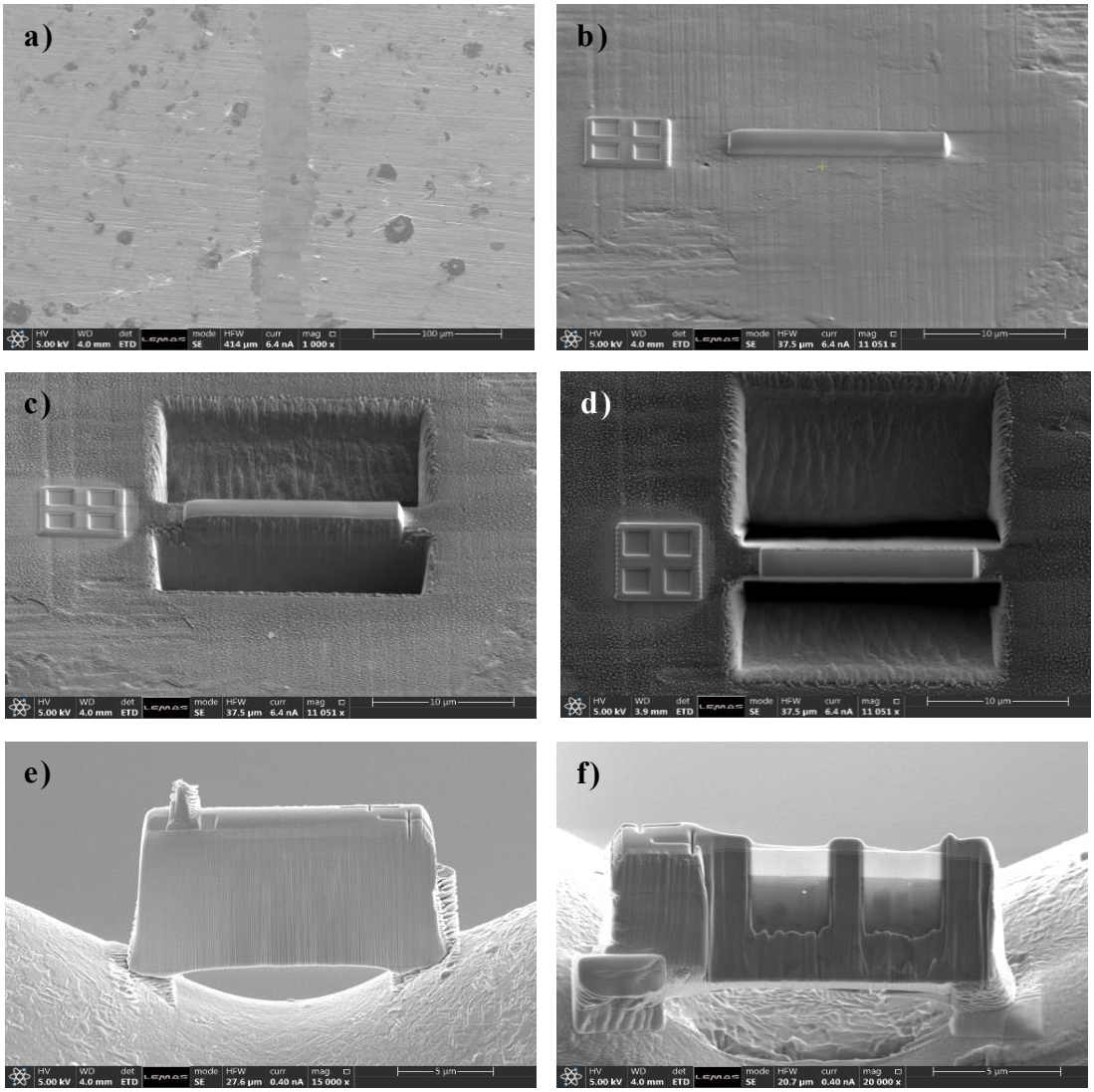

Figure 3.5 FIB sample preparation a) Wear scar prior to TEM section preparation. b) After the protective Pt layer has been deposited. c) After either side of the TEM section is milled away. d) After either side of the TEM section is milled away – top view. e) After the TEM section is removed from the bulk sample and attached to a Cu TEM grid. f) after section thinning to produce two electron transparent 'windows'

3.8 Transmission electron microscopy

Transmission Electron Microscopy (TEM) is a microscopy technique that utilises a beam of electrons, that transmits through an ultra-thin (<100 nm) specimen. The electron beam interacts with the specimen as it passes through, scattering the electrons, before they impact on a detector, producing an image outlined in Figure 3.6.

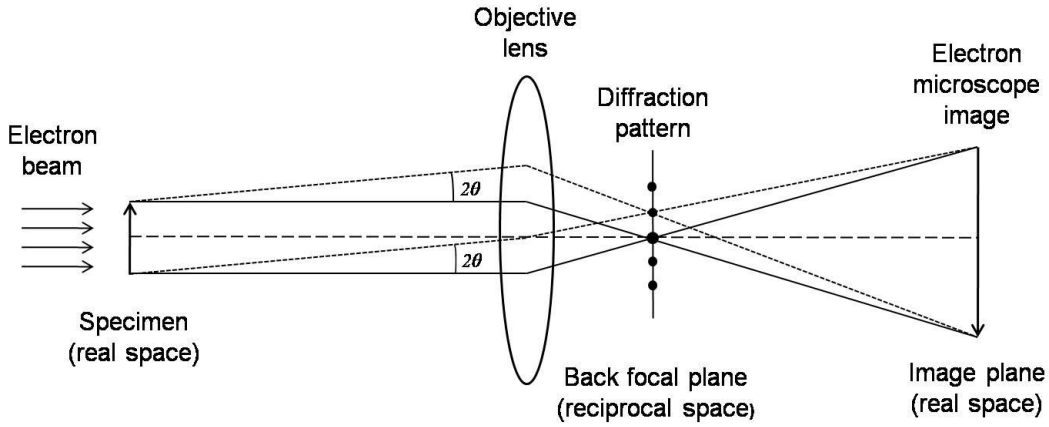

Figure 3.6 The optical electron beam diagram of TEM

An FEI Titan Themis Cubed 300 TEM was utilised at an electron voltage of 300kV and a magnification of 185kx to observe changes in the lattice structure and orientation of crystallites. Images were taken along the wear scar interface to observe lamellar orientation. Typical interlamellar spacing between MoS_2 lamellae ranges from 6.2-10 angstrom [140].

4. Chapter Four Effect of Water and Oxygen in the Testing Environment on the Lubricity of MoS_2 Coatings

4.1 Introduction

The aim of this chapter was to outline the effect that water and oxygen have on the tribological performance of MoS_2 coatings and explore the impact these species have both independently, and in synergy. The results displayed in this chapter are from unaged MoS_2 coatings that underwent sliding in nitrogen or air containing environments, at relative humidity levels of 0%, 25% and 50%. Post sliding analysis was then carried out using white light interferometry, SEM, EDX, Raman spectroscopy and TEM; to investigate the mechanical, bonding and chemical changes that occurred as a result.

4.2 Tribology results

The average coefficients of friction of as deposited, unaged, MoS_2 coatings tested in either nitrogen or air at 0, 25 and 50% relative humidity (RH) are displayed in

Figure 4.1a) and b), respectively. The friction coefficient increases drastically when humidity is increased, and steady-state coefficient of

friction is more than 2.5x higher at 50% relative humidity when compared with samples tested in a dry gas environment. Coefficient of friction is also higher in atmospheric oxygen containing environments, compared with nitrogen environments, with like levels of humidity.

The characteristics of friction over time differ considerably in dry and humid environments. In all environments tested, the coefficient of friction initially drops rapidly before hitting a minimum point. In dry environments, the coefficient of friction only rises a small amount. However, the friction response in humid environments displays a sharp rise immediately after the minimum coefficient of friction, before getting to steady state after some time.

Figure 4.1c) displays the steady state coefficients of friction in each environment. The values for the minimum coefficient of friction and steady state coefficient of friction are outlined in

Table 4-1 below.

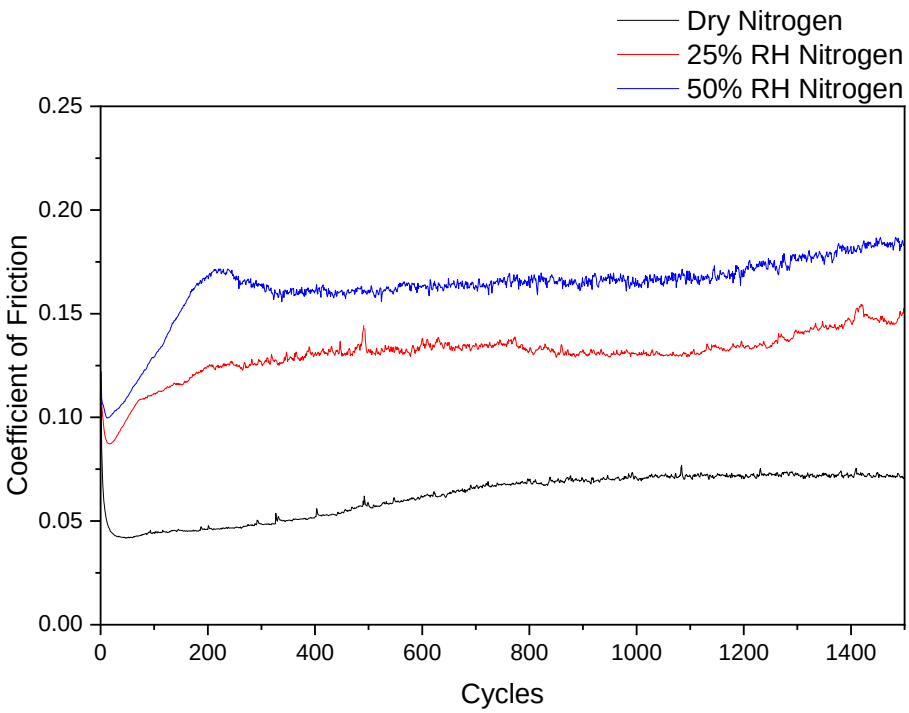
Dry Nitrogen
25% RH Nitrogen
50% RH Nitrogen
Coefficient of Friction
0.25
0.20
0.15
0.10
0.05
0.00
0
200
400
600
800
1000
1200
1400
Cycles

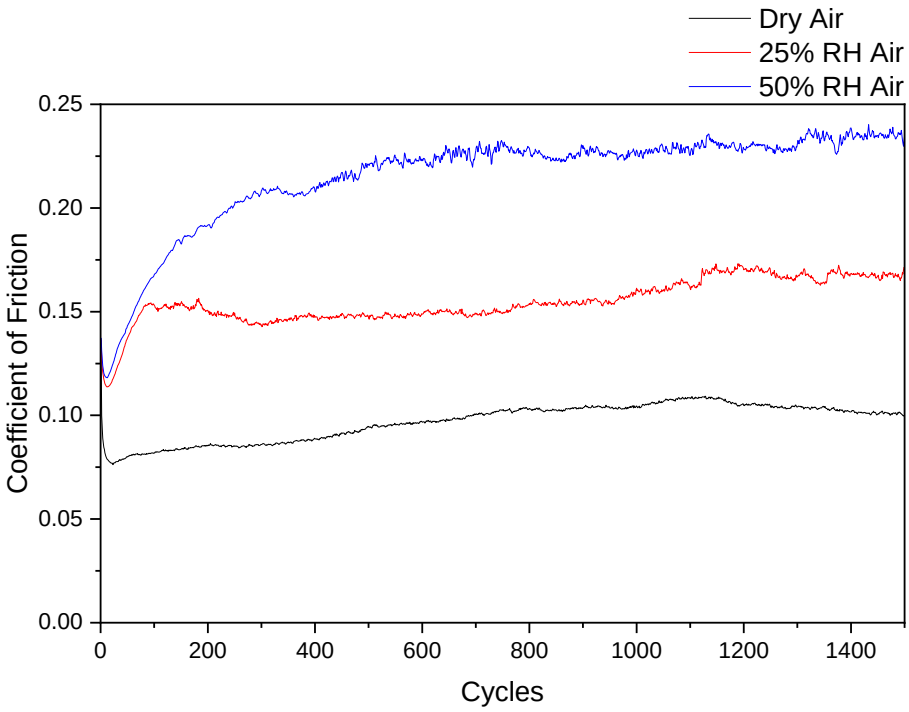
Dry Air
25% RH Air
50% RH Air
Coefficient of Friction
0.25
0.20
0.15
0.10
0.05
0.00
0
200
400
600
800
1000
1200
1400
Cycles

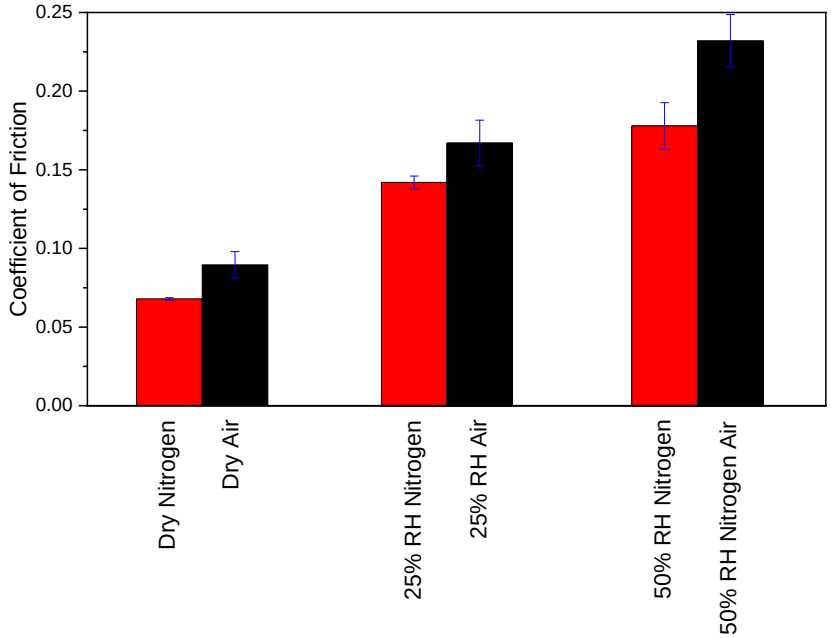

Figure 4.1 a) Unaged MoS_2 sample tested in dry, 25% and 50% RH N_2 for 1500 cycles. b) Unaged MoS_2 sample tested in dry, 25% and 50% RH air for 1500 cycles. c) Comparison of the steady state coefficient of friction of one week aged MoS_2 coatings.

Table 4-1 comparison of minimum and steady state coefficient of friction for each testing environment.

Testing Environment	Minimum coefficient of friction, μ	Steady state coefficient of friction, μ
Dry N_2	0.042	0.068
Dry air	0.077	0.090
25% RH N_2	0.087	0.143
25% RH air	0.114	0.168
50% RH N_2	0.100	0.178
50% RH air	0.118	0.233

4.3 White light interferometry

Figure 4.2a-c) shows white light interferometry results of the wear scars for samples that underwent sliding in dry, 25% RH and 50% RH N_2, respectively. Due to the surface topography of the samples, wear volume is difficult to estimate, however it can be seen that wear is

well within the realms of the coating on all samples. There is some asperity shearing and smoothing visible in the wear scar. Line scans were taken inside and outside of the wear volume to give roughness values of; Dry N_2, Ra = 64 nm and Ra_{ws} = 27.6 nm 25% RH N_2, Ra = 67 nm and Ra_{ws} = 26.1 nm and 50% RH N_2, Ra = 78 nm and Ra_{ws} = 28.9 nm.

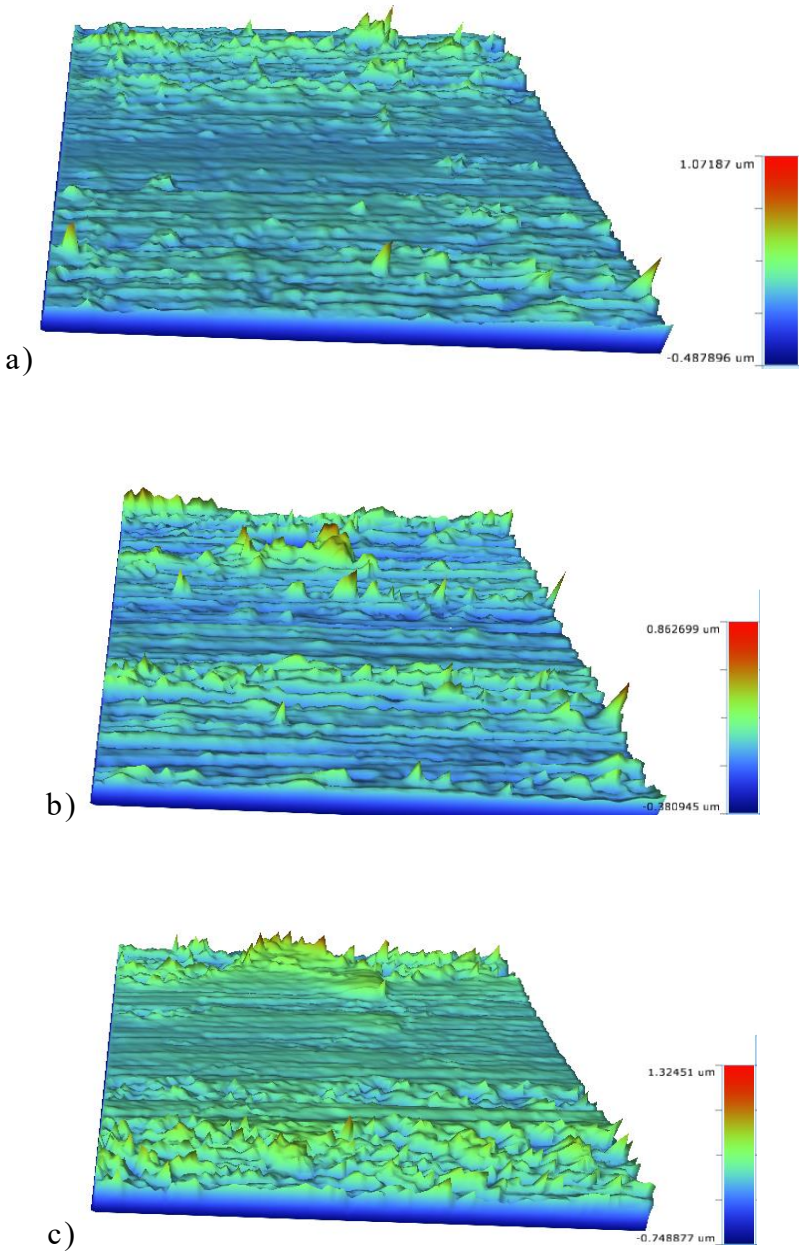

Figure 4.2 white light interferometry results taken around the wear scar after sliding of unaged MoS_2 in a) dry N_2, b) 25% RH N_2 and c) 50% RH N_2

Figure 4.2a-c) shows white light interferometry results of the wear scars for samples that underwent sliding in dry, 25% RH and 50% RH air, respectively. Wear volume has not been estimated, however, it can be seen that wear is well within the realms of the coating on all samples. The asperity shearing and smoothing of the samples in the wear scar is more prominent in the humid air aged samples. Especially at 50% RH air. Line scans were taken inside and outside of the wear volume to give roughness values of; Dry air, Ra = 53 nm and Ra_{ws} = 49.1 nm, 25% RH air, Ra = 71.3 nm and Ra_{ws} = 47.6 nm and 50% RH air, Ra = 98 nm and Ra_{ws} = 23.1 nm. Wear depth outlined in Table 4-2

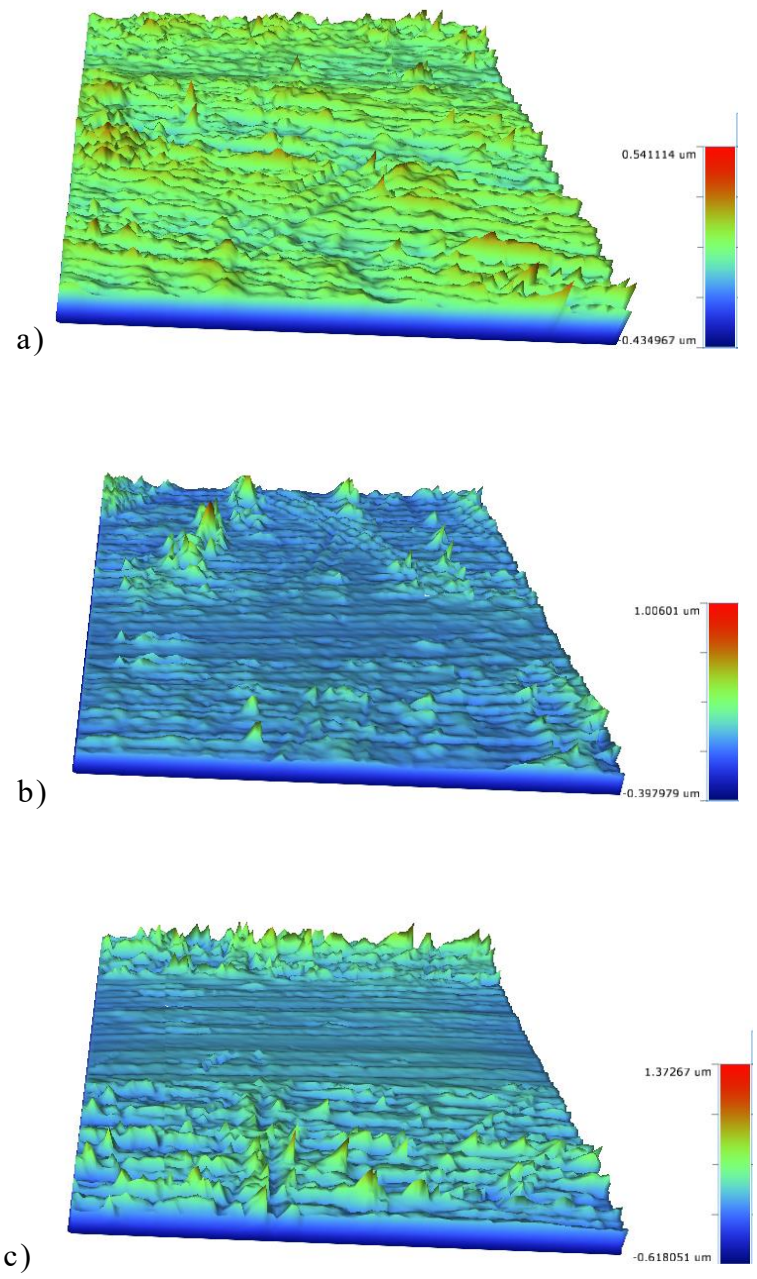

Figure 4.3 white light interferometry results taken around the wear scar after sliding of unaged MoS_2 in a) dry N_2, b) 25% RH N_2 and c) 50% RH N_2

Table 4-2 Wear depth for unaged MoS_2

	Nitrogen	Air
0% RH	0.101 μm	0.223 μm
25% RH	0.203 μm	0.301 μm
50% RH	0.452 μm	0.513 μm

4.4 Raman spectroscopy

MoS_2 has four prominent first order modes of vibration; E_{2g}^2 with a peak position of ~34cm^{-1}, E_{1g} at ~287 cm^{-1}, E_{2g}^1 at ~383 cm^{-1} and A_{1g} at ~409 cm^{-1} [137]. Figure 4.4 and Figure 4.5 show the Raman spectroscopy inside and outside of wear scar on unaged MoS_2 samples that have been tested in dry, 25 and 50% RH N_2 and air, respectively. At all humidity levels, the first order Raman peaks are visible. All peaks for both inside and outside of the wear scar for the dry, 25%

and 50% RH nitrogen tested samples, and air tested samples fall within the same range, indicating no bonding changes due to sliding.

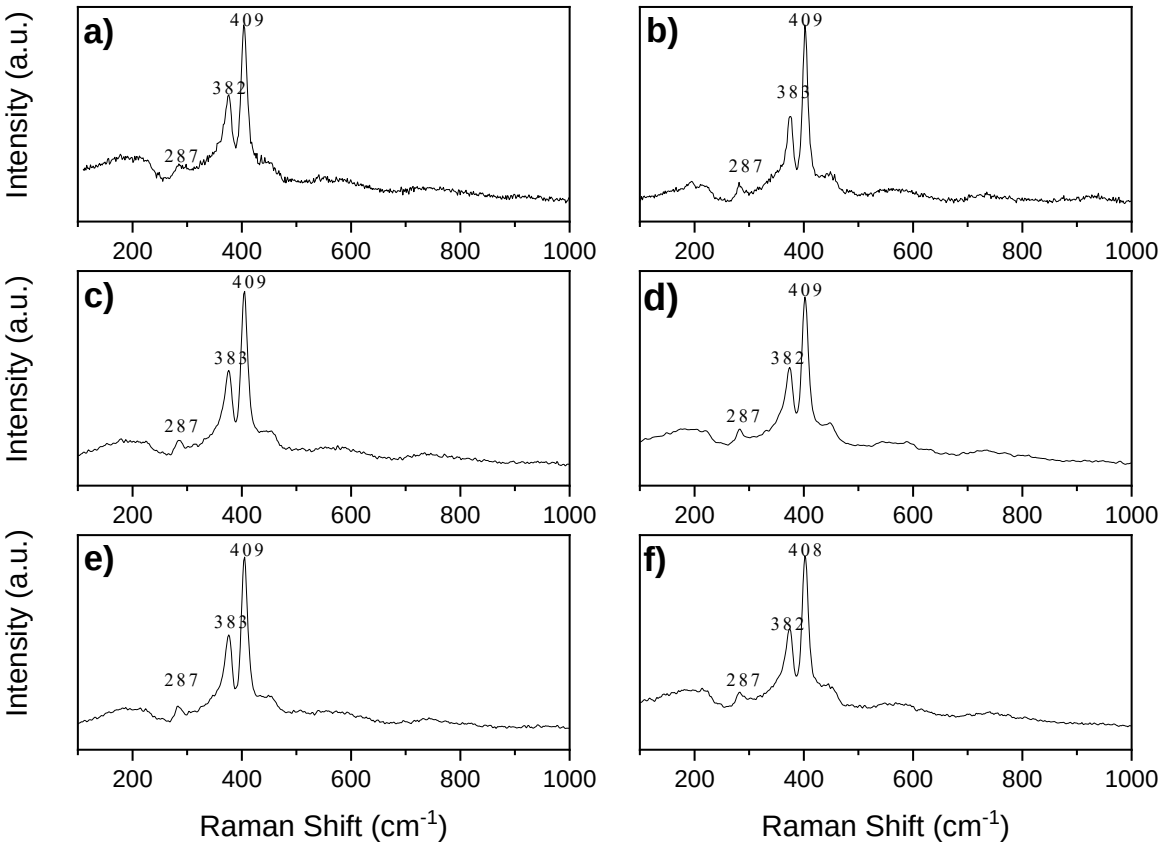

Figure 4.4 Raman spectroscopy unaged MoS_2 a) outside of the wear scar after sliding in dry nitrogen b) inside of the wear scar after sliding in dry nitrogen c) outside of the wear scar after sliding in 25% RH nitrogen d) inside of the wear scar after sliding in 25% RH nitrogen e) outside of the wear scar sliding in 50% RH nitrogen f) inside of the wear scar after sliding in 50% RH nitrogen.

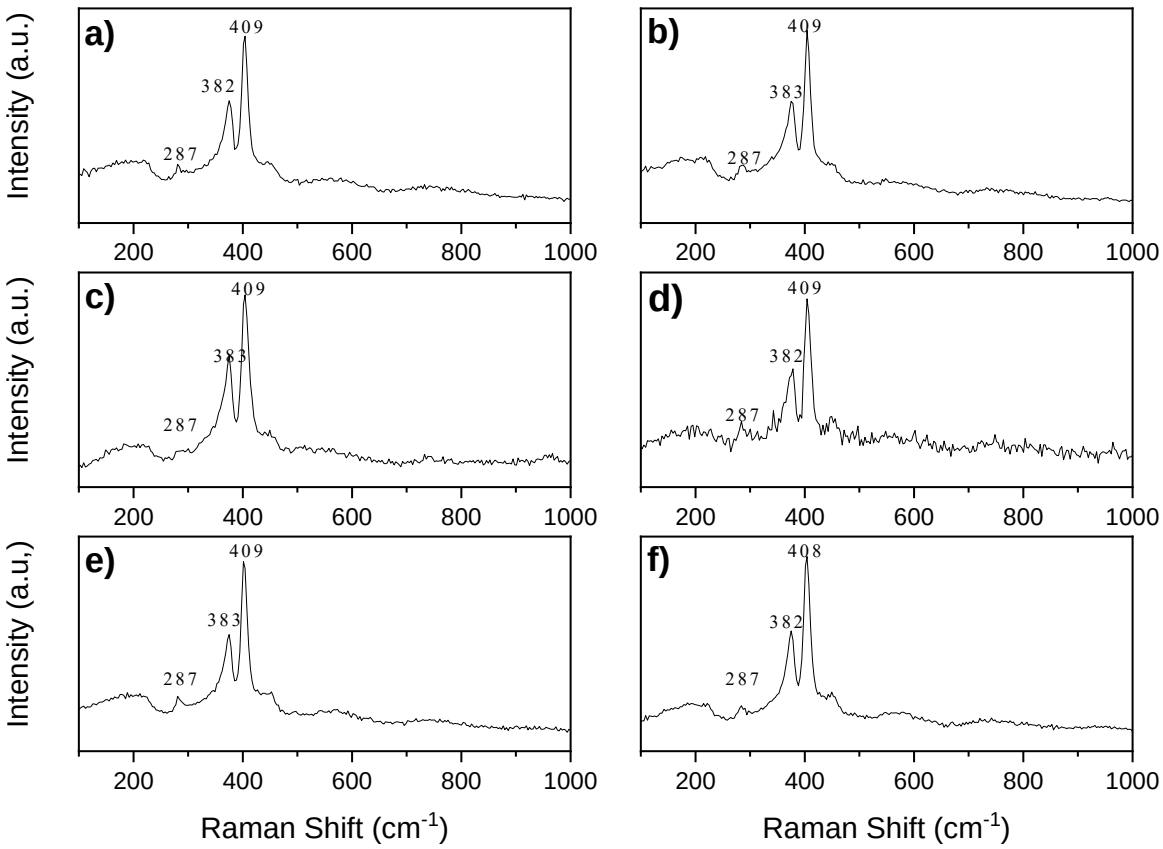

Figure 4.5 Raman spectroscopy unaged MoS_2 a) outside of the wear scar after sliding in dry air b) inside of the wear scar after sliding in dry air c) outside of the wear scar after sliding in 25% RH air d) inside of the wear scar after sliding in 25% RH air e) outside of the wear scar sliding in 50% RH air f) inside of the wear scar after sliding in 50% RH air

4.5 Transmission electron microscopy

The TEM images for unaged samples tested in dry and 50% RH N_2 as well as those tested in dry and 50% RH air are displayed in Figure 4.6 a-d). Where, [A] is the protective Pt, [B] is the iridium layer that was deposited to reduce sample charging, [C] is a carbon layer from previous analysis, [D] is the MoS_2 frictionally transformed region, [E] is the MoS_2 bulk, and the arrows detail the reciprocating sliding direction.

FIB sections were taken inside the wear scar to observe how the structure of the coating was affected by the environment that it was slid in. As can be seen in the dry N_2 tested sample in Figure 4.6 a) the lamellae in the wear portion of the image has a basal orientation parallel to the sliding direction throughout the wear scar. This aligns

well with why the coefficient of friction was lowest in this sample. However, after sliding in dry air, the lamellae in the wear scar were less uniformly aligned as shown in Figure 4.6 b). Although some of the lamellae displayed basal alignment parallel to the sliding direction, large portions of the wear scar exhibit lamellae at around a 45° angle. This less optimal basal alignment resulted in a higher friction coefficient when compared the dry N_2 slid sample. The reduction of basally aligned lamellae also suggests that atmospheric oxygen restricted the crystallographic reorientation of the coating. The sample that was tested in 50% RH air, displayed in Figure 4.6c), showed a lack of basal alignment in the wear scar, but to an even greater extent. Much of the lamellae in the wear scar are near perpendicular with the sliding direction. Thus, leading to significant increases in the coefficient of friction when compared to both the dry N_2 and dry air samples. Therefore showing that water in the sliding environment has a far greater affinity than oxygen alone to restrict preferential basal alignment. Finally Figure 4.6 d) shows the TEM image following 50% RH air sliding. The wear scar exhibits a majority of lamellae perpendicular or near perpendicular with the sliding direction. This led to the highest coefficient of the samples tested. Therefore, showing that water and oxygen together act synergistically in restricting crystallographic reorientation to preferential basally aligned lamellae.

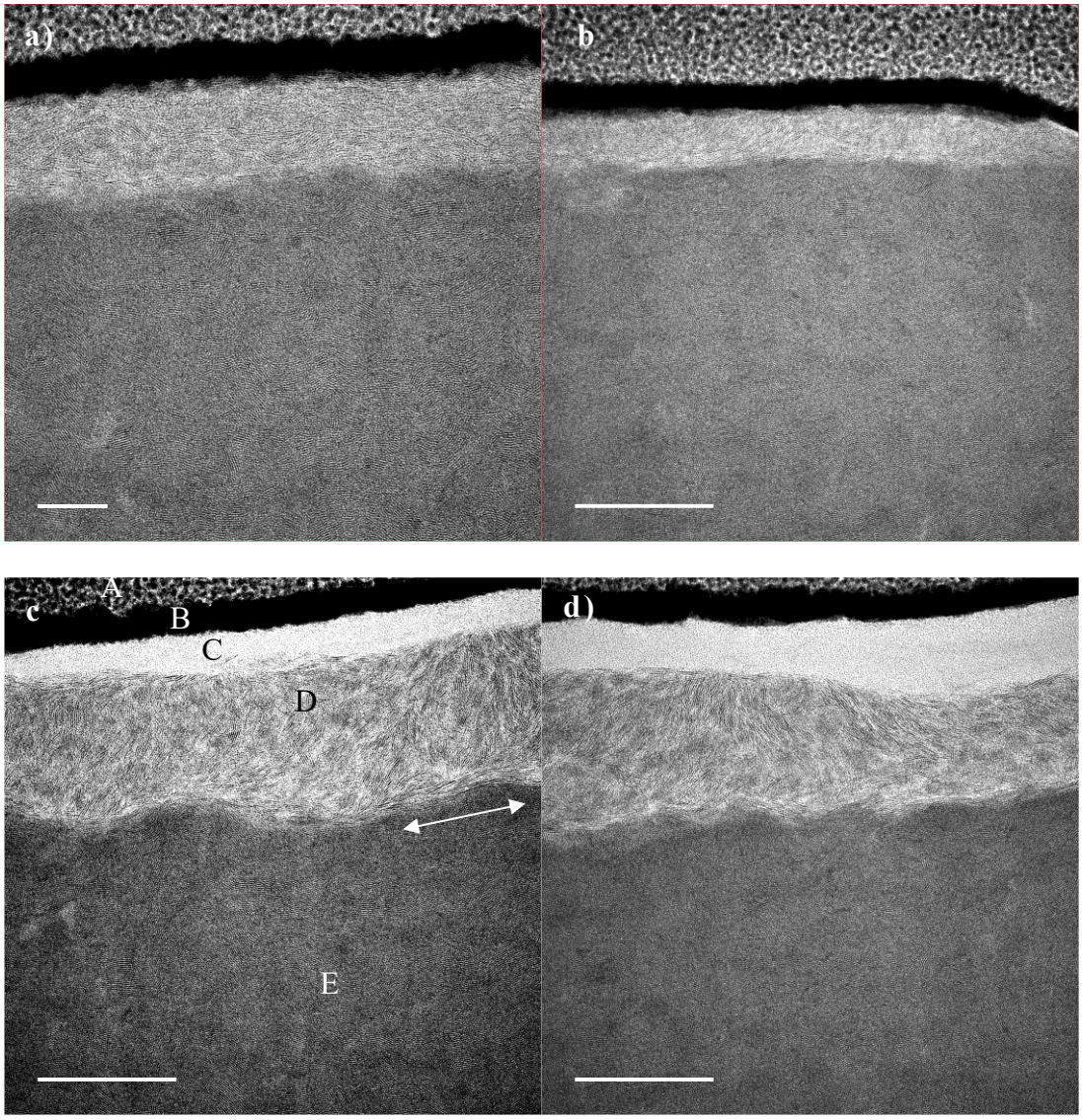

Figure 4.6 TEM of unaged MoS_2 after sliding in: a) dry nitrogen, b) dry air, c) 50% RH Nitrogen and d) 50% RH air.

4.6 Summary

The aim of this chapter was to elucidate the impact the water and oxygen in the sliding environment had on the tribological performance of MoS_2 coatings. Followed by an investigation into chemical and physical changes that may arise due to the environmental factors and the energy input from tribological testing. With a view to gaining an understanding into why water and oxygen degrade MoS_2 during sliding. The results presented in this chapter show:

- Humidity is the most significant driving factor in the increase of coefficient of friction when sliding in ambient environments containing oxygen, water and nitrogen. With a steady state coefficient of friction over 2.5x higher in 50% RH air compared to the dry air counterpart and 3.4x higher compared with sliding in a dry N_2 environment.
- The presence of oxygen in the sliding environment also leads to higher steady state coefficients of friction in all comparable relative humidity levels in the nitrogen slid counterparts.
- TEM showed a restriction of preferential basal reorientation of MoS_2 lamellae, with the most marked restriction coming from the sample after sliding in 50% RH air.

- No observable chemical or bonding changes were detected either inside or outside of the wear scars using Raman spectroscopy after sliding.

These results show that both oxygen and water play a role synergistically in restricting easy lamellar shear of MoS_2, and thus leading to higer coefficients of friction. Furthermore no oxidation was observed in these tests.

5. Chapter Five Effect of Water and Oxygen in the Storage Environment of MoS_2 Coatings

5.1 Introduction

Whilst most studies have focused on the direct tribology-environment interactions, few have examined the role of storage conditions, particularly room storage, on the subsequent friction properties. This chapter explores the medium term effects that the ageing environment have on MoS_2 as a lubricious coating. The results displayed are for samples aged for one to three weeks in either nitrogen or air (O_2 + N_2) with relative humidity (RH) levels ranging from 0-50% RH. Surface and subsurface characterisation of the coatings before and after ageing is also presented.

5.2 Tribology results

5.2.1 One week aged

When comparing the friction coefficients of samples aged at the same levels of relative humidity, but in differing base gasses, there is a clear difference in friction coefficient between the two, as outlined in Figure 5.1 a) and b). A rapid reduction in the coefficient of friction was observed, reaching $\mu = 0.05 \pm 0.01$ within the first 30 cycles for

N_2 aged samples and $\mu = 0.07 \pm 0.02$ for air aged samples. Further analysis showed that the time taken to reach the minimum coefficient of friction was also affected by the ageing environment. Samples aged in a dry N_2 environment, reached a minimum coefficient of friction, $\mu = 0.048$, after 19 cycles of sliding (total distance = 19 mm). This then increased, reaching a steady state coefficient of friction, $\mu = 0.07$. In comparison, samples aged in 25% RH and 50% RH N_2 reached a coefficient of friction of, $\mu = 0.054$ in 55 cycles and $\mu = 0.051$ in 67 cycles, respectively.

Samples aged in air consistently yield higher coefficients of friction throughout the duration of the test than their nitrogen aged counterparts. This is true for all humidity levels explored in this test set. It can also be seen that the gap in the coefficient of friction increases with humidity and that steady-state friction is achieved in fewer cycles in coatings aged in nitrogen compared to coatings aged in air

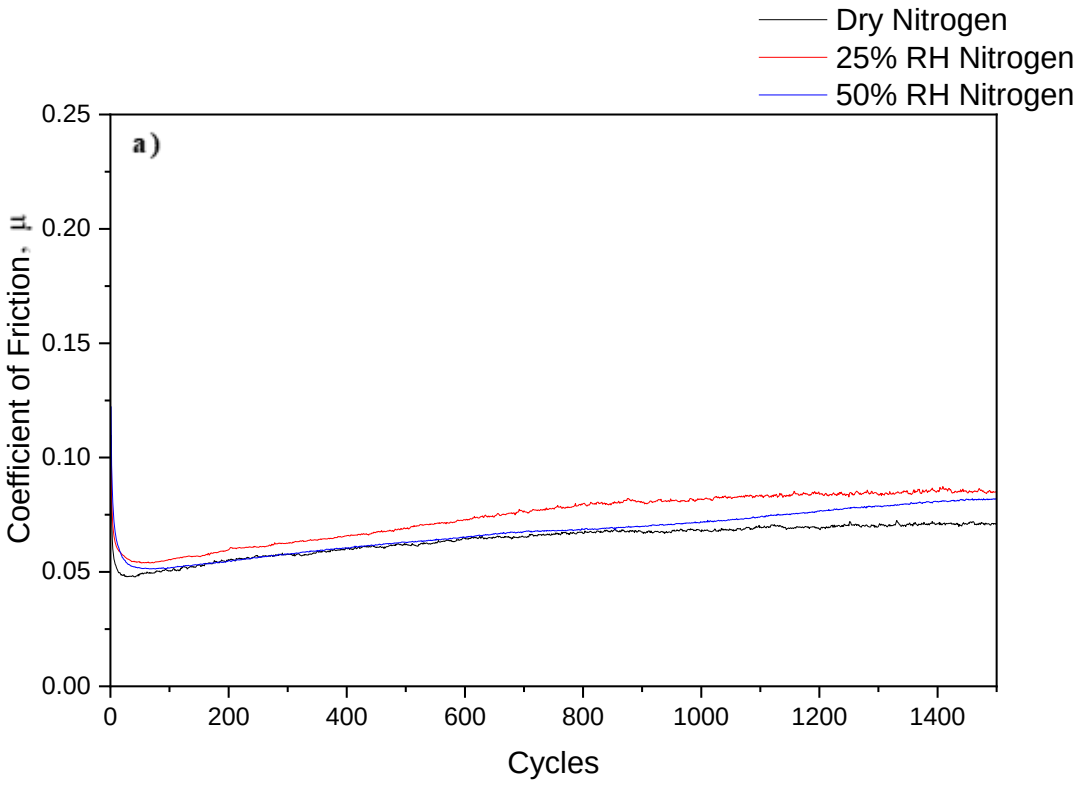
Dry Nitrogen
25% RH Nitrogen
50% RH Nitrogen
a)
Coefficient of Friction, μ
0.25
0.20
0.15
0.10
0.05
0.00
0
200
400
600
800
1000
1200
1400
Cycles

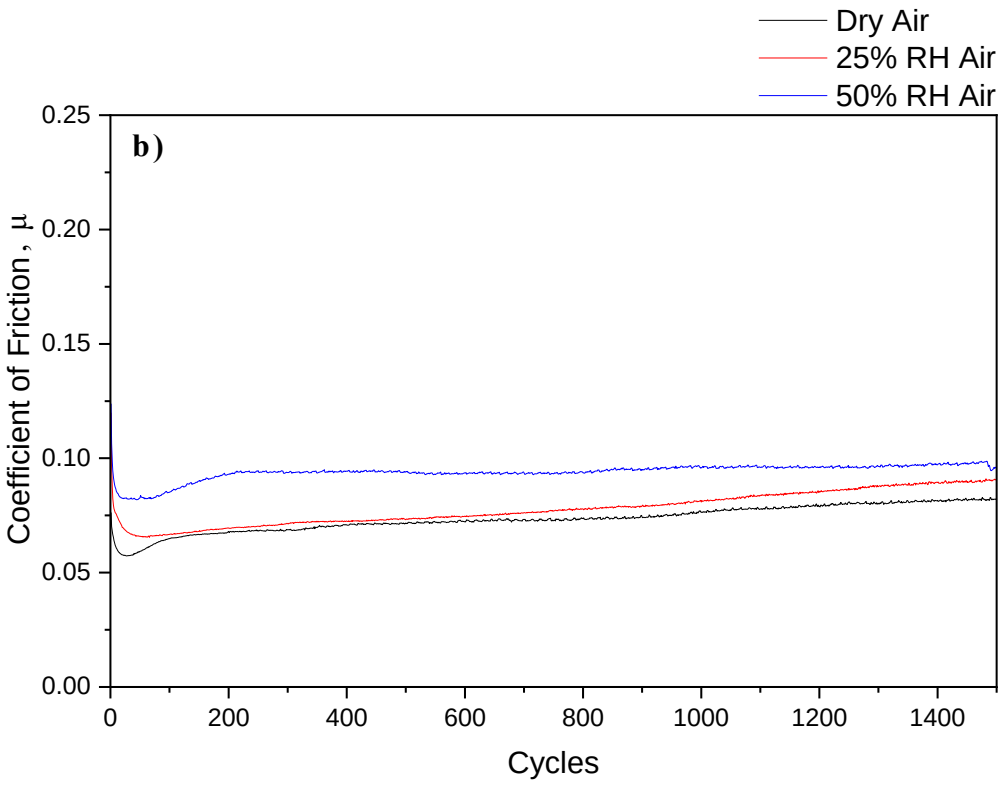

Figure 5.1 MoS_2 samples aged for one week in, a) N_2 environments at relative humidity levels of 0% (dry), 25% and 50%. Followed by sliding on the NTR for 1500 cycles in a dry N_2 environment, and, b) Air environments at relative humidity levels of 0% (dry), 25% and 50%. Followed by sliding on the NTR for 1500 cycles in a dry N_2 environment.

A comparison of steady state coefficients of friction, for MoS2 coatings aged for one week, can be found in Figure 5.2. The steady state coefficient of friction increased along with humidity in all samples. N_2 aged samples showed an increase in steady state

coefficient of friction from 0% RH, to 50% RH, going from μ =0.07 ± 0.005 to μ =0.08 ± 0.008 representing a 12.5% increase. Air aged samples showed an increase in the coefficient of friction with increasing humidity in the ageing environment from μ = 0.08 in 0% RH air to μ = 0.1 ± 0.01, an increase of 20%.

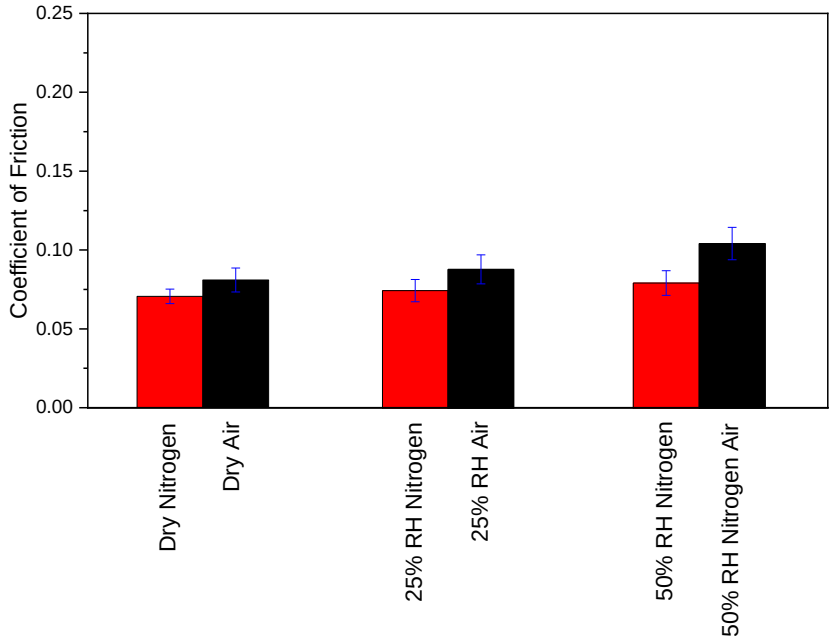

Figure 5.2 Comparison of the steady state coefficient of friction of one week aged MoS_2 coatings. Error shows maximum variance between repeats and is outlined in section 3.4.1

5.2.1 Two week aged

Figure 5.3 a) and b) show the coefficient of friction for AISI 440C - MoS_2 couples after 2 weeks of ageing in either nitrogen (a) or air (b) at 0, 25 and 50% RH. A rapid reduction in the coefficient of friction was observed, reaching $\mu = 0.074 \pm 0.01$ within the first 30 cycles for N_2 aged samples and $\mu = 0.085 \pm 0.02$ for air aged samples. Samples aged in a dry N_2 environment, reached a minimum coefficient of friction, $\mu = 0.06$; this then increased, reaching a steady state coefficient of friction, $\mu = 0.074$. In comparison, samples aged in 25% RH and 50% RH N_2 reached a minimum coefficient of friction of, $\mu = 0.073$ and $\mu = 0.084$, respectively.

The dry air aged sample displayed steady state $\mu = 0.088$. 25% and 50% relative humidity aged samples had a steady state $\mu = 0.09$ and $\mu = 0.11$ increase respectively. It can also be seen that the gaseous composition of the ageing environment affects the friction response, with air aged samples displaying higher coefficients of friction compared with nitrogen aged samples, at all like humidity levels.

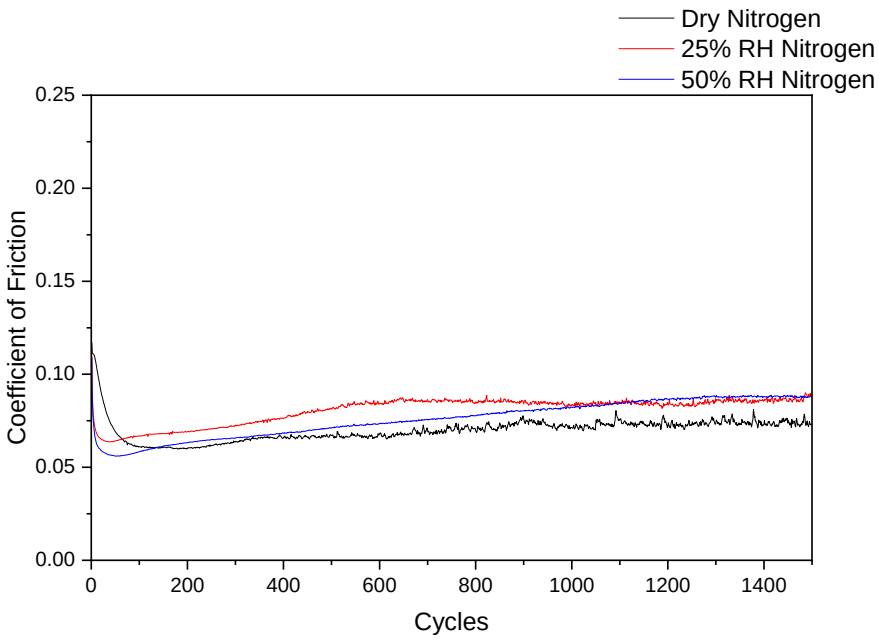
Dry Nitrogen
25% RH Nitrogen
50% RH Nitrogen
Coefficient of Friction
0.25
0.20
0.15
0.10
0.05
0.00
0
200
400
600
800
1000
1200
1400
Cycles

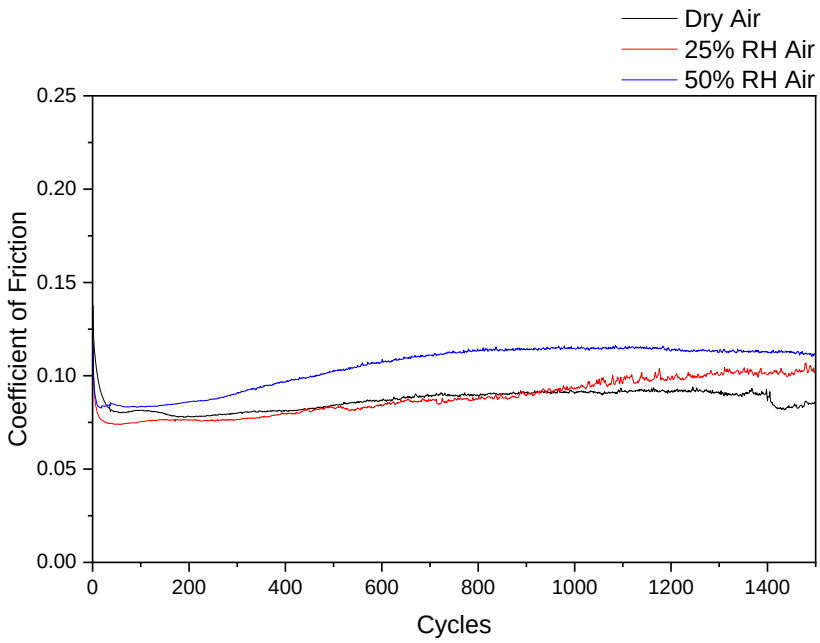
Dry Air
25% RH Air
50% RH Air
Coefficient of Friction
0.25
0.20
0.15
0.10
0.05
0.00
0
200
400
600
800
1000
1200
1400
Cycles

Figure 5.3 MoS_2 samples aged for two weeks in a) N_2 environments at relative humidity levels of 0% (dry), 25% and 50%. Followed by sliding on the NTR for 1500 cycles in a dry N_2 environment, and, b) Air environments at relative humidity levels of 0% (dry), 25% and 50%. Followed by sliding on the NTR for 1500 cycles in a dry N_2 environment.

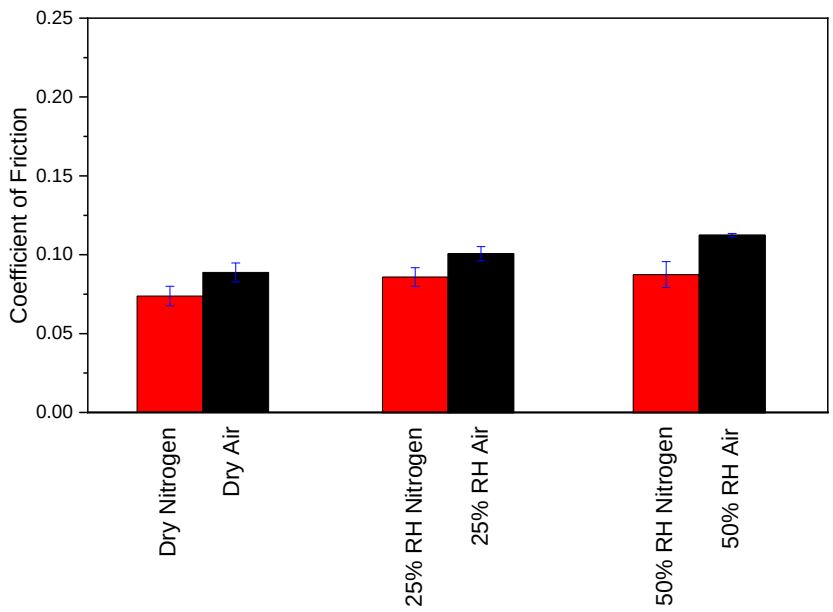

Figure 5.4 Comparison of the steady state coefficient of friction of two week aged MoS_2 coatings.

5.2.2 Three week aged

Figure 5.5 and Figure 5.6 show the coefficient of friction for AISI 440C - MoS_2 couples after 3 weeks of ageing in either nitrogen (Figure 5.5) or air (Figure 5.6) at 0, 25 and 50% RH. Samples aged in dry nitrogen display only small changes in coefficient of friction when compared to the unaged reference sample tested in dry nitrogen in Figure 5.7. After 3 weeks of ageing in dry nitrogen, the steady state coefficient of friction fell from $\mu = 0.067$ to $\mu=0.063$, a 6% drop when compared to the unaged reference. After ageing in 25% RH nitrogen, the coefficient of friction was $\mu=0.072$ representing an increase of 7.5%. Ageing for 3 weeks in 50% relative nitrogen led to a steady state coefficient of $\mu=0.079$, an increase of 17.9%. Air aged samples led to more drastic changes in the friction response of the coating.

The dry air aged sample displayed steady state $\mu=0.074$, a 10.4% increase from the unaged reference. 25% and 50% relative humidity aged samples had a steady state $\mu=0.093$ and $\mu=0.134$ a 38.8% and 100% increase respectively. It can also be seen that the gaseous composition of the ageing environment affects the friction response, with air aged samples displaying higher coefficients of friction compared with nitrogen aged samples, at all like humidity levels.

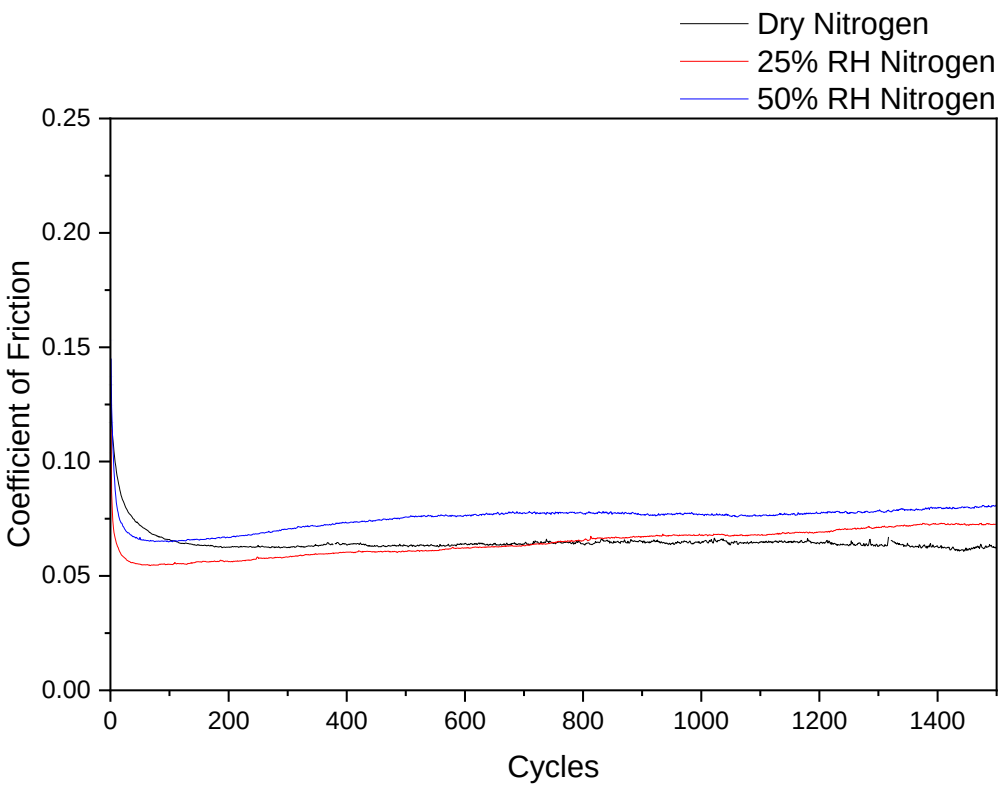

Figure 5.5 MoS_2 samples aged for three weeks in N_2 environments at relative humidity levels of 0% (dry), 25% and 50%. Followed by sliding on the NTR for 1500 cycles in a dry N_2 environment.

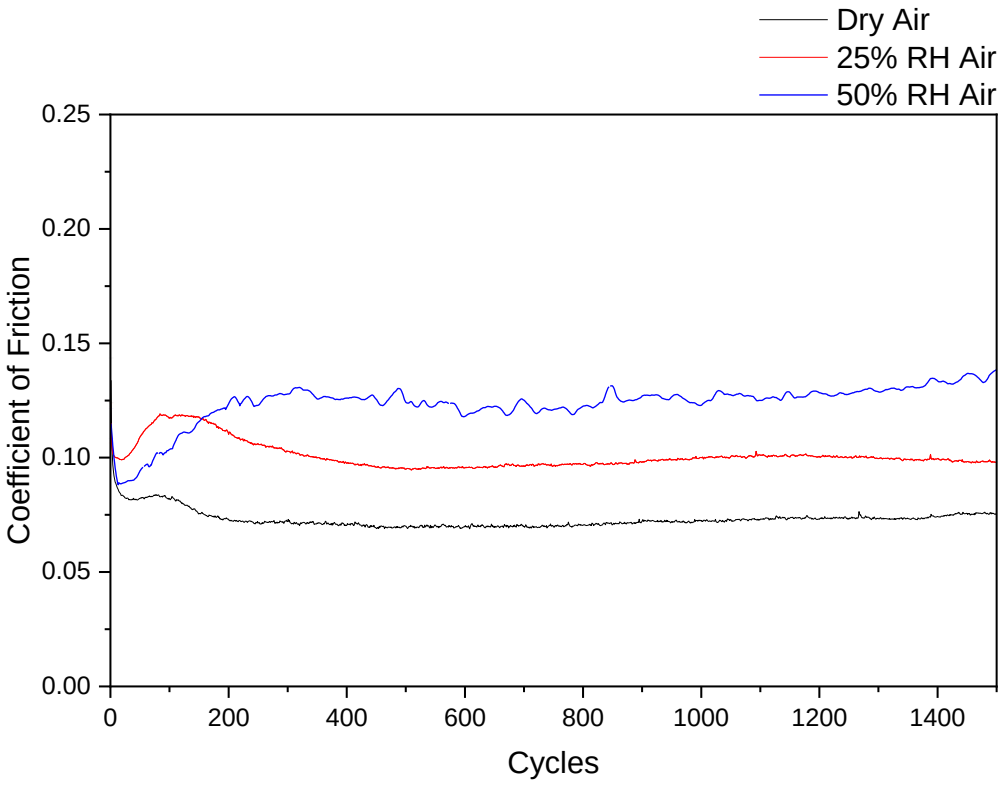

Figure 5.6 MoS_2 samples aged for three weeks in Air environments at relative humidity levels of 0% (dry), 25% and 50%. Followed by sliding on the NTR for 1500 cycles in a dry N_2 environment.

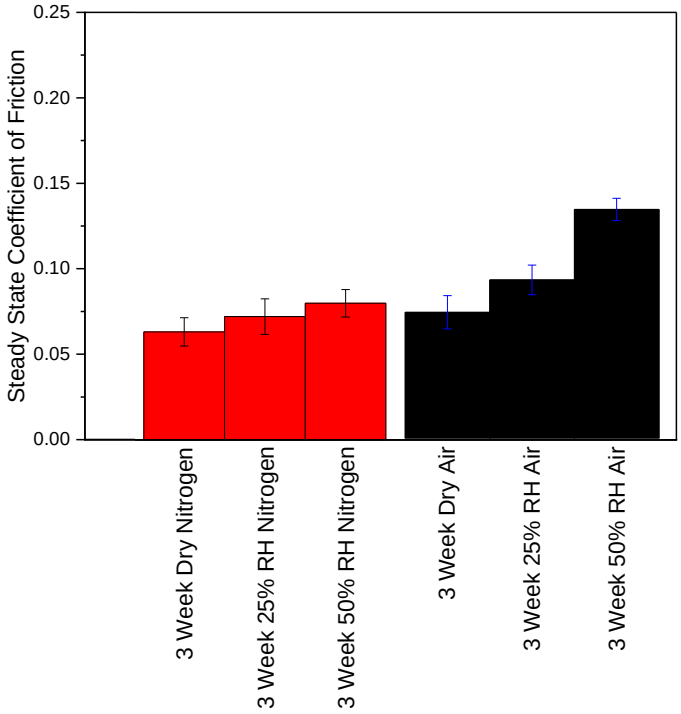

Figure 5.7 Comparison of the steady state coefficient of friction of three week aged MoS_2 coatings.

5.3 White light interferometry

5.3.1 One week aged

Figure 5.8 a-c) shows white light interferometry results of the wear scars for results for one week, N_2 aged samples that have undergone 1500 cycles of sliding in a dry N_2 environment. Due to the surface topography of the samples, wear volume is difficult to estimate;

however, it can be seen that wear is well within the realms of the coating on all samples. There is some asperity shearing and smoothing visible in the wear scar. Line scans were taken inside and outside of the wear volume to give roughness values of; Dry N_2, Ra = 68 nm and Ra_{ws} = 37.6 nm 25% RH N_2, Ra = 71 nm and Ra_{ws} = 40 nm and 50% RH N_2, Ra = 69 nm and Ra_{ws} = 28 nm.

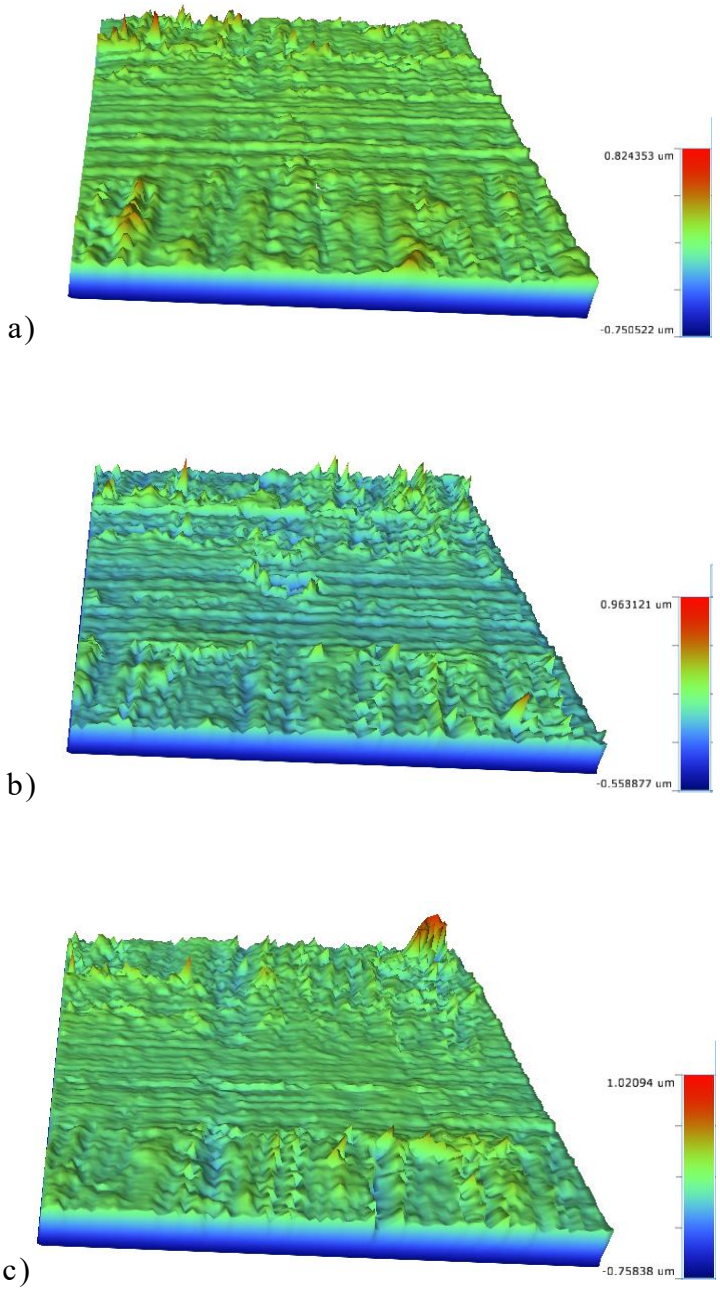

Figure 5.8 White light interferometry scan obtained from the MoS2 coated surfaces with a focus on the wear scar after 1 week ageing in a) dry N_2, b) 25% RH N_2 and c) 50% RH N_2, followed by friction testing in dry nitrogen.

Figure 5.9 a-c) shows white light interferometry shows white light interferometry results of the wear scars for results for one week, N_2 aged samples that have undergone 1500 cycles of sliding in a dry N_2 environment. Wear volume has not been estimated; however, it can be seen that wear is well within the realms of the coating on all samples. Line scans were taken inside and outside of the wear volume to give roughness values of; Dry air, Ra = 61 nm and Ra_{ws} = 28.4 nm, 25% RH air, Ra = 65 nm and Ra_{ws} = 31 nm and 50% RH air, Ra = 97 nm and Ra_{ws} = 27.7 nm. The average wear depth is outlined in Table 5-1

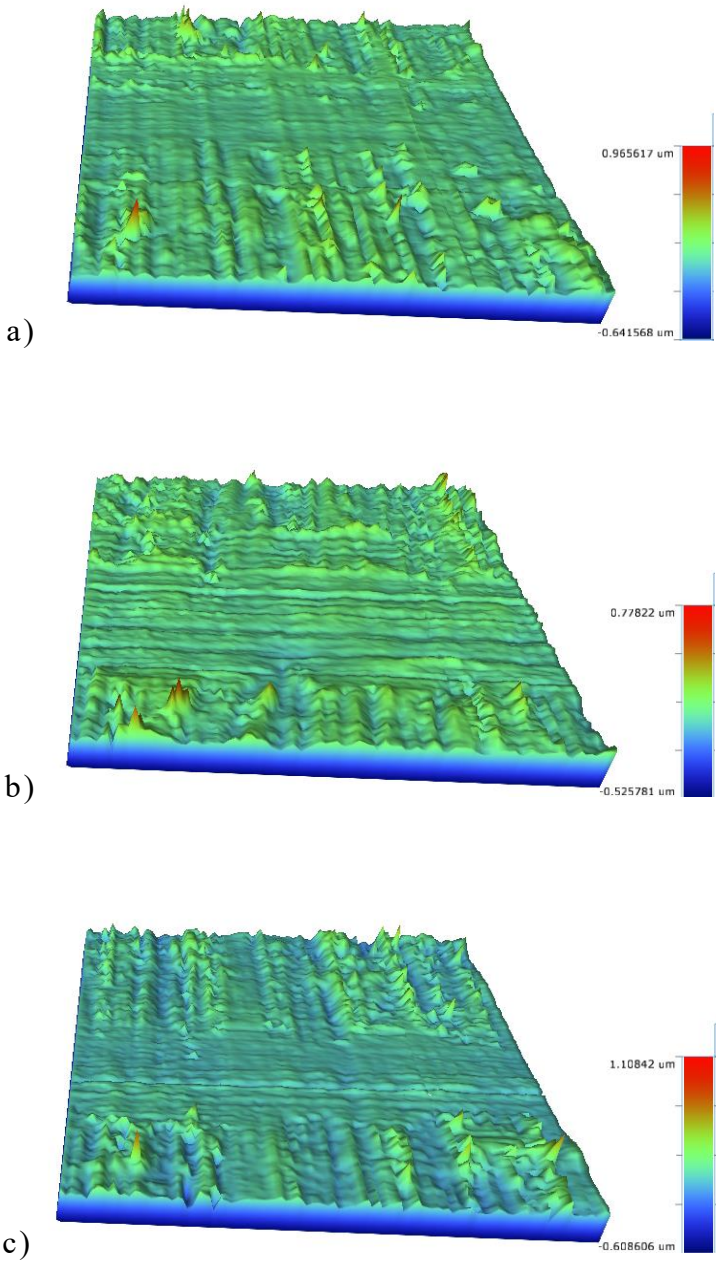

Figure 5.9 VSI results obtained from the MoS2 coated surfaces after 1 week ageing in a) dry air, b) 25% RH air and c) 50% RH air, followed by friction testing in dry nitrogen.

Table 5-1 Wear depth of one week aged MoS_2 samples

	Nitrogen	Air
0% RH	0.134 µm	0.145 µm
25% RH	0.241 µm	0.149 µm
50% RH	0.138 µm	0.130 µm

5.3.2 Two week aged

Figure 5.10 a-c) shows white light interferometry results of the wear scars for results for one week, N_2 aged samples that have undergone 1500 cycles of sliding in a dry N_2 environment. Due to the surface topography of the samples, wear volume is difficult to estimate; however, it can be seen that wear is well within the realms of the coating on all samples. There is some asperity shearing and smoothing visible in the wear scar. Line scans were taken inside and outside of

the wear volume to give roughness values of; Dry N_2, Ra = 68 nm and Ra_{ws} = 35.4 nm 25% RH N_2, Ra = 70 nm and Ra_{ws} = 40 nm and 50% RH N_2, Ra = 64 nm and Ra_{ws} = 58 nm.

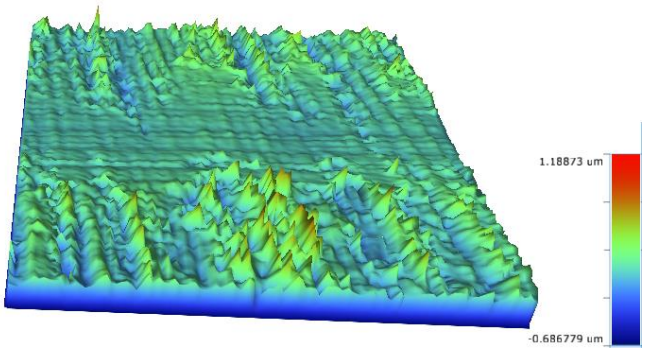

a)

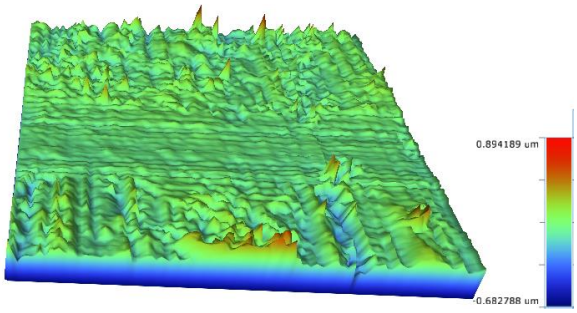

b)

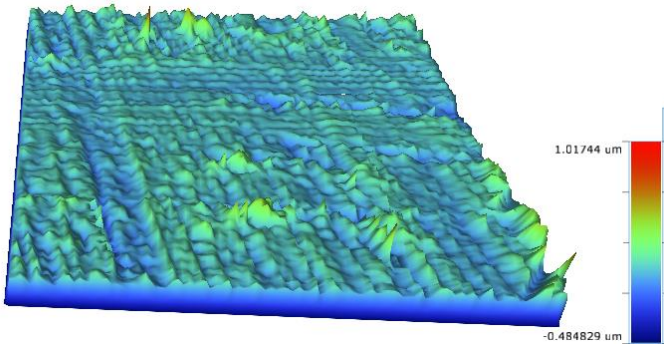

c)

Figure 5.10 White light interferometry scan obtained from the MoS2 coated surfaces with a focus on the wear scar after 2 weeks ageing in a) dry N_2, b) 25% RH N_2 and c) 50% RH N_2, followed by friction testing in dry nitrogen.

Figure 5.11 a-c) shows white light interferometry shows white light interferometry results of the wear scars for results for one week, N_2 aged samples that have undergone 1500 cycles of sliding in a dry N_2 environment. Wear volume has not been estimated, however, it can be seen that wear is well within the realms of the coating on all samples. Line scans were taken inside and outside of the wear volume to give roughness values of; Dry air, Ra = 71 nm and Ra_{ws} = 44 nm, 25% RH air, Ra = 75 nm and Ra_{ws} = 81 nm and 50% RH air, Ra = 63 nm and Ra_{ws} = 51 nm. Wear depth outlined in Table 5-2.

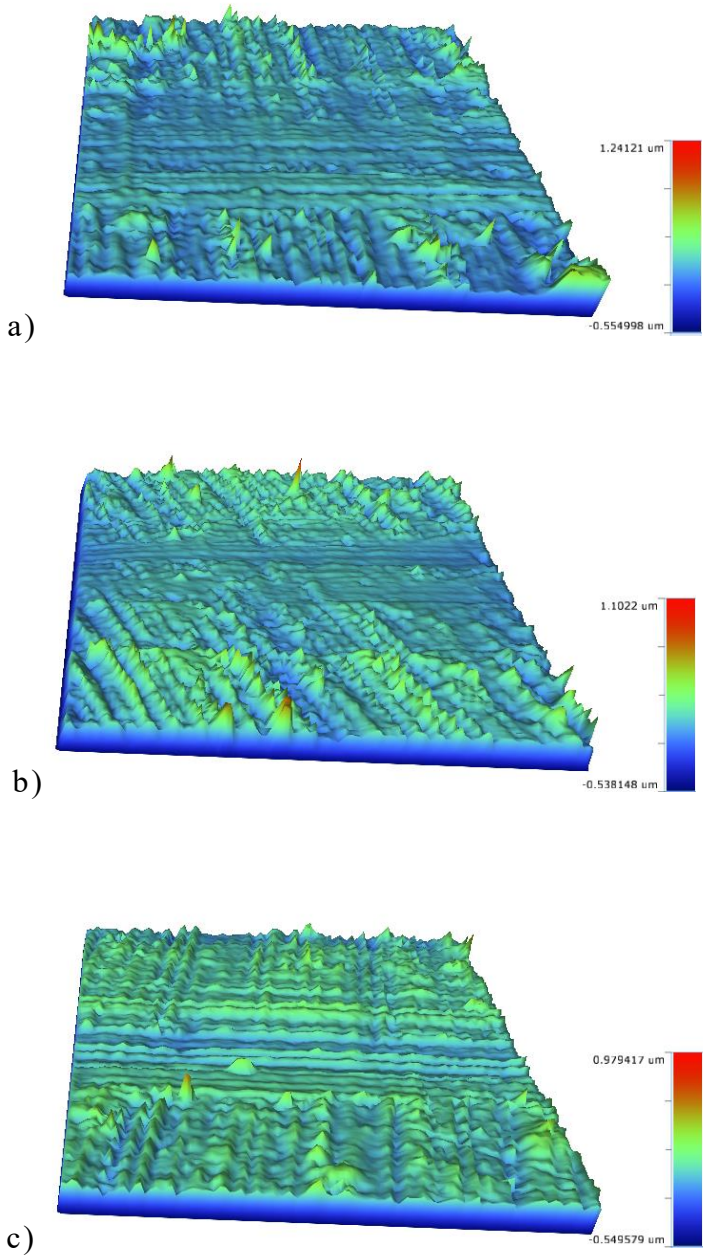

Figure 5.11 White light interferometry scan obtained from the MoS_2 coated surfaces with a focus on the wear scar after 2 weeks ageing in dry air followed by friction testing in dry nitrogen.

Table 5-2 Wear depth of two week aged MoS_2

	Nitrogen	Air
0% RH	0.117 µm	0.147 µm
25% RH	0.135 µm	0.149 µm
50% RH	0.138 µm	0.141 µm

5.3.3 Three week aged

Figure 5.12a-c) shows white light interferometry results of the wear scars for results for one week, N_2 aged samples that have undergone 1500 cycles of sliding in a dry N_2 environment. Due to the surface topography of the samples, wear volume is difficult to estimate; however, it can be seen that wear is well within the realms of the coating on all samples. There is some asperity shearing and smoothing visible in the wear scar. Line scans were taken inside and outside of

the wear volume to give roughness values of; Dry N_2, Ra = 51 nm and Ra_{ws} = 31.2 nm 25% RH N_2, Ra = 71 nm and Ra_{ws} = 28.6 nm and 50% RH N_2, Ra = 78 nm and Ra_{ws} = 54 nm.

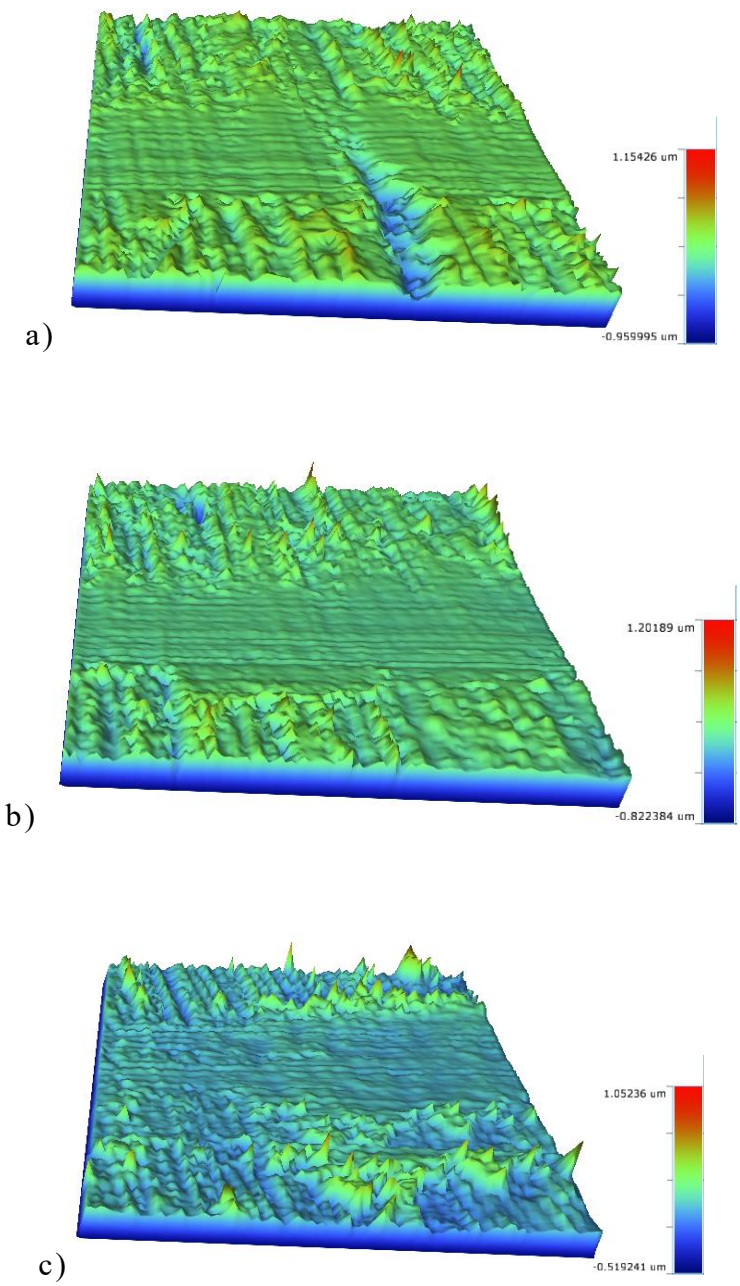

Figure 5.12 White light interferometry scan obtained from the MoS2 coated surfaces with a focus on the wear scar after 2 weeks ageing in a) dry N_2, b) 25% RH N_2, and c) 50% RH N2 followed by friction testing in dry nitrogen.

Figure 5.13 a-c) shows white light interferometry shows white light interferometry results of the wear scars for results for one week, N_2 aged samples that have undergone 1500 cycles of sliding in a dry N_2 environment. Wear volume has not been estimated; however, it can be seen that wear is well within the realms of the coating on all samples. Line scans were taken inside and outside of the wear volume to give roughness values of; Dry air, Ra = 83 nm and Ra_{ws} = 64 nm, 25% RH air, Ra = 89 nm and Ra_{ws} = 57 nm and 50% RH air, Ra = 65 nm and Ra_{ws} = 58 nm. Wear depths for all samples outlined in Table 5-3.

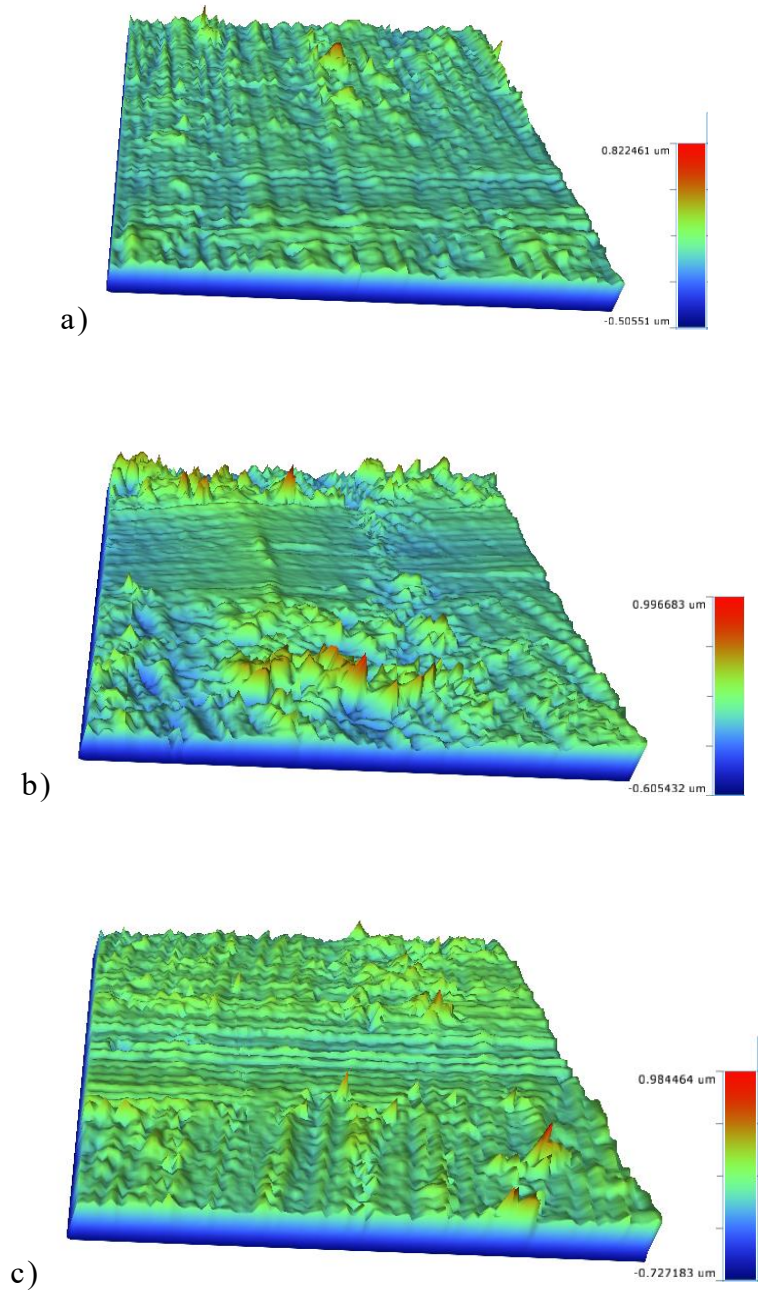

Figure 5.13 White light interferometry scan obtained from the MoS_2 coated surfaces with a focus on the wear scar after 3 weeks ageing in a) dry N_2, b) 25% RH N_2, and c) 50% RH N2 followed by friction testing in dry nitrogen

Table 5-3 Wear depth of 3 week aged MoS_2

	Nitrogen	Air
0% RH	0.155 µm	0.195 µm
25% RH	0.293 µm	0.228 µm
50% RH	0.222 µm	0.332 µm

5.4 Energy-dispersive X-Ray spectroscopy

5.4.1 One week aged

The wear did not fully penetrate through the coating, as confirmed by EDS maps displayed in Figure 5.14, where a strong signal for molybdenum and sulphur can be seen in the wear scar, added to the lack of iron or chromium signals, as would be expected had the stainless-steel substrate below been exposed.

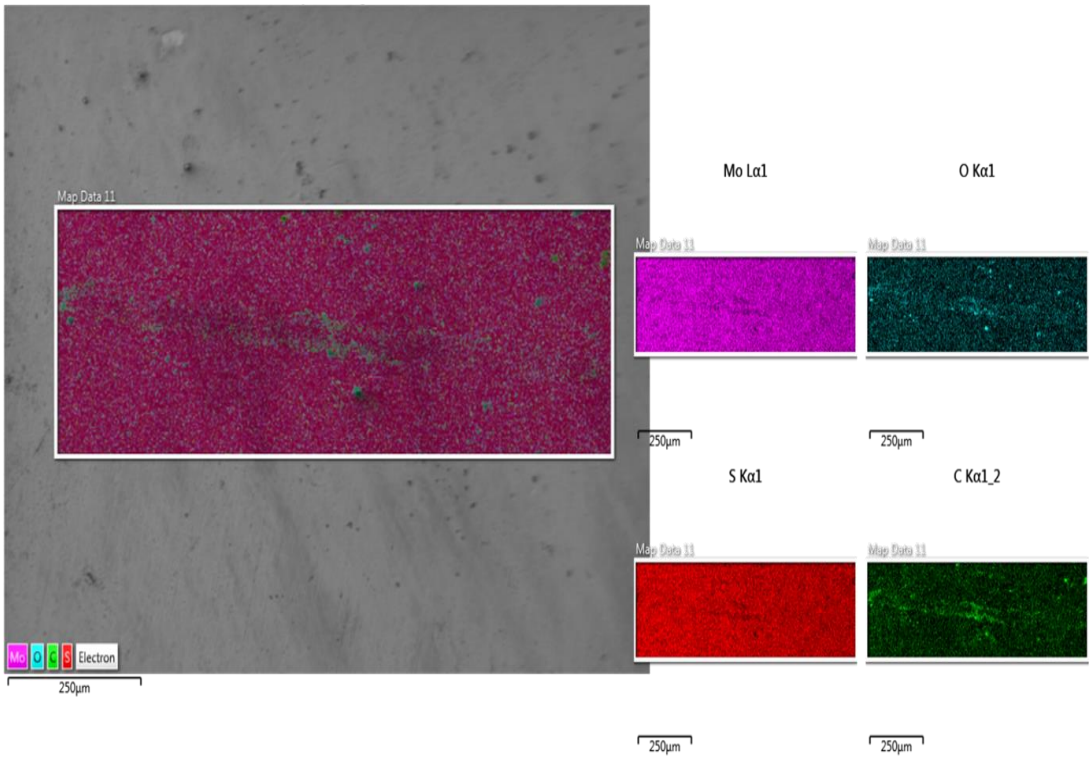

Figure 5.14 EDS mapping of the wear scar of an MoS_2 sample aged for one week in dry N_2.

Figure 5.15 shows the EDS elemental map output of the sample aged for two weeks in 25% RH N_2. As can be seen from the elemental mapping, the coating was not fully penetrated during sliding. In the EDS image, an increased oxygen signal can be observed in and around the very edges of the wear scar and, are significantly more prominent than in the dry nitrogen aged sample.

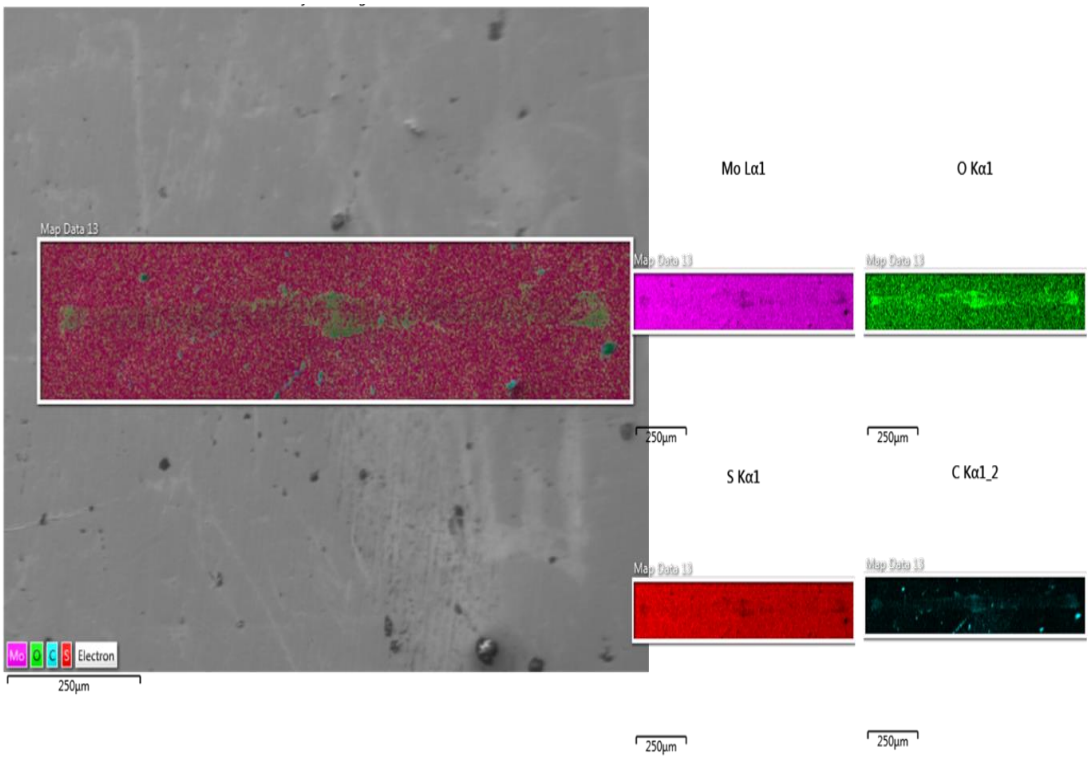

Figure 5.15 EDS mapping of the wear scar of an MoS_2 sample aged for one week in 25% RH N_2.

Figure 5.16 shows the EDS elemental map output of sample aged for two weeks in 50% RH N_2. As can be seen from the elemental mapping, the coating was not fully penetrated during sliding. Furthermore, it is following the trend of increased oxygen signal in higher humidity environments.

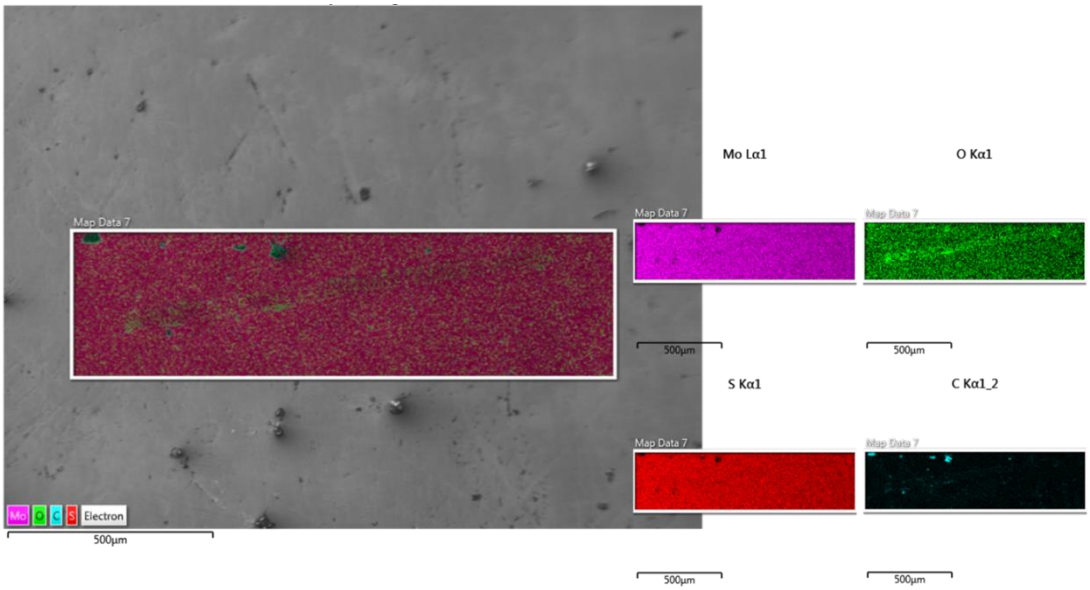

Figure 5.16 EDS mapping of the wear scar of an MoS_2 sample aged for one week in 50% RH N_2.

Figure 5.17 shows the EDS elemental map output of sample aged for one week in dry air. As with previous coatings, the coating was not fully penetrated during sliding. There is an increased oxygen signal concentrated in the wear scar when compared with the dry nitrogen aged sample. However, still less intensity of oxygen signal compared to the humid nitrogen counterparts.

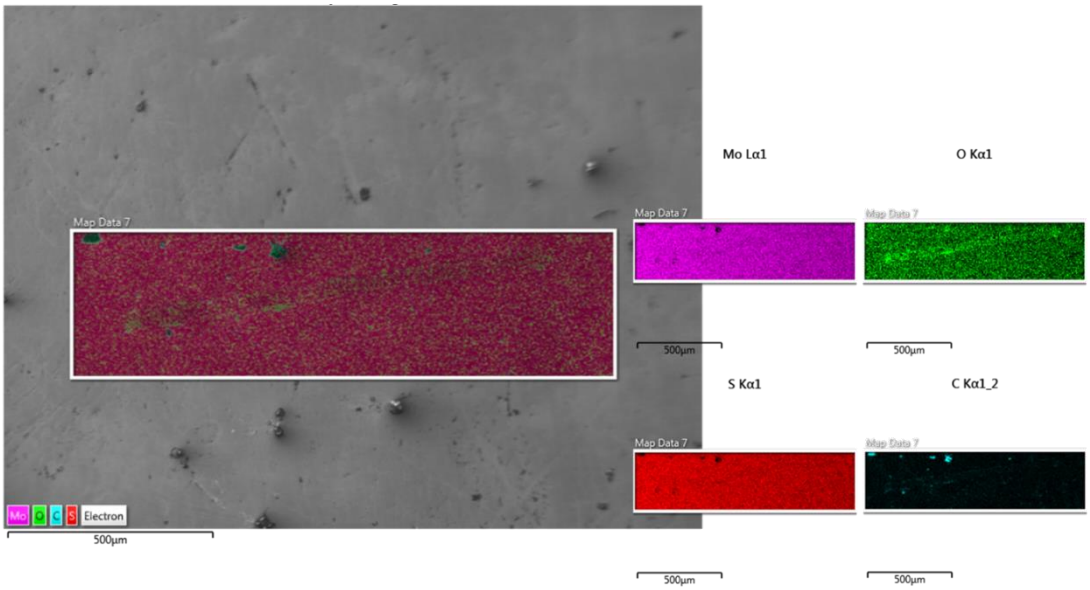

Figure 5.17 EDS mapping of the wear scar of an MoS_2 sample aged for one week in dry air.

Figure 5.18 shows the EDS elemental map output of sample aged for one week in 25% RH air. The oxygen signal in this peak is more intense in the wear scar than any of the previously displayed results.

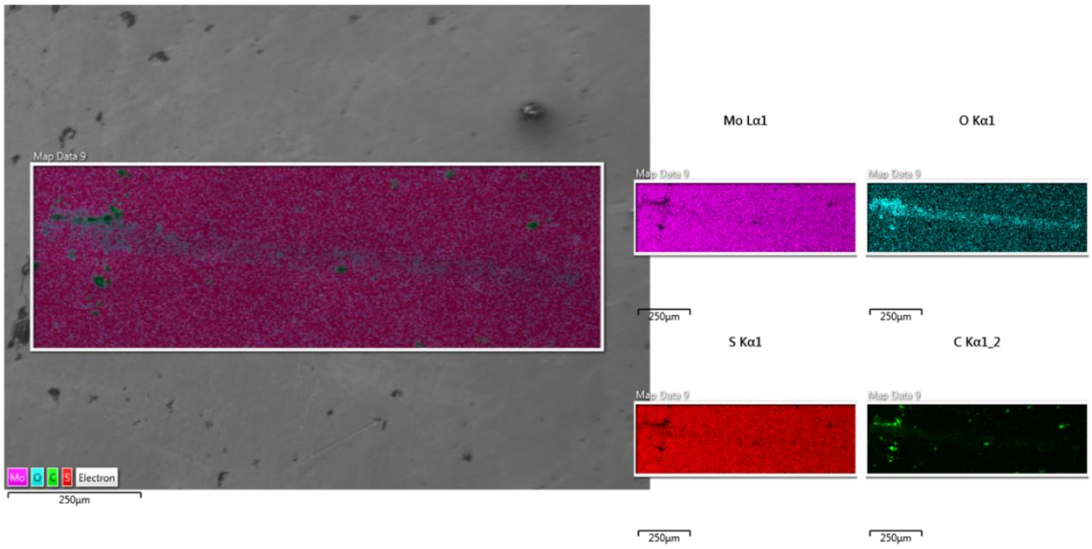

Figure 5.18 EDS mapping of the wear scar of an MoS_2 sample aged for one week in 25% RH air.

The EDS elemental map output of sample aged for two weeks in 50% RH air is displayed in Figure 5.19. As can be seen from the elemental mapping, the coating was not fully penetrated during sliding. Furthermore, it is following the trend of increased oxygen signal in higher humidity and oxygen containing environments. A comparison of all of the one week aged EDS mapping for oxygen can be seen in Table 5-4.

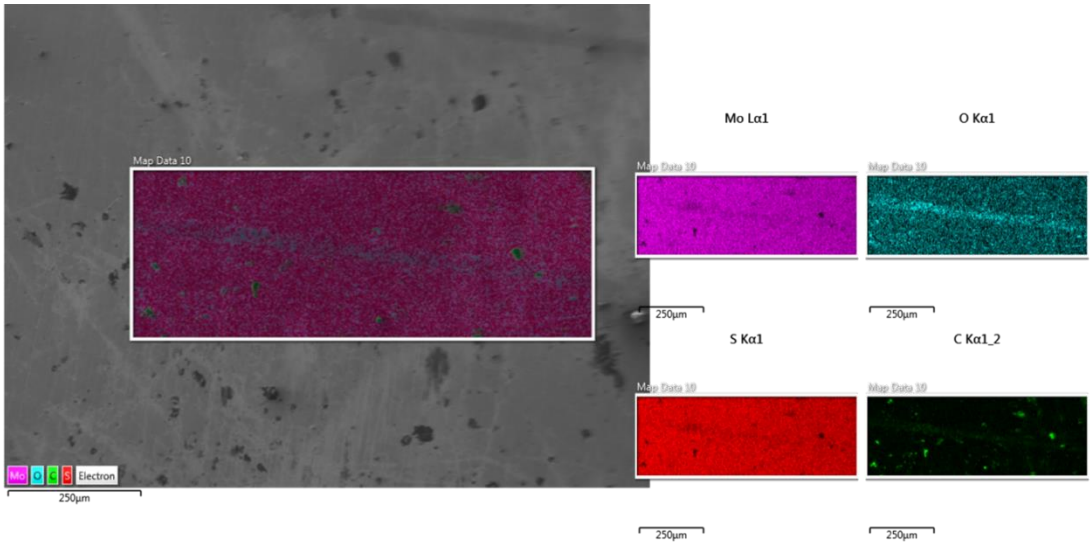

Figure 5.19 EDS mapping of the wear scar of an MoS_2 sample aged for one week in 50% RH air.

Table 5-4 Comparison of oxygen signal from EDX spectra of two week aged samples

Relative Humidity (%)	Nitrogen	Air
0	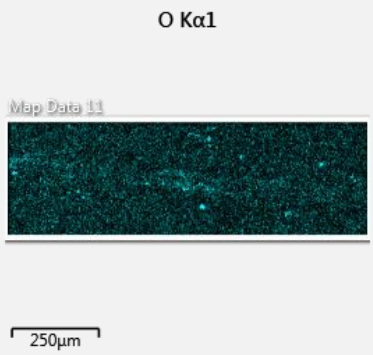	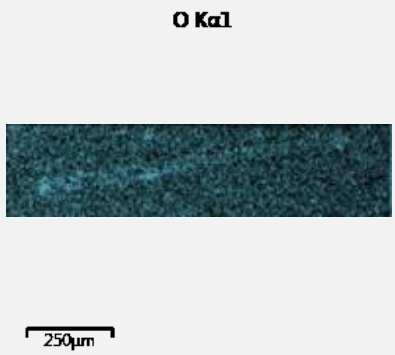
25	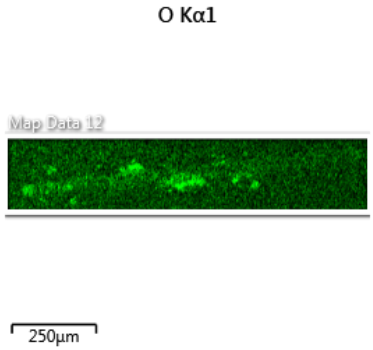	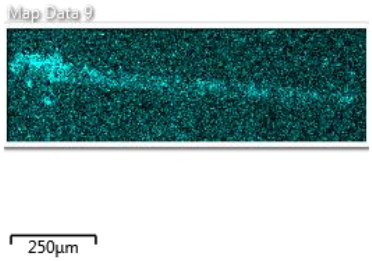
50	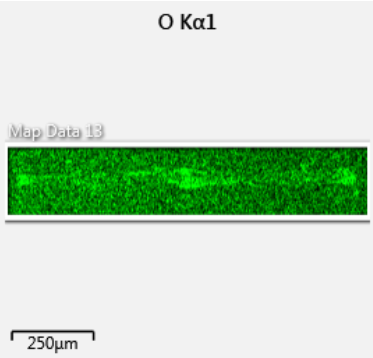	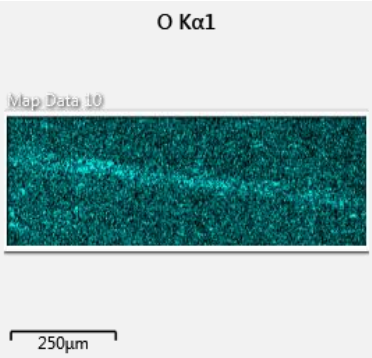

5.4.2 Two week aged

EDS mapping of the wear scar displayed in Figure 5.20 shows an increased oxygen signal in the wear scar. However, unlike previously described samples there is a significant signal for carbon, this is likely surface contamination.

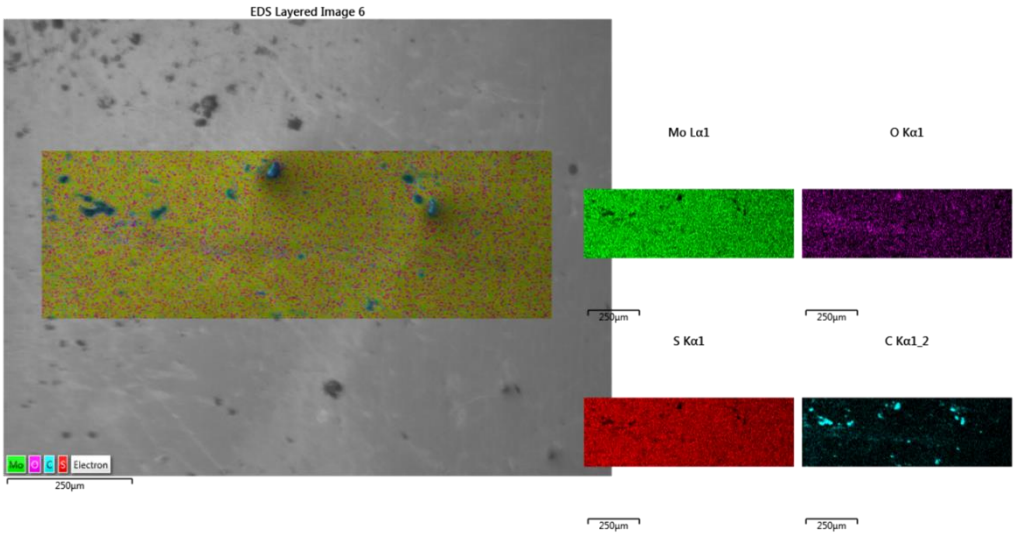

Figure 5.20 EDS mapping of the wear scar of an MoS_2 sample aged for two weeks in dry N_2.

EDS mapping of the wear scar and close surrounding area, displayed in Figure 5.21 shows a concentrated oxygen signal in the wear scar.

Furthermore, there is a significantly increased oxygen signal around the rest of the EDS map outside of the wear scar.

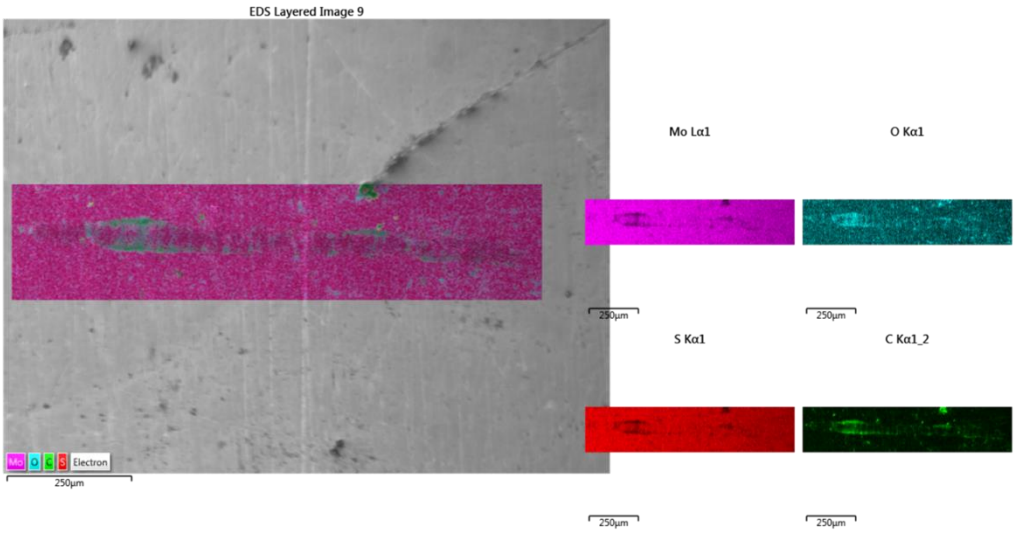

Figure 5.21 EDS mapping of the wear scar of an MoS_2 sample aged for two weeks in 25% RH N_2.

EDS mapping of the wear scar and close surrounding area, displayed in Figure 5.22, shows a slightly concentrated oxygen signal in the wear scar. Furthermore, there is a significantly increased oxygen signal around the rest of the EDS map outside the wear scar.

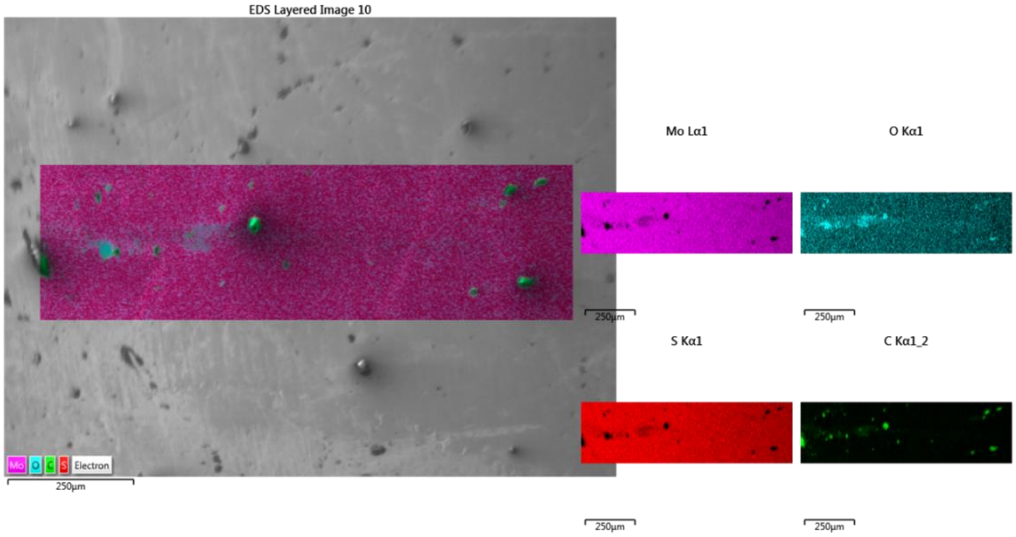

Figure 5.22 EDS mapping of the wear scar of an MoS_2 sample aged for two week in 50% RH N_2.

EDS mapping of the wear scar and close surrounding area, displayed in Figure 5.23, shows a slightly concentrated oxygen signal in the wear scar. Furthermore, there is a significantly increased oxygen signal around the rest of the EDS map outside of the wear scar. There is minimal carbon signal in the wear track, indicating the coating has not worn through to the base substrate

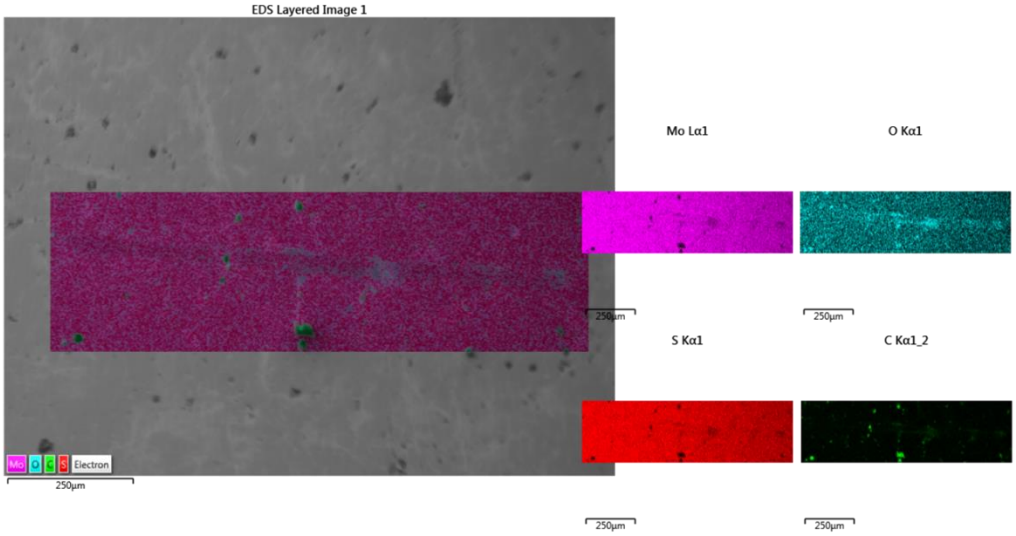

Figure 5.23 EDS mapping of the wear scar of an MoS_2 sample aged for two weeks in dry air.

Figure 5.24shows the EDS elemental map output of sample aged for one week in 25% RH air. The oxygen signal is focused within the wear scar. However, there is a spot of higher intensity oxygen at one point in the wear scar.

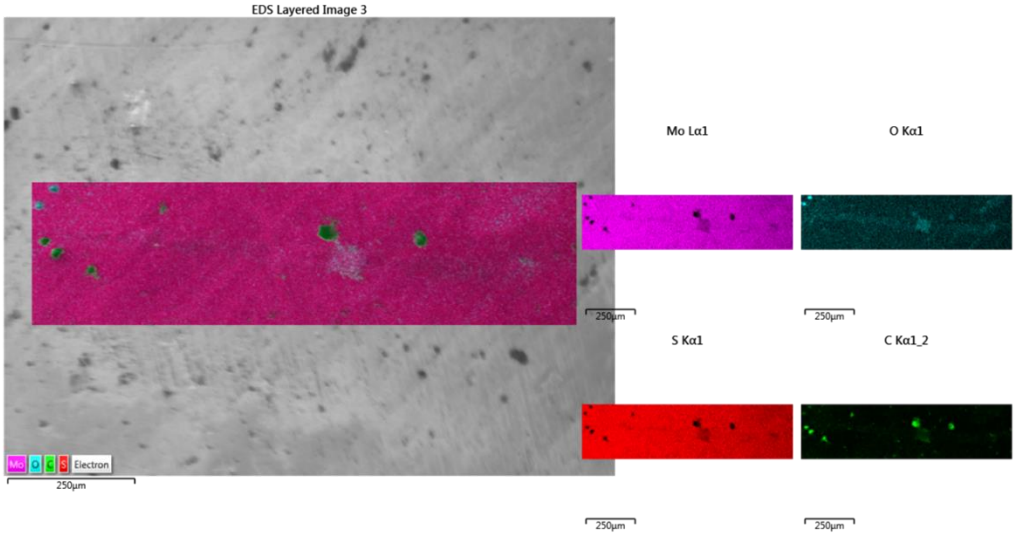

Figure 5.24 EDS mapping of the wear scar of an MoS_2 sample aged for two week in 25% RH air.

The EDS elemental map output of sample aged for two weeks in 50% RH air is displayed in Figure 5.25. As can be seen from the elemental mapping, the coating was not fully penetrated during sliding. Furthermore, it is following the trend of increased oxygen signal in higher humidity and oxygen containing environments. A comparison of all of the one week aged EDS mapping for oxygen can be seen in

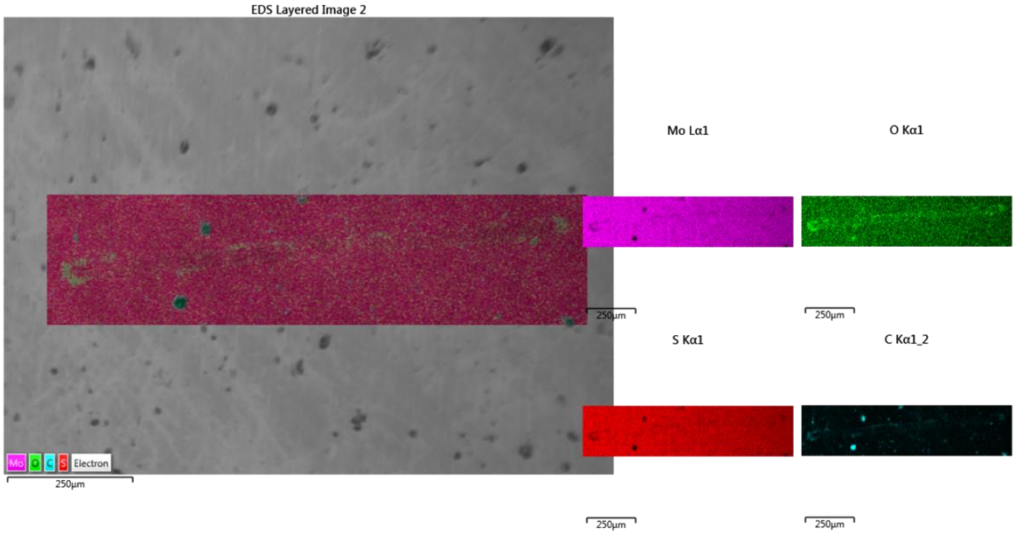

Figure 5.25 EDS mapping of the wear scar of an MoS_2 sample aged for two weeks in 50% RH air.

Table 5-5 Comparison of oxygen signal from EDS spectra of two week aged samples

Relative Humidity (%)	Nitrogen	Air
0		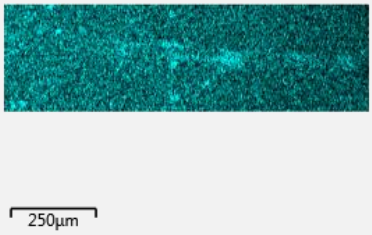
25	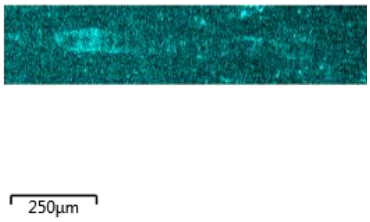	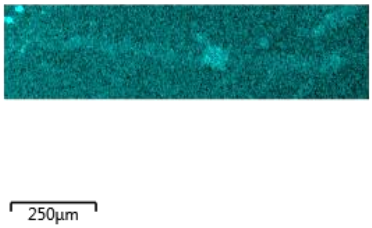
50	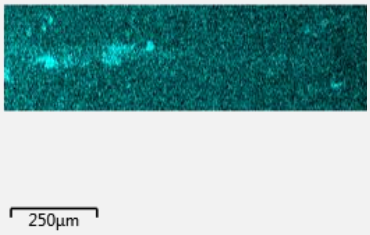	

5.4.3 Three week aged

Figure 5.26 – Figure 5.31 show the EDS elemental map signal at 5 keV in the wear scar of both air and nitrogen samples aged for 3 weeks in 0, 25 and 50% RH. The intensity of the oxygen signal is concentrated in the wear scar in all air aged samples, with intensity increasing with humidity. Oxygen can also be observed in the 25% and the 50% RH nitrogen aged samples. The intensity of the oxygen signal is higher in air aged than nitrogen aged at all like humidity levels.

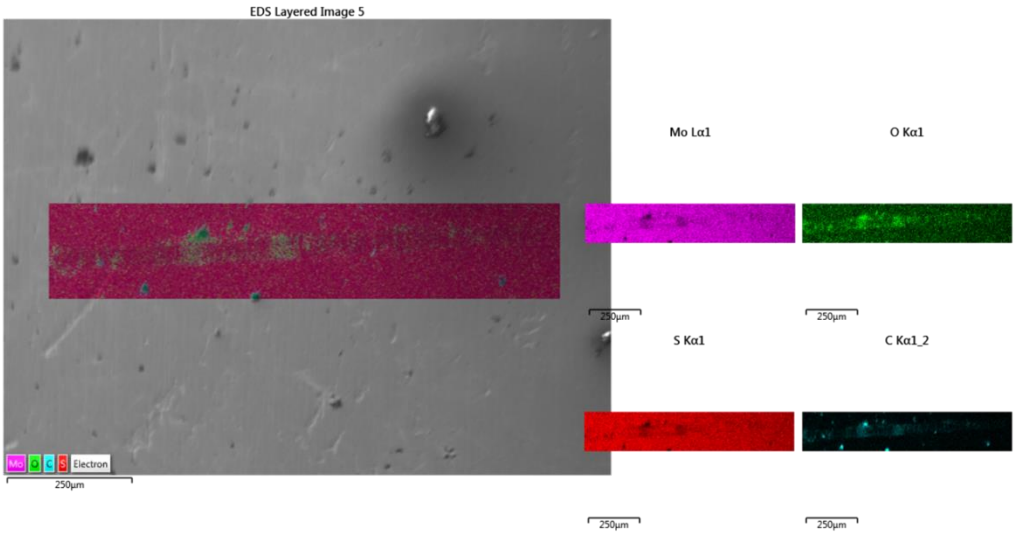

Figure 5.26 EDS mapping of the wear scar of an MoS_2 sample aged for three weeks in dry N_2.

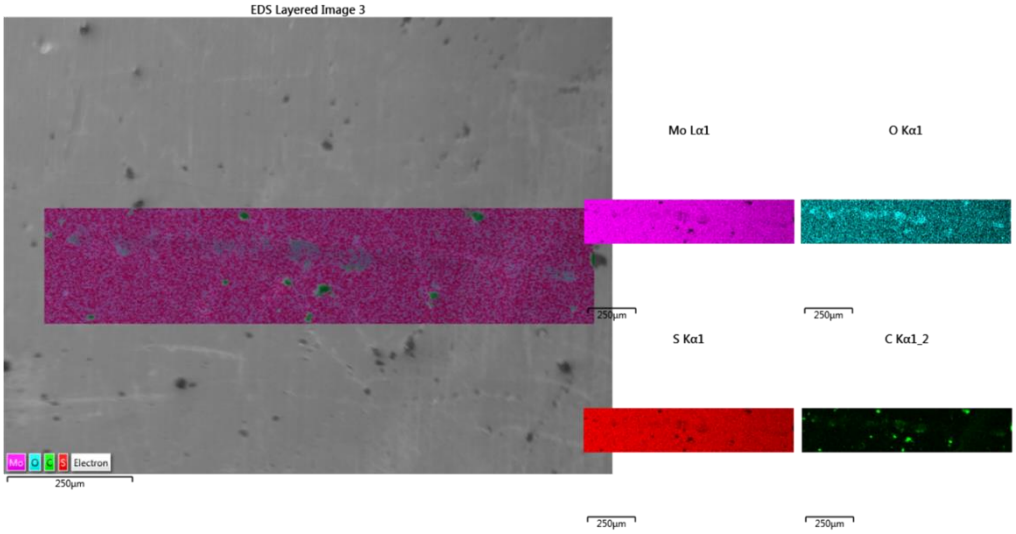

Figure 5.27 EDS mapping of the wear scar of an MoS_2 sample aged for three week in 25% RH N_2.

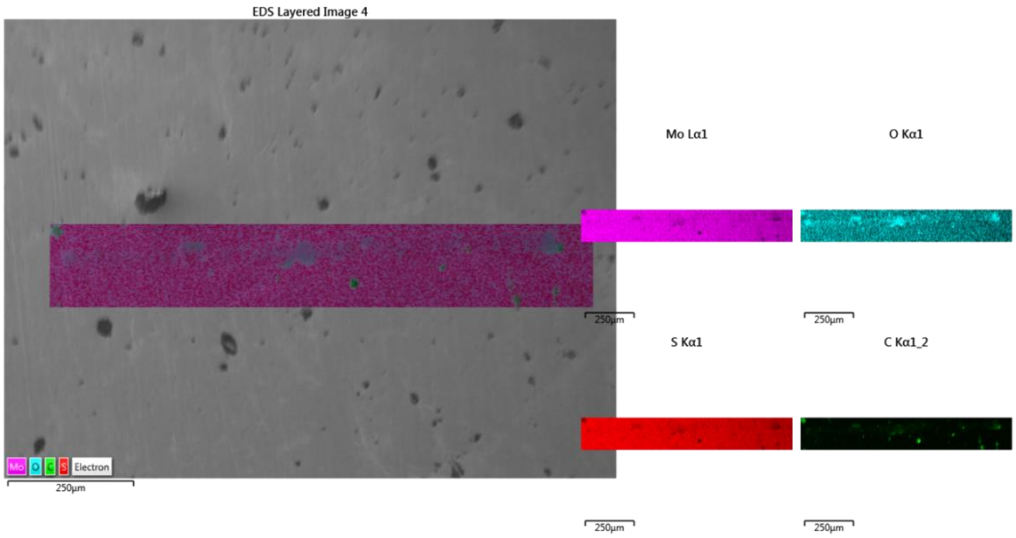

Figure 5.28 EDS mapping of the wear scar of an MoS_2 sample aged for three week in 50% RH N_2.

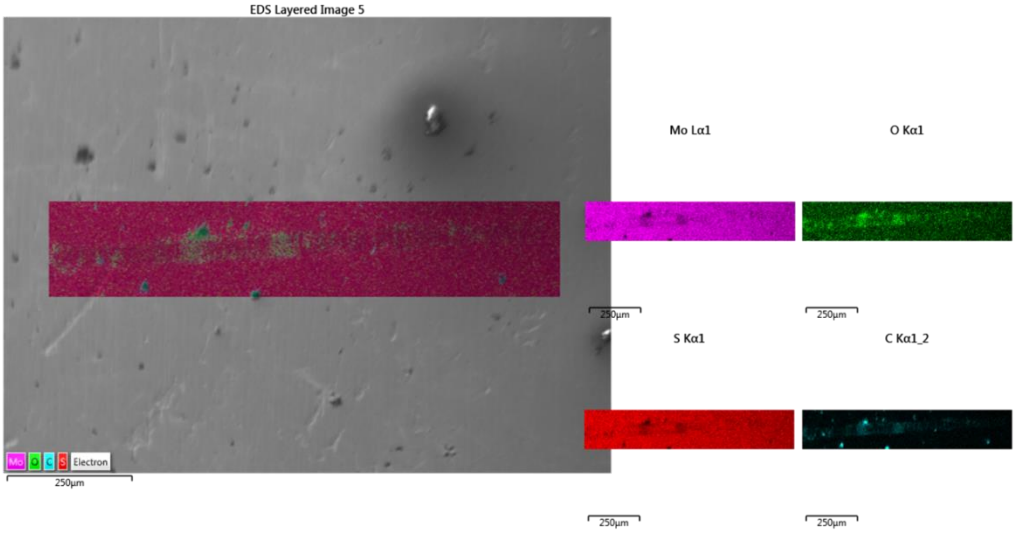

Figure 5.29 EDS mapping of the wear scar of an MoS_2 sample aged for three weeks in dry air.

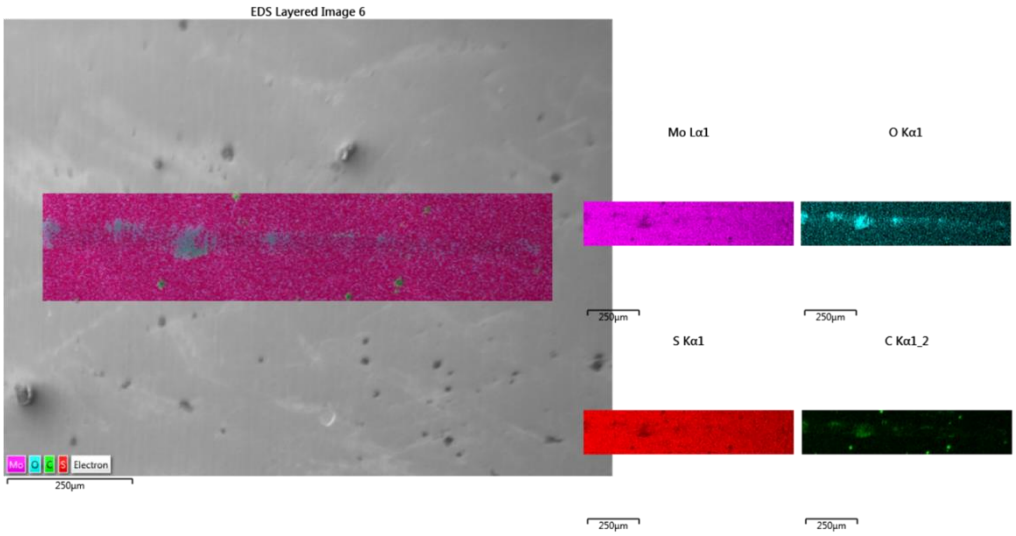

Figure 5.30 EDS mapping of the wear scar of an MoS_2 sample aged for three weeks in 25% RH air.

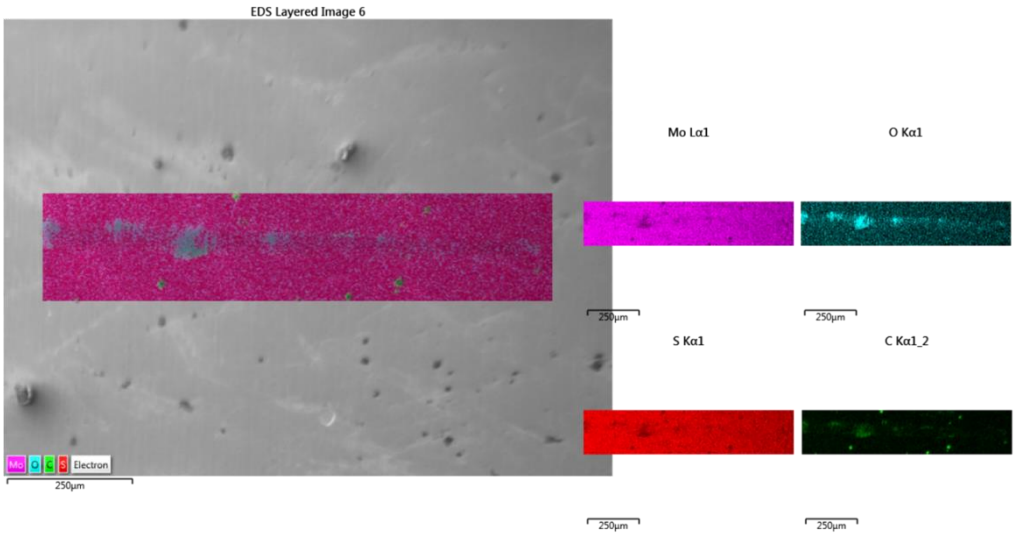

Figure 5.31 EDS mapping of the wear scar of an MoS_2 sample aged for three weeks in 50% RH air.

Table 5-6 Comparison of oxygen signal from EDS spectra of three week aged samples

Relative Humidity (%)	Nitrogen	Air
0	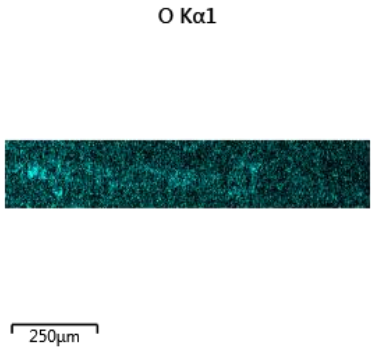	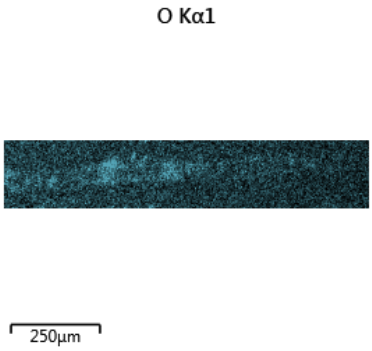
25	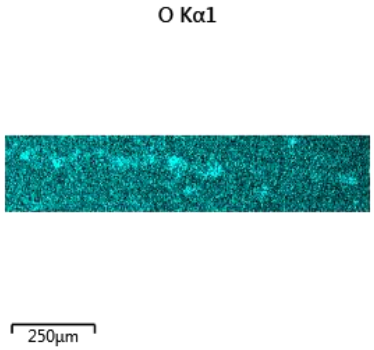	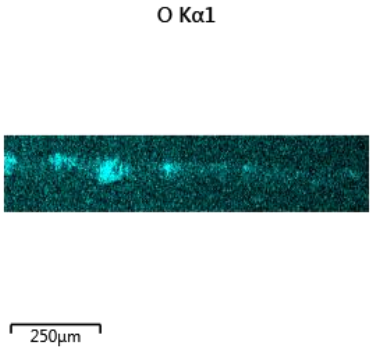
50	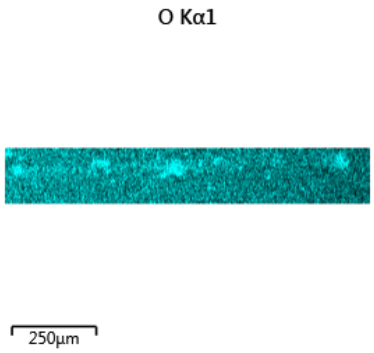	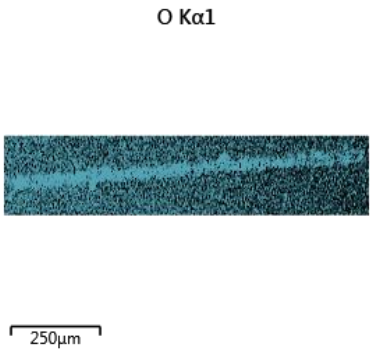

5.5 Raman spectroscopy

5.5.1 One week aged

Figure 5.32 and Figure 5.33 show the Raman spectroscopy inside and outside of wear scar on MoS_2 samples aged for one week in dry, 25 and 50% RH N_2 and air respectively. At all humidity levels, the first order Raman peaks are visible. All peaks for both inside and outside of the wear scar for the dry, 25% and 50% RH nitrogen tested samples and air tested samples fall within the same range, indicating no bonding changes due to sliding.

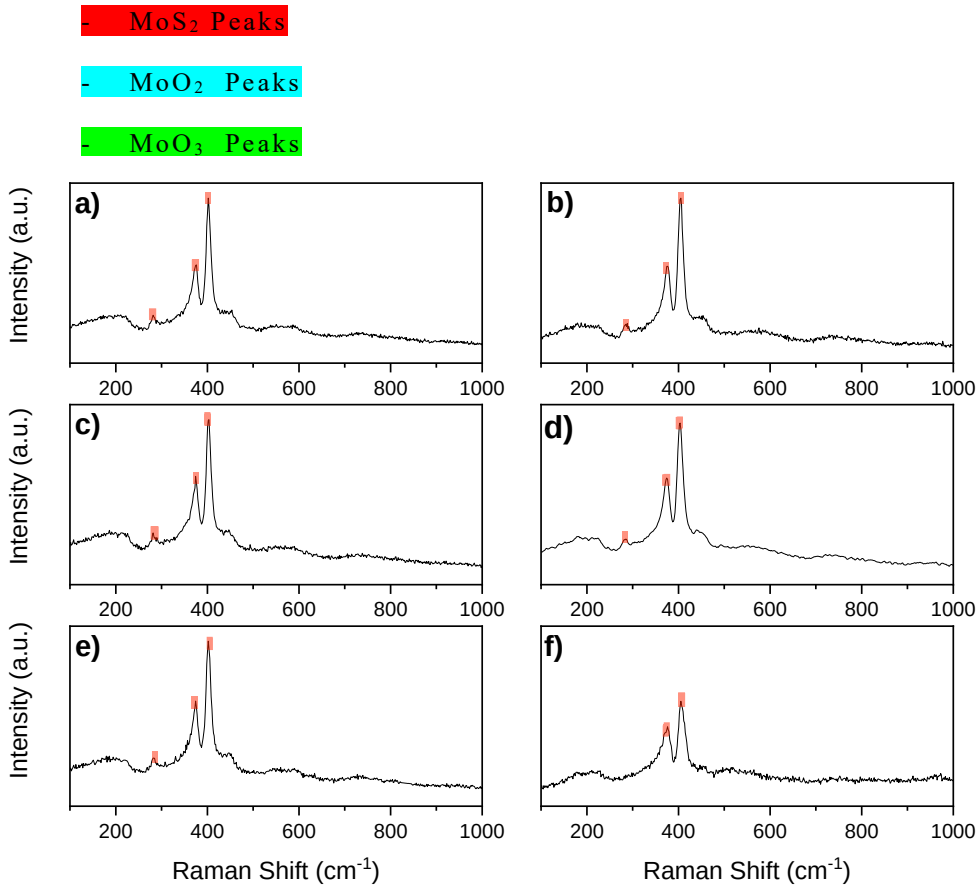

Figure 5.32 Raman spectroscopy of one week aged MoS_2 a) outside of the wear scar after ageing in dry nitrogen b) inside of the wear scar after ageing in dry nitrogen c) outside of the wear scar after ageing in 25% RH nitrogen d) inside of the wear scar after ageing in 25% RH nitrogen e) outside of the wear scar ageing in 50% RH nitrogen f) inside of the wear scar after ageing in 50% RH nitrogen.

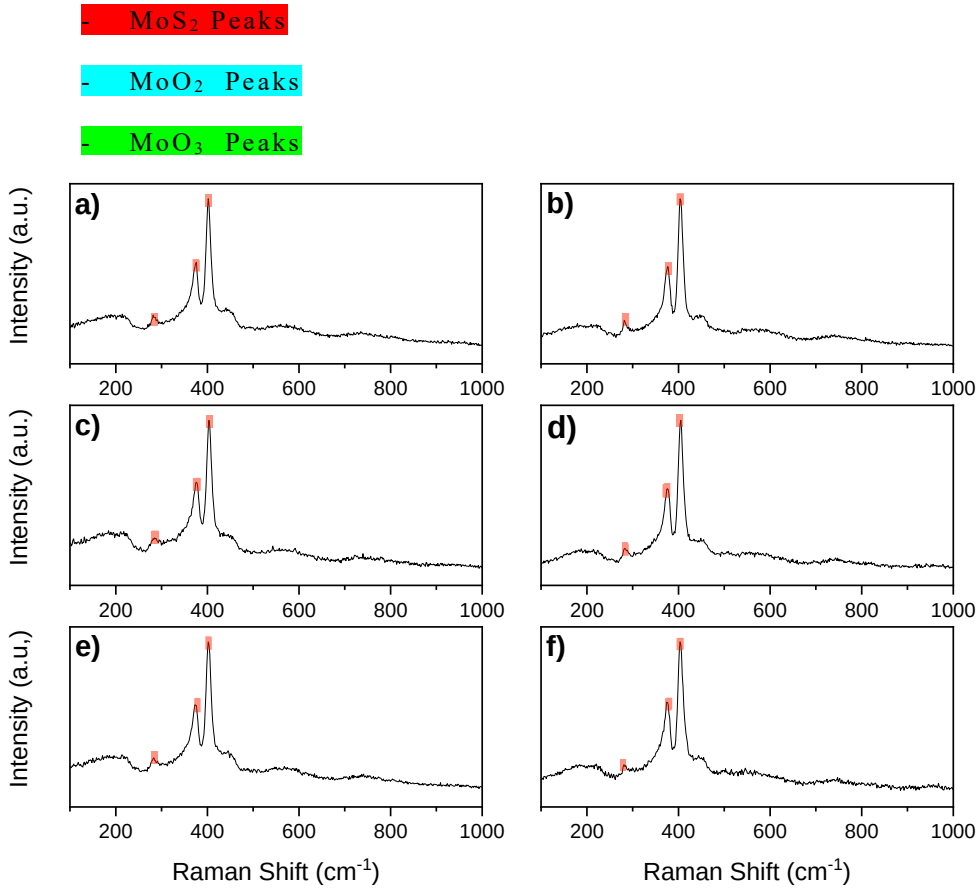

Figure 5.33 Raman spectroscopy of one week aged MoS_2 a) outside of the wear scar after ageing in dry air b) inside of the wear scar after ageing in dry air c) outside of the wear scar after ageing in 25% RH air d) inside of the wear scar after ageing in 25% RH air e) outside of the wear scar after ageing in 50% RH air f) inside of the wear scar after ageing in 50% RH air.

5.5.2 Two week aged

Figure 5.36 shows the Raman spectroscopy inside and outside of wear scar on 2-week nitrogen aged MoS_2 samples in dry, 25 and 50% RH. At all humidity levels, the first order Raman peaks are visible. All peaks for both inside and outside of the wear scar for the dry, 25% and 50% RH nitrogen aged samples fall within the same range, indicating no change due to sliding.

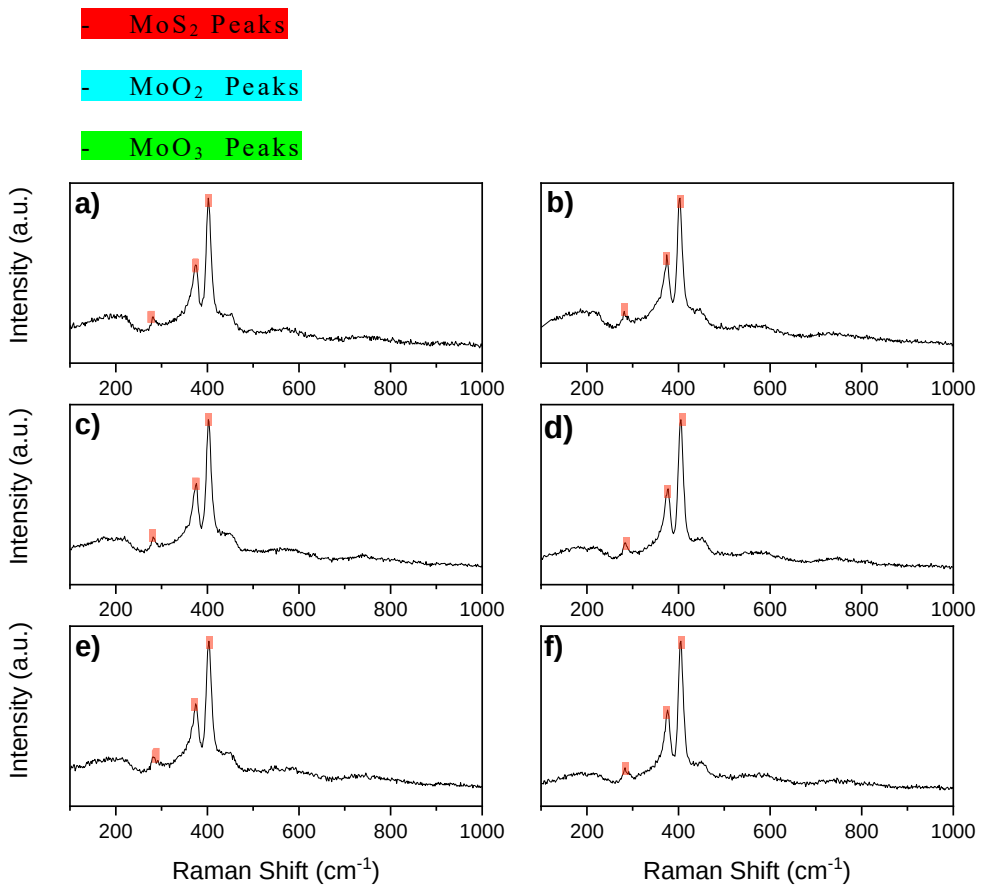

Figure 5.34 Raman spectroscopy of two week aged MoS_2 a) outside of the wear scar after ageing in dry nitrogen b) inside of the wear scar after ageing in dry nitrogen c) outside of the wear scar after ageing in 25% RH nitrogen d) inside of the wear scar after ageing in 25% RH nitrogen e) outside of the wear scar ageing in 50% RH nitrogen f) inside of the wear scar after ageing in 50% RH nitrogen.

Figure 5.35 shows the Raman spectroscopy inside and outside of wear scar on 2-week air aged MoS_2 samples in dry, 25 and 50% relative

humidity air. Clear differences can be seen between the worn and unworn spectrum. In the dry air aged sample, the E_{1g} at 286-287 cm^{-1}, E_{2g}^{1} at 380-382 cm^{-1} and A_{1g} at 408-409 cm^{-1} peaks are prominent denoting MoS_2. However, peaks at 202-203 cm^{-1}, 360 cm^{-1}, 566 cm^{-1}, 729-730 cm^{-1} corresponding to MoO_2 [141, 142] can also be observed in the wear scar. These peaks become more prominent at the higher levels of humidity. On the *25% and 50% RH aged* samples further MoO_2 peaks at 227 cm^{-1} and 489 cm^{-1} are visible and become more intense relative to the other peaks as humidity increases.

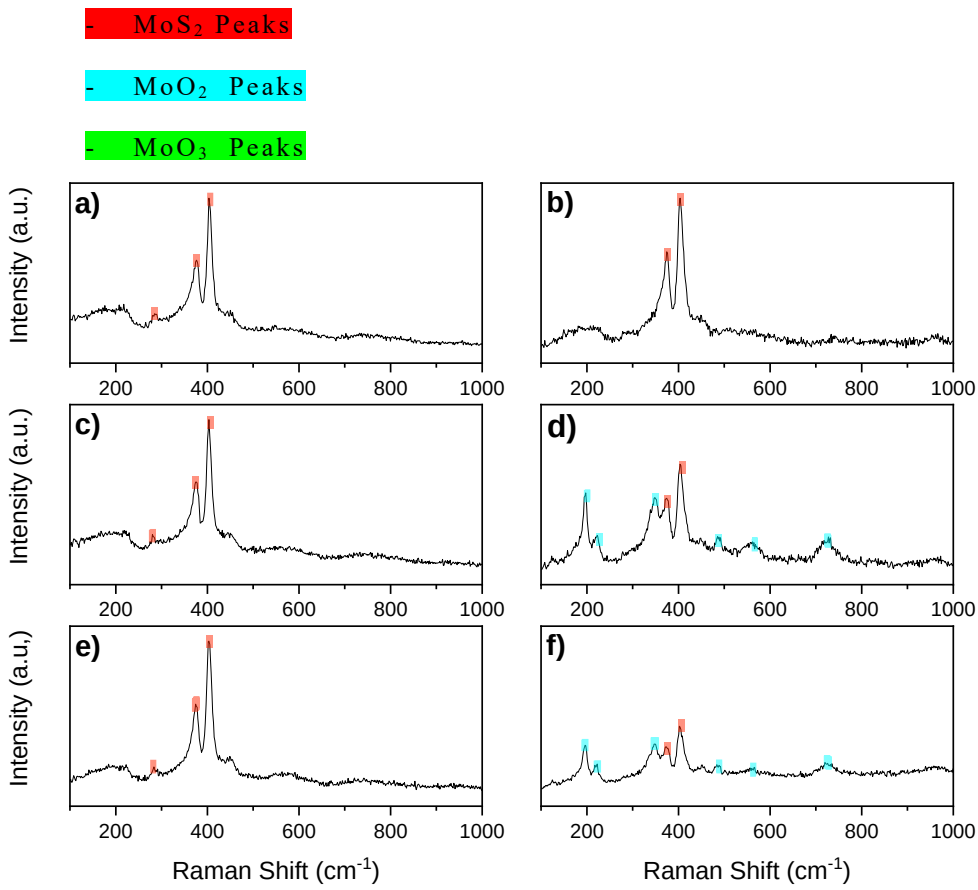

Figure 5.35 Raman spectroscopy of two week aged MoS_2 a) outside of the wear scar after ageing in dry air b) inside of the wear scar after ageing in dry air c) outside of the wear scar after ageing in 25% RH air d) inside of the wear scar after ageing in 25% RH air e) outside of the wear scar after ageing in 50% RH air f) inside of the wear scar after ageing in 50% RH air.

5.5.3 Three week aged

MoS_2 has four prominent first order modes of vibration; E_{2g}^2 with a peak position of ~34cm^{-1}, E_{1g} at ~287 cm^{-1}, E_{2g}^1 at ~383 cm^{-1} and A_{1g}

at ~409 cm^{-1} [137]. Figure 5.36 shows the Raman spectroscopy inside and outside of wear scar on 3-week nitrogen aged MoS_2 samples in dry, 25 and 50% RH. At all humidity levels, the first order Raman peaks are visible. All peaks for both inside and outside of the wear scar for the dry, 25% and 50% RH *nitrogen aged* samples fall within the same range, indicating no change due to sliding.

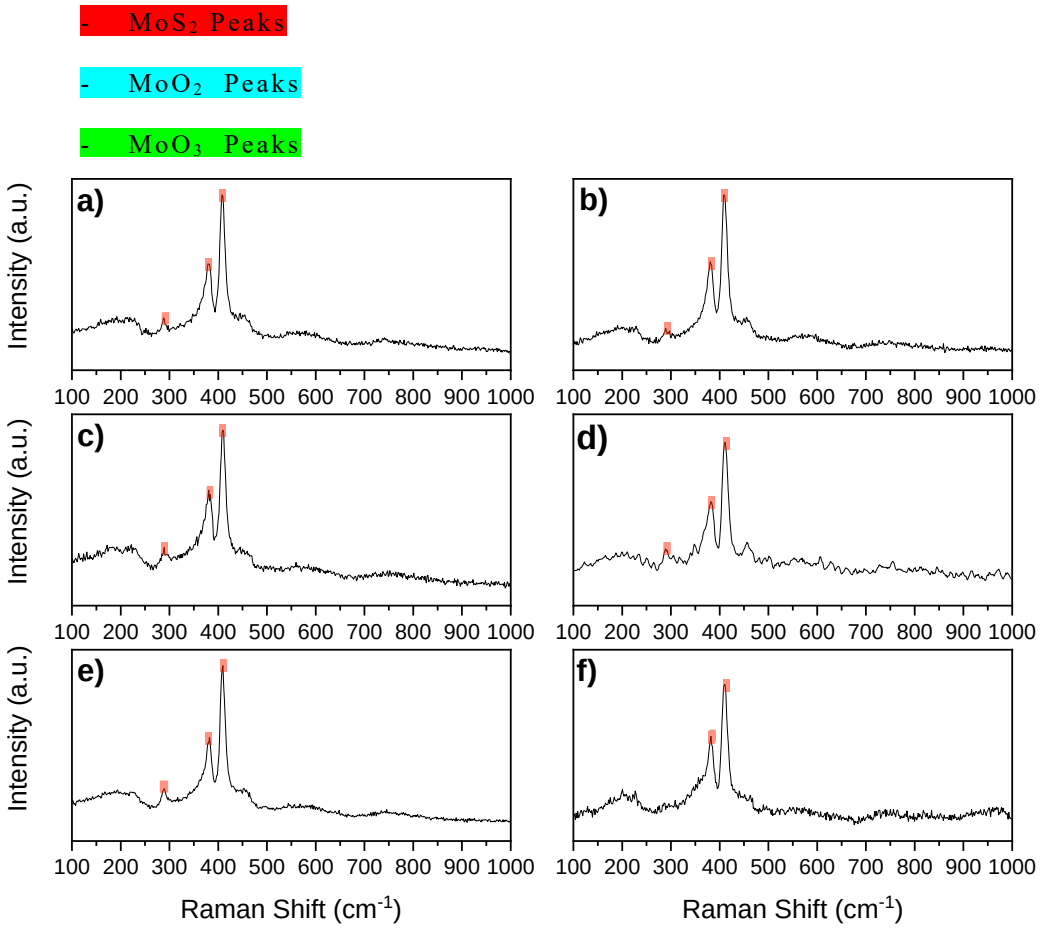

Figure 5.36 Raman spectroscopy of three week aged MoS_2 a) outside of the wear scar after ageing in dry nitrogen b) inside of the wear scar after ageing in dry nitrogen c) outside of the wear scar after ageing in 25% RH nitrogen d) inside of the wear scar after ageing in 25% RH nitrogen e) outside of the wear scar ageing in 50% RH nitrogen f) inside of the wear scar after ageing in 50% RH nitrogen.

Figure 5.37 shows the Raman spectroscopy inside and outside of wear scar on 3-week air aged MoS_2 samples in dry, 25 and 50% relative humidity air. Clear differences can be seen between the worn and unworn spectrum. In the dry air aged sample, the E_{1g} at 286-287 cm^{-1}, E_{2g}^1 at 380-382 cm^{-1} and A_{1g} at 408-409 cm^{-1} peaks are prominent denoting MoS_2. However, peaks at 202-203 cm^{-1}, 360 cm^{-1}, 566 cm^{-1}, 729-730 cm^{-1} corresponding to MoO_2 [141, 142] can also be observed in the wear scar. These peaks become more prominent at the higher levels of humidity. On the *25% and 50% RH aged* samples further MoO_2 peaks at 227 cm^{-1} and 489 cm^{-1} are visible and become more intense as humidity increases. Weak MoO_3 peaks are also visible at 825-826 cm^{-1} in *25% and 50% RH aged* samples [143]. However, the E_{2g}^1 peaks of the *25 and 50% RH aged* samples are slightly blue shifted (~3 cm^{-1}), and the spacing between the E_{2g}^1 and A_{1g} peaks is increased. This is often attributed to increased strain in the material lattice [144]. All Raman peak assignment can be seen in section 5.5, Table 5-8.

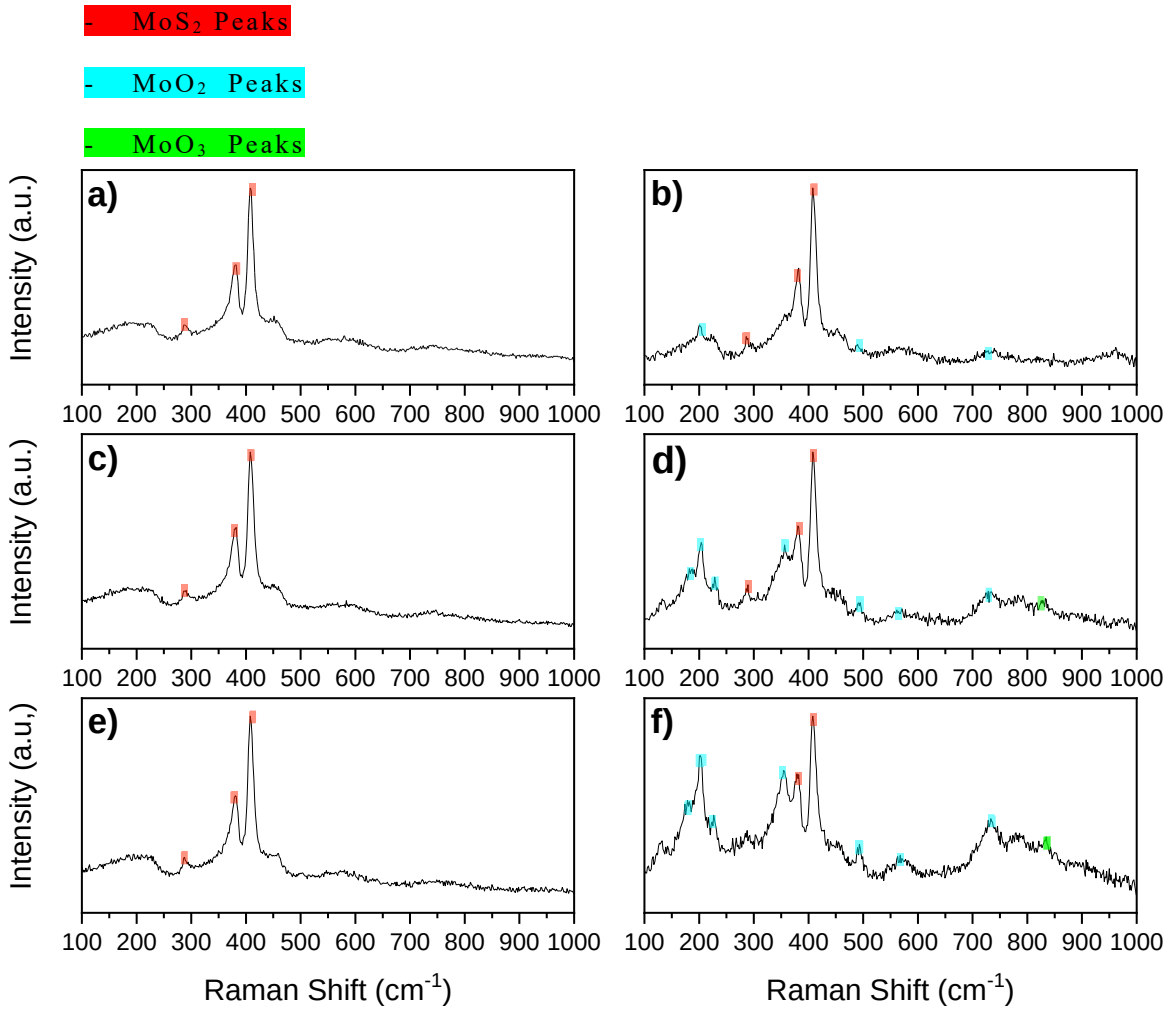

Figure 5.37 Raman spectroscopy of three week aged MoS_2 a) outside of the wear scar after ageing in dry air b) inside of the wear scar after ageing in dry air c) outside of the wear scar after ageing in 25% RH air d) inside of the wear scar after ageing in 25% RH air e) outside of the wear scar after ageing in 50% RH air f) inside of the wear scar after ageing in 50% RH air.

5.6 Transmission electron microscopy

Figure 5.38 (a-d) shows TEM images within the wear scar of MoS_2 samples that had been aged for three weeks in nitrogen or air, in either dry or 50% RH conditions, and tested on the NTR in a dry nitrogen environment. The dry nitrogen aged sample shows significant crystallographic reorientation with basal orientation of lamellae in the wear scar, parallel to the sliding direction, throughout the depth of the wear scar. Where, [A] is the protective Pt, [B] is the iridium layer that was deposited to reduce sample charging, [C] is a carbon layer from previous analysis, [D] is the MoS_2 frictionally transformed region, [E] is the MoS_2 bulk, and the arrows detail the reciprocating sliding direction. The dry air aged sample displays some reorientation of the lamellae in the direction of the wear scar. However, less uniformity and an increased number of crystallites perpendicular to the sliding direction was observed.

After 3 weeks of ageing in 50% RH nitrogen, the sample displays a good basal orientation, as defined by lamellae parallel to the material surface in the direction of sliding. The three-week *50% RH air aged* sample wear scar displays significantly less uniformity of lamellae orientation. Large proportions of the wear scar exhibit crystallites perpendicular to the direction of sliding. Though, there is some basal

orientation parallel to the sliding direction at the outer limits of the wear scar.

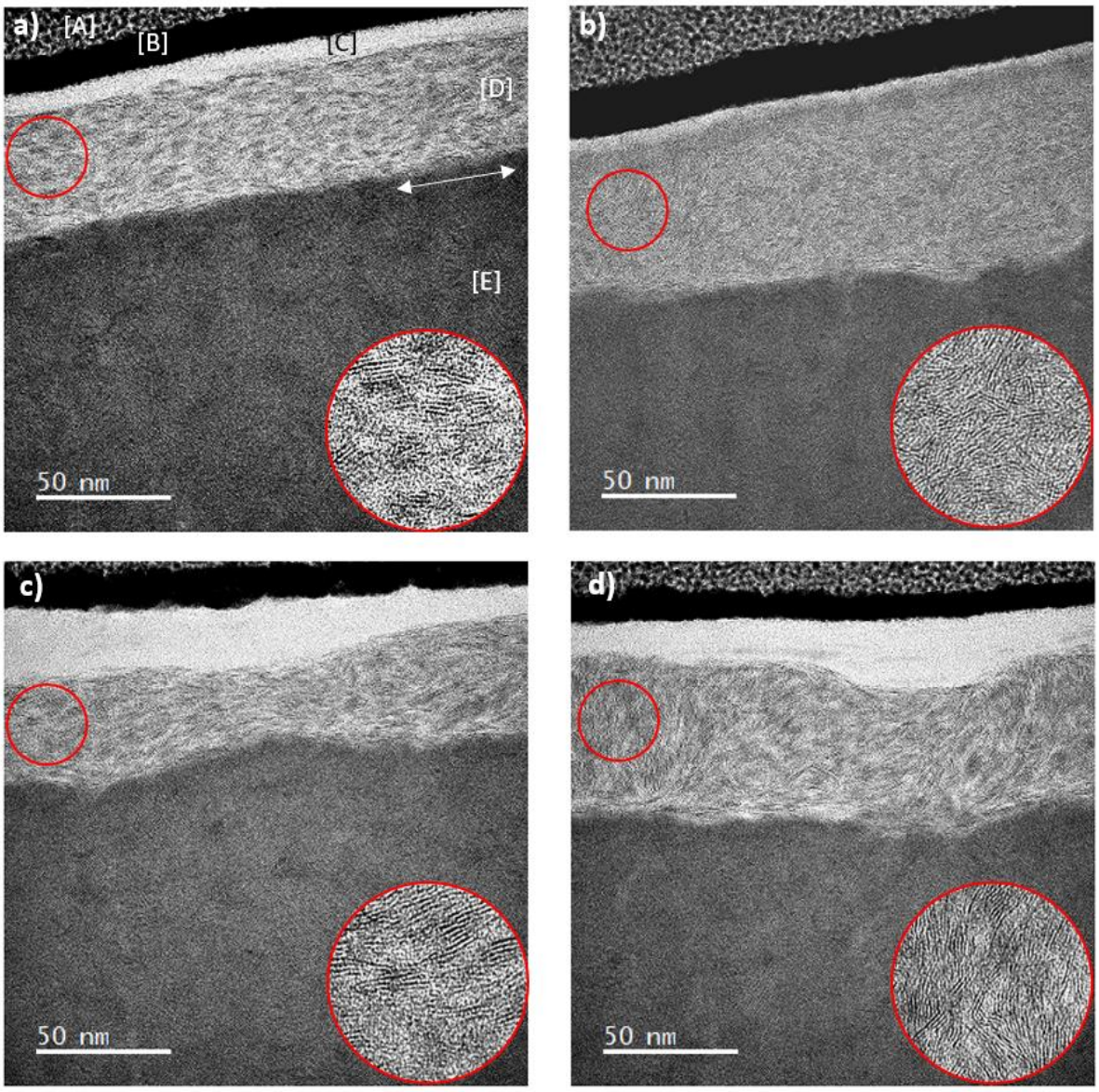

Figure 5.38 TEM image of the wear scar of MoS2 with magnified section inset temperature throughout 23° C a) after ageing for three weeks in dry N2. Where, [A] is the protective Pt, [B] is the iridium layer that was deposited to reduce sample charging, [C] is a carbon layer from previous analysis, [D] is the MoS_2 frictionally transformed, [E] is the MoS_2 bulk, and the arrows detail the reciprocating sliding direction. b) after ageing for three weeks in dry air. c) after ageing for three weeks in 50% RH N2. d) after ageing for three weeks in 50% RH Air.

5.7 Summary

The aim of this chapter was to elucidate the impact the water and oxygen in the storage environment had on the tribological performance of MoS_2 coatings. Followed by an investigation into chemical and physical changes that may arise due to the environmental factors and the energy input from tribological testing. With a view to gaining an understanding of why water and oxygen degrade MoS_2. The results presented in this chapter show:

- Coefficients of friction increased over time on MoS_2 coatings stored in environments containing water and/or oxygen.
- Water and oxygen displayed a synergistic effect in increasing coefficients of friction, with the highest coefficients of friction observed on coatings aged in 50% RH air as outlined in Table 5-7.
- Oxygen and water in the storage environment restricted easy lamellae reorientation to become basally orientated, parallel to the sliding direction, as observed on the TEM.
- No observable oxidation using Raman spectroscopy were present in the absence of sliding. However, after ageing in humid, oxygen containing environments, the input energy from the sliding was enough to cause oxidation in the wear track of the MoS_2 coating, with MoO_2 and MoO_3 peaks being observed outlined in Table 5-8.

Table 5-7 steady state coefficients of friction of aged samples

	Steady state coefficient of friction					
	N_2			Air		
Aging period	0% RH	25% RH	50% RH	0% RH	25% RH	50% RH
1 week	0.067	0.074	0.072	0.08	0.088	0.1
2 weeks	0.074	0.075	0.079	0.088	0.09	0.11
3 weeks	0.063	0.072	0.079	0.074	0.1	0.134

Table 5-8 Raman Peak assignment

Raman Peak (cm^{-1})	Assignment
287, 383, 409	MoS_2
190, 202, 227, 363, 489, 565, 728	MoO_2
197, 819	MoO_3

6. Chapter Six Discussion

6.1 Introduction

The aim of this thesis was to better understand how 'benign' environmental conditions affect the friction mechanisms of MoS_2 coatings; both directly and due to storage. Elucidating the impact that the environment may have on solid MoS_2 coatings and understanding the reasons why environmental conditions reduce performance to lead to a framework for best practice use of this lubricious coating, both in storage and operation.

In order to meet the aims of this project, the following objectives were set:

- To observe the role that water and oxygen in the sliding environment have on the lubricity of MoS_2 coatings and explore any structural or chemical changes they may cause.

- To investigate how introducing water and oxygen into the storage environment affects the lubricious performance of MoS_2 coatings once they are returned to operation in an ideal, inert environment.

- To elucidate the mechanisms of how water and oxygen cause performance reductions in MoS_2 coatings

6.2 Impact of water and oxygen in the sliding environment

The results presented here agree with the trend of increased coefficients of friction in humid environments. It can clearly be seen from friction tests in different sliding environments that humidity has, by far, the most significant impact on the transient running in processes and resultant steady-state coefficient of friction of the MoS_2 coating. The steady state coefficients of friction are over 2.5x higher in samples tested in 50% RH, compared to the dry tested counterparts. This has frequently been attributed to the adsorption of water, restricting crystallographic reorientation of MoS_2 coatings, thus, leading to higher coefficients of friction as outlined by Khare et al. [65, 66]. It was also observed that the gaseous composition of the sliding environment leads to changes in the friction response of MoS_2 coatings. Environments containing gaseous oxygen resulted in a higher coefficient of friction at all like levels of humidity, when

compared to nitrogen sliding environments. This is contrary to much of the literature where it is stated that physisorbed water is the sole attributer to friction increases when sliding at room temperature, in humid air [66]. It was also suggested in the literature, that there was little difference in friction response in MoS_2 coatings, when alternating between dry nitrogen and air [79]. The results presented in this study show increases in the coefficient of friction in dry air when compared to dry nitrogen of $\mu = 0.022$. However, the increase in coefficients of friction between the two base gasses is more significant at higher humidity levels. Displaying increases in the coefficient of friction from 50% RH N_2 to 50% RH air of $\mu = 0.55$ This suggests that there may be a synergistic effect between oxygen and water, which leads to a higher coefficient of friction in MoS_2 coatings.

6.3 Impact of water and oxygen in the storage environment

After three weeks of ageing in nitrogen at relative humidity levels of 0, 25 and 50%, there were only modest changes in the steady state friction coefficients when compared to unaged samples. In dry nitrogen, there was a small drop of around 6% in the coefficient of friction when compared with the unaged reference sample. It has been suggested that nitrogen may itself act as a lubricant [145]. Therefore,

after 3 weeks, the MoS_2 coating may have adsorbed nitrogen leading to reduced resistance to crystallographic reorientation and lower coefficients of friction between lamellae. The TEM in Figure 5.38a supports this statement, as the wear scar shows basal alignment of crystallites parallel to the sliding direction, throughout the depth of the wear. At relative humidity levels of 25% and 50% the nitrogen aged samples displayed friction coefficients 7.5% and 17.9% respectively, higher than the unaged sample. This can likely be attributed to larger concentrations of water adsorption, causing a slight restriction of easy lamellar shear between MoS_2 planes. This is highlighted in Figure 5.38c, where the crystallites show decreased uniformity compared to the dry nitrogen aged sample, although still displaying mainly preferentially orientated crystallites in the wear scar. When comparing the chemical composition of the coatings both inside and outside of the wear scar, no significant changes can be seen using Raman at any humidity level; suggesting there are no bonding changes due to ageing or tribology.

The friction results after ageing in 3 weeks of air, at varying humidity levels, displayed in Figure 5.6, suggest that the ageing environment can permanently poison the friction response of MoS_2 coatings. The changes in the steady state coefficient of friction were much more substantial than those obtained from the nitrogen aged samples. When

comparing the results to the unaged sample, the coefficient of friction was higher at all humidity levels tested. In the *25% RH air aged* sample, the steady state coefficient of friction increased by more than a third. The *50% RH air aged* sample displayed a steady state coefficient of friction double that of the unaged reference, as outlined in Table 4-1.Table 4-1 comparison of minimum and steady state coefficient of friction for each testing environment. These results show that oxygen and water in the ageing/storage environment lead to significant degradation of the lubricity and performance of MoS_2 coatings in as little as 3 weeks. The TEM image in Figure 5.38d after 3 weeks of ageing in 50% RH air, shows significantly less ordered crystallites, with a large number of crystallites perpendicular to the sliding direction, which explains the increase in friction. Furthermore, it is clear that both water and oxygen together are needed to prevent the preferential, basal, crystallographic realignment of MoS_2.

The results from the Raman spectroscopy taken outside of the wear scar of the three-week air aged coatings in Figure 5.37 show no clear chemical or bonding changes, and all possess the characteristic vibration peaks of MoS_2. However, the E^1_{2g} peaks of the *25 and 50% RH aged* samples are slightly blue shifted (~3 cm^{-1}), and the spacing between the E^1_{2g} and A_{1g} peaks is increased. This is often attributed to increased strain in the material lattice [144]. As this is only prevalent

in the air aged samples, it can be deduced that both oxygen and water are adsorbed and sit interstitially between lamellae, thus increasing lattice strain. In the spectrum relating to the dry air aged sample wear scar, all characteristic MoS_2 peaks can be observed, but, some low intensity peaks, which are characteristic of MoO_2 are also visible. The intensity of these peaks increase in the spectrum relating to the *25% RH air aged* sample wear scar, and further peaks appear at Raman shifts of 227 cm^{-1}, 358 cm^{-1} and 566 cm^{-1}. These peaks become more intense in the *50% RH aged* wear scar spectra. These results suggest that gaseous oxygen is essential for oxidation to occur during room temperature sliding of MoS_2, as environments containing no gaseous oxygen presented no signs of oxidation in the coating. Furthermore, the introduction of water, through humidity, helps to facilitate oxidation and leads to more oxidation in the wear scar.

6.4 Summary

The aim of this study was to elucidate the impact that water and oxygen have in both the ageing and sliding environments on the performance of MoS_2 coatings. It has been shown that ageing alone at room temperature in nitrogen or humid air does not lead to oxidation of MoS_2; this is because the activation energy has not been reached to facilitate oxidation. It is reported in the literature that MoS_2 does not

oxidise until a threshold temperature of 350℃ has been met [111], although the introduction of water may reduce this to below 100℃ [109]. Therefore, the energy from the mechanical input during sliding, must have exceeded the activation energy for oxidation to occur. It is hypothesised that this may be due to the flash temperature at the asperity contact, which can be multiple orders higher than the bulk temperature of the material [37], leading to a reaction between the MoS_2, O_2 and H_2O. One key point to note, is that the sliding environment had no oxygen or water, meaning that for oxidation to occur, the water and oxygen must have been adsorbed during the ageing environment and not have 'escaped' the coating when returned to a dry nitrogen environment. The hypothesis for how water and oxygen degrade MoS_2 coatings is outlined below in Figure 6.1.

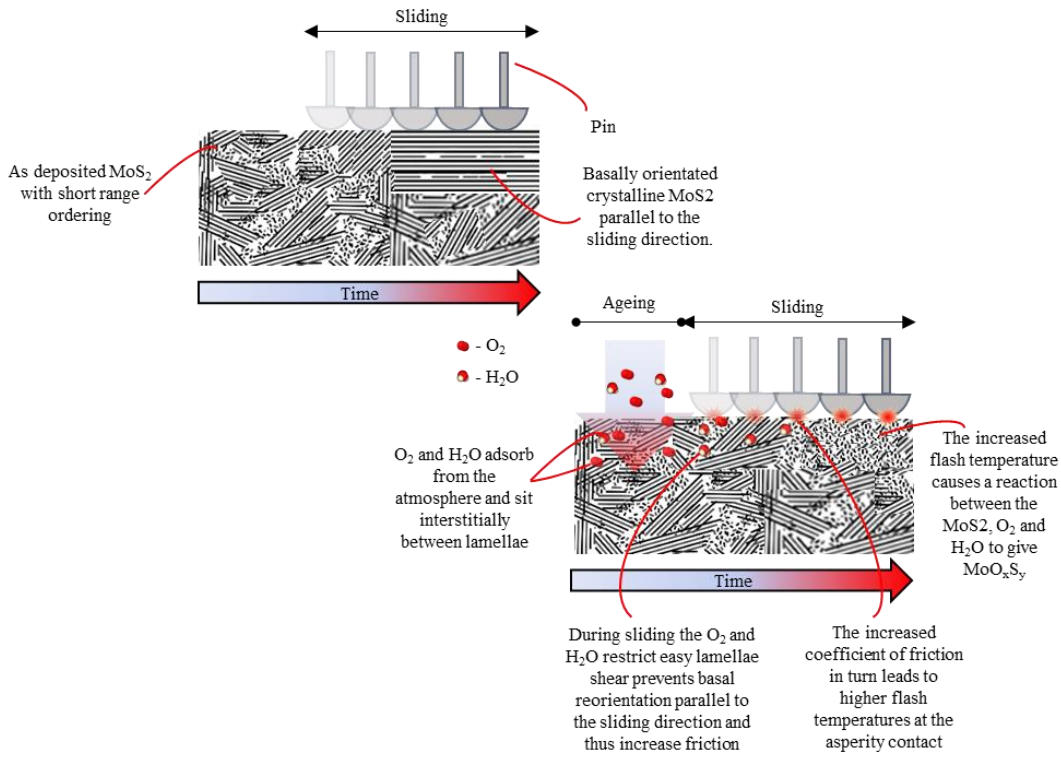

Figure 6.1 Schematic outlining hypothesis on the impact of water and oxygen on the degradation of MoS_2 coatings.

A simple heat model can be used to calculate the maximum temperature during sliding:

The maximum temperature during sliding is shown in Equation 6-1:

Equation 6-1

$$T_{max} = T_{initial} + \left(\frac{Q_{max}}{mCp}\right)$$

Where:

$T_{initial}$: Initial temperature of the material = 294.15 (K)

Q_{max}: Heat generated due to frictional heating (J)

m: Mass of the material = $8.06 \times 10^{-4}\ kg$

Cp: Specific heat of the material = $0.7\, J \cdot (kg \cdot K)^{-1}$ (J/kg.K)

The heat generated due to frictional heating can be calculated using Equation 6-2:

Equation 6-2

$$\boldsymbol{Q_{max} = \mu N v A \times \left(1 - e^{\left(-\frac{t}{\kappa}\right)}\right)}$$

Where:

μ: Coefficient of friction = 0.134

N: Normal force = $0.1N$

v: Sliding velocity = $0.5 \times 10^{-3}\ m^3$

A: Contact area = $16.057 \times 10^{-3}\ m^3$

t: Sliding time = $3000\ s$

κ: Thermal conductivity = $34.5\ W \cdot (kg \cdot K)^{-1}$

Equation 6-3

$$Q_{max} = 0.134 \times 0.1 \times (0.5 \times 10^{-3}) \times (16.057 \times 10^{-3}) \times \left(1 - e^{-\frac{3000}{0.7}}\right)$$

$$Q_{max} = 1.07 \times 10^{-7}\ J$$

Therefore:

Equation 6-4

$$T_{max} = 294.15 + \left(\frac{1.07 \times 10^{-7}}{8.04 \times 10^{-4} \times 0.7}\right)$$

$$T_{max} = 294.15\ K$$

However, this doesn't take into consideration asperity contact which can be orders of magnitude higher than the bulk maximum temperature. Especially as slow speed sliding [146].

7. Chapter Eight Conclusions and Further work

The purpose of this work was to study the effect that water and oxygen has on MoS_2 coatings, exploring how both the testing environment and the ageing environment degrade the coating and elucidate the effects of each substance individually.

- The largest impact on reduction of lubricity for unaged samples was the relative humidity in the testing environment, with friction coefficients increasing with humidity. However, the role of oxygen was not insignificant, with higher coefficients of friction at every like humidity level in air, when compared to nitrogen tested samples.
- In aged samples, the chemical and physical attributes of the coating did not change until the introduction of sliding, after the ageing process. Outside of the wear scars, no chemical changes were observed with Raman Spectroscopy.
- Nitrogen aged samples displayed no chemical changes before or after sliding at all humidity levels tested. However, small increases in friction were observed with increasing humidity, and TEM images of dry and 50% RH samples suggested a slight restriction of crystallographic orientation.

- In Air aged samples of 25% and 50% RH, molybdenum oxysulphides (MoO_xS_y) were observed inside the wear scar, displaying MoO_2 and MoO_3 characteristic peaks and friction coefficients increased significantly with humidity. It can be hypothesised that oxygen and water adsorb into the coating and together prevent preferential basal orientation parallel to the sliding direction. This is highlighted in the TEM image of the three-week, *50% RH air aged* sample, where crystallites are arranged mainly perpendicular to the sliding direction. Due to the lack of basal orientation, friction is increased, which leads to increased flash temperatures at the asperity contact. This meets the needed activation energy to facilitate oxidation of the MoS_2 with the already adsorbed water and oxygen species. It is clear from the evidence presented in this study that, water and oxygen work synergistically in degrading the performance of MoS_2 coatings.

This work has outlined the impact that both the ageing and testing environment can have on the degradation of MoS_2 coatings, clearly showing that both oxygen and water play their role in the reduction of lubricity in the testing environment. Pointing to a need for proper

storage of MoS_2 coated components prior to being used in their ideal environments.

Although ageing alone led to no chemical state changes of MoS_2, the introduction of room temperature sliding after ageing in humid air environments is enough to cause oxidation. Thus, leading to the hypothesis that water and oxygen adsorb into or onto MoS_2 during ageing and the introduction of extra energy through sliding satisfies the activation energy needed to form oxides.

7.1 Future work

Although the data presented in this thesis backs up the hypothesis that water and oxygen work synergistically in degrading and oxidising MoS_2 coatings. Further work could be done to explore how much water may be adsorbed by the coating and how it affects crystallinity.

- Develop a mathematical model to calculate flash temperatures at the asperity contact in slow speed sliding for MoS_2

- Thermo gravimetric analysis could be used to quantify water adsorption into the coating and calculate the rate of oxygen and water adsorption.

- XRD to observe if species sitting interstitially increase residual strain as would be expected.

- Extended dwell periods for Stop-dwell-start testing to observe any changes that may occur after a longer dwell, and if it may negate oxidation of the coating if it has been run in.

- Heating in a dry N_2 environment after storage to see if it prevents oxidation of the MoS_2 coating during sliding.

- In-situ sliding in the TEM to explore how aged MoS_2 coatings react differently and to observe crystallographic reorientation of MoS_2 lamellae and how the react when restricted by adsorbed species.

References

[1] J. Williams, *Engineering Tribology*. Cambridge University Press, 2005.

[2] H. Jost, "Tribology: How a word was coined 40 years ago," *ARCHIVE Proceedings of the Institution of Mechanical Engineers Part J Journal of Engineering Tribology 1994-1996 (vols 208-210),* vol. 223, pp. 240-244, 05/01 2009.

[3] D. C. Dowson, "History of Tribology," 1979.

[4] G. B. D. o. Education, Science, and H. P. JOST, *Lubrication-Tribology. Education and Research. A Report [of a Working Group] on the Present Position and Industry's Needs. [Chairman, H. Peter Jost.]*. 1966.

[5] K. Holmberg and A. Erdemir, "Influence of tribology on global energy consumption, costs and emissions," *Friction,* vol. 5, no. 3, pp. 263-284, 2017/09/01 2017.

[6] E. D. Erikson, T. G. Beat, D. D. Berger, and B. A. Frazier, "Vacuum outgassing of various materials," *Journal of Vacuum Science & Technology A,* vol. 2, no. 2, pp. 206-210, 1984/04/01 1984.

[7] C. Muratore and A. A. Voevodin, "Chameleon Coatings: Adaptive Surfaces to Reduce Friction and Wear in Extreme Environments," *Annual Review of Materials Research,* vol. 39, no. 1, pp. 297-324, 2009/08/01 2009.

[8] A. Savan, E. Pflüger, P. Voumard, A. Schröer, and M. Simmonds, "Modern solid lubrication: Recent developments and applications of MoS2," *Lubrication Science,*

https://doi.org/10.1002/ls.3010120206 vol. 12, no. 2, pp. 185-203, 2000/02/01 2000.

[9] M. R. Vaziriserehk, A. Martini, D. Strubbe, and M. Baykara, "Solid Lubrication with MoS 2 : A Review," *Lubricants,* vol. 7, 07/02 2019.

[10] P. Voumard, A. Savan, and E. Pflüger, "Advances in solid lubrication with MoS2 multilayered coatings," *Lubrication Science,* https://doi.org/10.1002/ls.3010130204 vol. 13, no. 2, pp. 135-145, 2001/02/01 2001.

[11] G. Stachowiak and A. Batchelor, *Engineering Tribology* (Engineering Tribology (Fourth Edition)). Boston: Butterworth-Heinemann, 2014.

[12] M. Dienwiebel and J. W. M. Frenken, "12 - Superlubricity between Graphite Surfaces," in *Superlubricity*, A. Erdemir and J.-M. Martin, Eds. Amsterdam: Elsevier Science B.V., 2007, pp. 199-206.

[13] W. O. Winer, "Molybdenum disulfide as a lubricant: A review of the fundamental knowledge," *Wear,* vol. 10, no. 6, pp. 422-452, 1967/11/01/ 1967.

[14] M. Tagawa, J. Ikeda, H. Kinoshita, M. Umeno, and N. Ohmae, "Effect of Atomic Oxygen Exposures on the Tribological Properties of Molybdenum Disulfide Lubricants," in *Protection of Space Materials from the Space Environment*, Dordrecht, 2001, pp. 73-84: Springer Netherlands.

[15] K. Gao, Y. Wang, B. Zhang, and J. Zhang, "Effect of vacuum atomic oxygen irradiation on the tribological properties of fullerene-like carbon and MoS2 films," *Tribology International,* vol. 170, p. 107499, 2022/06/01/ 2022.

[16] L. Cui, Z. Lu, and L. Wang, "Environmental effect on the load-dependent friction behavior of a diamond-like carbon film," *Tribology International,* vol. 82, pp. 195-199, 2015/02/01/ 2015.

[17] B. Bhushan, "Micro/nanotribology and its applications to magnetic storage devices and MEMS," *Tribology International,* vol. 28, no. 2, pp. 85-96, 1995/03/01/ 1995.

[18] M. Barzegar, S. Blanks, B.-A. Sainsbury, and W. Timms, "MEMS technology and applications in geotechnical monitoring: a review," *Measurement Science and Technology,* vol. 33, no. 5, p. 052001, 2022/02/11 2022.

[19] T. Cao, T. Hu, and Y. Zhao, "Research Status and Development Trend of MEMS Switches: A Review," (in eng), *Micromachines (Basel),* vol. 11, no. 7, Jul 17 2020.

[20] P. Stoyanov, J. Z. Fishman, J. R. Lince, and R. R. Chromik, "Micro-tribological performance of MoS2 lubricants with varying Au content," *Surface and Coatings Technology,* vol. 203, no. 5, pp. 761-765, 2008/12/25/ 2008.

[21] H. P. Jost, "Tribology — Origin and future," *Wear,* vol. 136, no. 1, pp. 1-17, 1990/02/01/ 1990.

[22] K. Holmberg, P. Andersson, and A. Erdemir, "Global energy consumption due to friction in passenger cars," *Tribology International,* vol. 47, pp. 221-234, 2012/03/01/ 2012.

[23] K. Holmberg, "Reliability aspects of tribology," *Tribology International,* vol. 34, no. 12, pp. 801-808, 2001/12/01/ 2001.

[24] T. Liskiewicz, *Introduction to Tribology and Real Surfaces Lecture notes* (Work Unit 1). University of Leeds, 2018.

[25] M. Urbakh, J. Klafter, D. Gourdon, and J. Israelachvili, "The nonlinear nature of friction," *Nature,* vol. 430, no. 6999, pp. 525-528, 2004/07/01 2004.

[26] R. Leine and H. Nijmeijer, *Dynamics and Bifurcations of Non-Smooth Mechanical Systems*. Springer-Verlag Berlin Heidelberg, 2004, p. 236.

[27] D. Arnell, "2 - Mechanisms and laws of friction and wear," in *Tribology and Dynamics of Engine and Powertrain*, H. Rahnejat, Ed.: Woodhead Publishing, 2010, pp. 41-72.

[28] G. Pintaude, "Hardness as an indicator of material strength: a critical review," *Critical Reviews in Solid State and Materials Sciences,* pp. 1-19, 2022.

[29] "Elastic and Elastic-Plastic Contact," in *Introduction to Contact Mechanics*, A. C. Fischer-Cripps, Ed. Boston, MA: Springer US, 2007, pp. 175-188.

[30] R. Budynas and K. Nisbett, *Shigleys Mechanical Engineering Design*, 10th Edition ed. McGraw-Hill Education, 2014, p. 1104.

[31] I. M. Hutchings, "Leonardo da Vinci's studies of friction," *Wear,* vol. 360-361, pp. 51-66, 2016/08/15/ 2016.

[32] Y. J. S. I. J. o. M. Desplanques and Manufacturing, "Amontons-Coulomb Friction Laws, A Review of the Original Manuscript," *SAE Int. J. Mater. Manf.,* vol. 8, no. 1, pp. 98-103, 2014.

[33] H. Heshmat, *Tribology of Interface Layers*, 1st ed. Boca Raton: CRC Press, 2010, p. 464.

[34] L. Anderson and R. Boulatov, "Chapter Three - Polymer Mechanochemistry: A New Frontier for Physical Organic

Chemistry," in *Advances in Physical Organic Chemistry*, vol. 52, I. H. Williams and N. H. Williams, Eds.: Academic Press, 2018, pp. 87-143.

[35] I. Hutchings and P. Shipway, "5 - Sliding wear," in *Tribology (Second Edition)*, I. Hutchings and P. Shipway, Eds.: Butterworth-Heinemann, 2017, pp. 107-164.

[36] P. Ptáček, F. Šoukal, and T. Opravil, "Introduction to the Transition State Theory," 2018.

[37] G. Sutter and N. Ranc, "Flash temperature measurement during dry friction process at high sliding speed," *Wear,* vol. 268, no. 11, pp. 1237-1242, 2010/05/12/ 2010.

[38] F. E. Kennedy, "Thermal and thermomechanical effects in dry sliding," *Wear,* vol. 100, no. 1, pp. 453-476, 1984/12/01/ 1984.

[39] M. Conte, B. Pinedo, and A. Igartua, "Frictional heating calculation based on tailored experimental measurements," *Tribology International,* vol. 74, pp. 1-6, 2014/06/01/ 2014.

[40] A. E. M. Beedle, M. Mora, C. T. Davis, A. P. Snijders, G. Stirnemann, and S. Garcia-Manyes, "Forcing the reversibility of a mechanochemical reaction," *Nature Communications,* vol. 9, no. 1, p. 3155, 2018/08/08 2018.

[41] J. Pelleg, "Mechanism of Diffusion," in *Diffusion in Ceramics*, J. Pelleg, Ed. Cham: Springer International Publishing, 2016, pp. 31-39.

[42] X. Gao *et al.*, "Changes in the composition, structure and friction property of sputtered MoS2 films by LEO environment exposure," *Applied Surface Science,* vol. 330, pp. 30-38, 2015/03/01/ 2015.

[43] V. Kuznetsov *et al.*, "Microscopic Diffusion of Atomic Hydrogen and Water in HER Catalyst MoS2 Revealed by Neutron Scattering," *The Journal of Physical Chemistry C,* vol. 126, no. 51, pp. 21667-21680, 2022/12/29 2022.

[44] H. Li *et al.*, "Superlubricity between MoS2 Monolayers," (in eng), *Adv Mater,* vol. 29, no. 27, Jul 2017.

[45] L. Burstein, "3 - Lubrication and roughness," in *Tribology for Engineers*, J. P. Davim, Ed.: Woodhead Publishing, 2011, pp. 65-120.

[46] I. L. Singer, S. Fayeulle, and P. D. Ehni, "Wear behavior of triode-sputtered MoS 2 coatings in dry sliding contact with steel and ceramics," *Wear,* vol. 195, no. 1, pp. 7-20, 1996/07/01/ 1996.

[47] A. Erdemir, "Genesis of superlow friction and wear in diamondlike carbon films," *Tribology International,* vol. 37, no. 11, pp. 1005-1012, 2004/11/01/ 2004.

[48] A. Erdemir, "The role of hydrogen in tribological properties of diamond-like carbon films," *Surface and Coatings Technology,* vol. 146-147, pp. 292-297, 2001/09/01/ 2001.

[49] A. Erdemir, O. L. Eryilmaz, I. B. Nilufer, and G. R. Fenske, "Synthesis of superlow-friction carbon films from highly hydrogenated methane plasmas," *Surface and Coatings Technology,* vol. 133-134, pp. 448-454, 2000/11/01/ 2000.

[50] A. S. H. Makhlouf, "1 - Current and advanced coating technologies for industrial applications," in *Nanocoatings and Ultra-Thin Films*, A. S. H. Makhlouf and I. Tiginyanu, Eds.: Woodhead Publishing, 2011, pp. 3-23.

[51] A. P. M. Baptista, F. Silva, J. Porteiro, J. L. Míguez, and G. J. T. C. Pinto, "Sputtering Physical Vapour Deposition (PVD)

Coatings: A Critical Review on Process Improvement and Market Trend Demands," vol. 8, p. 402, 2018.

[52] G. Faraji, H. S. Kim, and H. T. Kashi, "Introduction," in *Severe Plastic Deformation*, G. Faraji, H. S. Kim, and H. T. Kashi, Eds.: Elsevier, 2018, pp. 1-17.

[53] K. William, "Antifriction and antiabrasive metal," 19th August 1927, 1927.

[54] R. R. M. Johnston and A. J. W. Moore, "The burnishing of molybdenum disulphide on to metal surfaces," *Wear,* vol. 7, no. 6, pp. 498-512, 1964/11/01/ 1964.

[55] G. Salomon, A. W. J. De Gee, and J. H. Zaat, "Mechano-chemical factors in MoS2-film lubrication," *Wear,* vol. 7, no. 1, pp. 87-101, 1964/01/01/ 1964.

[56] C. Gao, L. Bredell, D. Kuhlmann-Wilsdorf, and D. D. Makel, "Micromechanics of MoS2 lubrication," *Wear,* vol. 162-164, pp. 480-491, 1993/04/13/ 1993.

[57] J. F. Curry *et al.*, "Highly Oriented MoS2 Coatings: Tribology and Environmental Stability," *Tribology Letters,* vol. 64, no. 1, p. 11, 2016/09/03 2016.

[58] J. Tian *et al.*, "Shear-induced interfacial reconfiguration governing superlubricity of MoS2-Ag film enabled by diamond-like carbon," *Applied Surface Science,* vol. 578, p. 152068, 2022/03/15/ 2022.

[59] L. Kong, K. Huang, X. Cao, Z. Lu, G. a. Zhang, and H. Hu, "Effect of MoS2 content on friction and wear properties of Mo and S co-doped CrN coatings at 25–600 °C," *Ceramics International,* vol. 47, no. 15, pp. 21450-21458, 2021/08/01/ 2021.

[60] K. Hebbar Kannur *et al.*, "An insight on the MoS2 tribo-film formation to determine the friction performance of Mo-S-N sputtered coatings," *Surface and Coatings Technology,* vol. 408, p. 126791, 2021/02/25/ 2021.

[61] E. Serpini *et al.*, "Nanoscale frictional properties of ordered and disordered MoS2," *Tribology International,* vol. 136, pp. 67-74, 2019/08/01/ 2019.

[62] R. K. Upadhyay and A. Kumar, "Effect of humidity on the synergy of friction and wear properties in ternary epoxy-graphene-MoS2 composites," *Carbon,* vol. 146, pp. 717-727, 2019/05/01/ 2019.

[63] J. F. Curry, "Friction and Environmental Sensitivity of Molybdenum Disulfide: Effects of Microstructure," LeHigh University, 2942, 2017.

[64] T. Gradt and T. Schneider, "Tribological Performance of MoS2 Coatings in Various Environments," *Lubricants* vol. 4, no. 32, 2016.

[65] H. S. Khare and D. L. Burris, "Surface and Subsurface Contributions of Oxidation and Moisture to Room Temperature Friction of Molybdenum Disulfide," *Tribology Letters,* vol. 53, no. 1, pp. 329-336, 2014/01/01 2014.

[66] H. S. Khare and D. L. Burris, "The Effects of Environmental Water and Oxygen on the Temperature-Dependent Friction of Sputtered Molybdenum Disulfide," *Tribology Letters,* vol. 52, no. 3, pp. 485-493, 2013/12/01 2013.

[67] B. Vierneusel, T. Schneider, S. Tremmel, S. Wartzack, and T. Gradt, "Humidity resistant MoS2 coatings deposited by unbalanced magnetron sputtering," *Surface and Coatings Technology,* vol. 235, pp. 97-107, 2013/11/25/ 2013.

[68] S. Watanabe, J. Noshiro, and S. Miyake, "Friction properties of WS2/MoS2 multilayer films under vacuum environment," *Surface and Coatings Technology,* vol. 188-189, pp. 644-648, 2004/11/01/ 2004.

[69] M. C. Simmonds, A. Savan, E. Pflüger, and H. Van Swygenhoven, "Mechanical and tribological performance of MoS2 co-sputtered composites," *Surface and Coatings Technology,* vol. 126, no. 1, pp. 15-24, 2000/04/03/ 2000.

[70] M. Belin, "The wear behavior of a thin MoS2 coating, as studied by triboscopic measurements in friction and electrical contact resistance," in *Tribology Series*, vol. 36, D. Dowson *et al.*, Eds.: Elsevier, 1999, pp. 439-448.

[71] C. Donnet, J. M. Martin, T. Le Mogne, and M. Belin, "Super-low friction of MoS2 coatings in various environments," *Tribology International,* vol. 29, no. 2, pp. 123-128, 1996/02/01/ 1996.

[72] C. Donnet, J. M. Martin, T. Le Mogne, and M. Belin, "The origin of super-low friction coefficient of MoS2 coatings in various environments," in *Tribology Series*, vol. 27, D. Dowson, C. M. Taylor, T. H. C. Childs, M. Godett, and G. Dalmaz, Eds.: Elsevier, 1994, pp. 277-284.

[73] P. D. Fleischauer, "Effects of Crystallite Orientation on Environmental Stability and Lubrication Properties of Sputtered MoS2 Thin Films," *A S L E Transactions,* vol. 27, no. 1, pp. 82-88, 1984/01/01 1984.

[74] M. B. Peterson, "Friction and Wear Investigation of Molybdenum Disulfide I: Effect of Moisture," 1953.

[75] K. Dreva, A. Morina, L. Yang, and A. Neville, "The effect of temperature on water desorption and oxide formation in MoS2 coatings and its impact on tribological properties,"

Surface and Coatings Technology, vol. 433, p. 128077, 2022/03/15/ 2022.

[76] A. J. Haltner and C. S. Oliver, "Effect of Water Vapor on Friction of Molybdenum Disulfide," *Industrial & Engineering Chemistry Fundamentals,* vol. 5, no. 3, pp. 348-355, 1966/08/01 1966.

[77] Y. Wang, Y. Du, J. Deng, and Z. Wang, "Friction reduction of water based lubricant with highly dispersed functional MoS2 nanosheets," *Colloids and Surfaces A: Physicochemical and Engineering Aspects,* vol. 562, pp. 321-328, 2019/02/05/ 2019.

[78] X. Zhang, F. Jia, B. Yang, and S. Song, "Oxidation of molybdenum disulfide sheet in water under in situ Atomic Force Microscopy observation," *J. Phys. Chem. C,* vol. 121, p. 9938, 2017.

[79] E. Serpini, A. Rota, A. Ballestrazzi, D. Marchetto, E. Gualtieri, and S. Valeri, "The role of humidity and oxygen on MoS2 thin films deposited by RF PVD magnetron sputtering," *Surface and Coatings Technology,* vol. 319, pp. 345-352, 2017/06/15/ 2017.

[80] X. Zhao and S. S. Perry, "The Role of Water in Modifying Friction within MoS2 Sliding Interfaces," *ACS Applied Materials & Interfaces,* vol. 2, no. 5, pp. 1444-1448, 2010/05/26 2010.

[81] C. Donnet, T. Le Mogne, and J. M. Martin, "Superlow friction of oxygen-free MoS2 coatings in ultrahigh vacuum," *Surface and Coatings Technology,* vol. 62, no. 1, pp. 406-411, 1993/12/10/ 1993.

[82] L. Qi, Y. Wang, L. Shen, and Y. Wu, "Chemisorption induced n-doping of MoS2 by oxygen," *Appl. Phys. Lett.,* vol. 108, p. 063103, 2016.

[83] P. D. Fleischauer and J. R. Lince, "A comparison of oxidation and oxygen substitution in MoS2 solid film lubricants," *Tribology International,* vol. 32, no. 11, pp. 627-636, 1999/11/01/ 1999.

[84] T. Onodera *et al.*, "A computational chemistry study on friction of h-MoS(2). Part I. Mechanism of single sheet lubrication," (in eng), *J Phys Chem B,* vol. 113, no. 52, pp. 16526-36, Dec 31 2009.

[85] J. Martincová, M. Otyepka, and P. Lazar, "Is Single Layer MoS2 Stable in the Air?," *Chemistry – A European Journal,* vol. 23, no. 53, pp. 13233-13239, 2017/09/21 2017.

[86] R. Szoszkiewicz, "Local Interactions of Atmospheric Oxygen with MoS(2) Crystals," (in eng), *Materials (Basel),* vol. 14, no. 20, Oct 11 2021.

[87] G. Wang, R. Pandey, and S. P. Karna, "Physics and chemistry of oxidation of two-dimensional nanomaterials by molecular oxygen," *WIREs Comput. Mol. Sci.,* vol. 7, p. e1280, 2017.

[88] G. Yu *et al.*, "The pivotal role of oxygen in establishing superlow friction by inducing the in situ formation of a robust MoS2 transfer film," *Journal of Colloid and Interface Science,* vol. 594, pp. 824-835, 2021/07/15/ 2021.

[89] B. C. Windom, W. G. Sawyer, and D. W. Hahn, "A Raman Spectroscopic Study of MoS2 and MoO3: Applications to Tribological Systems," *Tribology Letters,* vol. 42, no. 3, pp. 301-310, 2011/06/01 2011.

[90] J. Pető *et al.*, "Spontaneous doping of the basal plane of MoS2 single layers through oxygen substitution under ambient conditions," *Nature Chemistry,* vol. 10, no. 12, pp. 1246-1251, 2018/12/01 2018.

[91] H. Peelaers and C. G. Van de Walle, "Elastic Constants and Pressure-Induced Effects in MoS2," *The Journal of Physical Chemistry C,* vol. 118, no. 22, pp. 12073-12076, 2014/06/05 2014.

[92] A. P. S. Gaur, S. Sahoo, M. Ahmadi, S. P. Dash, M. J. F. Guinel, and R. S. Katiyar, "Surface Energy Engineering for Tunable Wettability through Controlled Synthesis of MoS2," *Nano Letters,* vol. 14, no. 8, pp. 4314-4321, 2014/08/13 2014.

[93] H.-P. Komsa and A. V. Krasheninnikov, "Native defects in bulk and monolayer MoS2 from first principles," *Physical Review B,* vol. 91, no. 12, p. 125304, 03/12/ 2015.

[94] J. Moser and F. Lévy, "Crystal reorientation and wear mechanisms in MoS2 lubricating thin films investigated by TEM," *Journal of Materials Research,* vol. 8, no. 1, pp. 206-213, 1993.

[95] J. J. Hu, R. Wheeler, J. Zabinski, P. Shade, A. Shiveley, and A. Voevodin, *Transmission Electron Microscopy Analysis of Mo–W–S–Se Film Sliding Contact Obtained by Using Focused Ion Beam Microscope and In Situ Microtribometer*. 2008, pp. 49-57.

[96] T. Han *et al.*, "Research on the Factors Affecting the Growth of Large-Size Monolayer MoS_2 by APCVD," (in eng), *Materials (Basel),* vol. 11, no. 12, Dec 17 2018.

[97] S. Adachi and N. Ueda, "Effect of Cold-Spray Conditions Using a Nitrogen Propellant Gas on AISI 316L Stainless Steel-Coating Microstructures," *Coatings,* vol. 7, no. 7, 2017.

[98] T. W. Scharf and I. Singer, *Monitoring Transfer Films and Friction Instabilities with In Situ Raman Tribometry*. 2003, pp. 3-8.

[99] J. M. Martin, C. Donnet, T. Le Mogne, and T. Epicier, "Superlubricity of molybdenum disulphide," *Physical Review B,* vol. 48, no. 14, pp. 10583-10586, 10/01/ 1993.

[100] J. M. Martin, H. Pascal, C. Donnet, T. Le Mogne, J. L. Loubet, and T. Epicier, "Superlubricity of MoS2: crystal orientation mechanisms," *Surface and Coatings Technology,* vol. 68-69, pp. 427-432, 1994/12/01/ 1994.

[101] J. P. Oviedo *et al.*, "In Situ TEM Characterization of Shear-Stress-Induced Interlayer Sliding in the Cross Section View of Molybdenum Disulfide," *ACS Nano,* vol. 9, no. 2, pp. 1543-1551, 2015/02/24 2015.

[102] T. Liang, W. G. Sawyer, S. S. Perry, S. B. Sinnott, and S. R. Phillpot, "Energetics of Oxidation in MoS2 Nanoparticles by Density Functional Theory," *The Journal of Physical Chemistry C,* vol. 115, no. 21, pp. 10606-10616, 2011/06/02 2011.

[103] C. Muratore, J. E. Bultman, S. M. Aouadi, and A. A. Voevodin, "In situ Raman spectroscopy for examination of high temperature tribological processes," *Wear,* vol. 270, no. 3, pp. 140-145, 2011/01/12/ 2011.

[104] R. Holinski and J. Gänsheimer, "A study of the lubricating mechanism of molybdenum disulfide," *Wear,* vol. 19, no. 3, pp. 329-342, 1972/03/01/ 1972.

[105] R. Holinski, *ASLE Proc. Int. Conf. on Solid Lub.,"* (null). 1971, p. 41.

[106] T. B. Stewart and P. D. Fleischauer, "Chemistry of sputtered molybdenum disulfide films," *Inorganic Chemistry,* vol. 21, no. 6, pp. 2426-2431, 1982/06/01 1982.

[107] A. W. J. De Gee, G. Salomon, and J. H. Zaat, "On the Mechanisms of MoS2-Film Failure in Sliding Friction," *A S L E Transactions,* vol. 8, no. 2, pp. 156-163, 1965/01/01 1965.

[108] M. Uemura, K. Saito, and K. Nakao, "A Mechanism of Vapor Effect on Friction Coefficient of Molybdenum Disulfide," *Tribology Transactions,* vol. 33, no. 4, pp. 551-556, 1990/01/01 1990.

[109] S. Ross and A. Sussman, "Surface oxidation of molybdenum disulfide," *J. Phys. Chem.,* vol. 59, p. 889, 1955.

[110] G. J. Dudder, X. Zhao, B. Krick, W. Gregory Sawyer, and S. S. Perry, *Environmental Effects on the Tribology and Microstructure of MoS2–Sb2O3–C Films*. 2011, pp. 203-213.

[111] W. L. Spychalski, M. Pisarek, and R. Szoszkiewicz, "Microscale Insight into Oxidation of Single MoS2 Crystals in Air," *The Journal of Physical Chemistry C,* vol. 121, no. 46, pp. 26027-26033, 2017/11/22 2017.

[112] M. Yamamoto, T. L. Einstein, M. S. Fuhrer, and W. G. Cullen, "Anisotropic etching of atomically thin MoS2," *J. Phys. Chem. C,* vol. 117, p. 25643, 2013.

[113] R. E. Kahrizsangi, M. H. Abbasi, and A. Saidi, "Model-fitting approach to kinetic analysis of non-isothermal oxidation of molybdenite," *Iran. J. Chem. Chem. Eng.,* vol. 26, p. 119, 2007.

[114] R. Szoszkiewicz and E. Riedo, "Nucleation time of nanoscale water bridges," *Phys. Rev. Lett.,* vol. 95, p. 135502, 2005.

[115] K. Santosh, R. C. Longo, R. M. Wallace, and K. Cho, "Surface oxidation energetics and kinetics on MoS2 monolayer," *J. Appl. Phys.,* vol. 117, p. 135301, 2015.

[116] T. N. Walter, F. Kwok, H. Simchi, H. M. Aldosari, and S. E. Mohney, "Oxidation and oxidative vapor-phase etching of few-layer MoS2," *J. Vac. Sci. Technol., B: Nanotechnol. Microelectron.: Mater., Process., Meas., Phenom.,* vol. 35, p. 021203, 2017.

[117] T. Krantz, C. Hakun, Z. Cameron, I. Shareef, and M. Dube, "Performance of MoS2 Coated Gears Exposed to Humid Air During Storage," *Materials Science,* 2018.

[118] J. R. Lince, S. H. Loewenthal, and C. S. Clark, "Degradation of Sputter-Deposited Nanocomposite MoS 2 Coatings for NIRCam during Storage in Air," 2016.

[119] B. C. Stupp, "Synergistic effects of metals co-sputtered with MoS2," *Thin Solid Films,* vol. 84, no. 3, pp. 257-266, 1981/10/16/ 1981.

[120] H. Torres, H. Rojacz, L. Čoga, M. Kalin, and M. Rodríguez Ripoll, "Local mechanical and frictional properties of Ag/MoS2-doped self-lubricating Ni-based laser claddings and resulting high temperature vacuum performance," *Materials & Design,* vol. 186, p. 108296, 2020/01/15/ 2020.

[121] C. Zhang *et al.*, "Microstructure and friction behavior of LaF3 doped Ti-MoS2 composite thin films deposited by unbalanced magnetron sputtering," *Surface and Coatings Technology,* vol. 359, pp. 334-341, 2019/02/15/ 2019.

[122] T. Zhimeng, W. Zemin, X. Lei, Z. Libo, H. Zhaohui, and L. Jianhua, "Thermal and tribological properties of MoS2 doped graphite/copper composites by microwave sintering,"

Journal of Materials Research and Technology, vol. 15, pp. 6001-6010, 2021/11/01/ 2021.

[123] X. Wang, Y. Xing, S. Ma, X. Zhang, K. Xu, and D. G. Teer, "Microstructure and mechanical properties of MoS2/titanium composite coatings with different titanium content," *Surface and Coatings Technology,* vol. 201, no. 9, pp. 5290-5293, 2007/02/26/ 2007.

[124] N. M. Renevier, V. C. Fox, D. G. Teer, and J. Hampshire, "Performance of low friction MoS2/titanium composite coatings used in forming applications," *Materials & Design,* vol. 21, no. 4, pp. 337-343, 2000/08/01/ 2000.

[125] V. Bellido-González *et al.*, "Tribological behaviour of high performance MoS2 coatings produced by magnetron sputtering," *Surface and Coatings Technology,* vol. 97, no. 1, pp. 687-693, 1997/12/01/ 1997.

[126] J. R. Lince, "Tribology of Co-sputtered Nanocomposite Au/MoS2 Solid Lubricant Films over a Wide Contact Stress Range," *Tribology Letters,* vol. 17, no. 3, pp. 419-428, 2004/10/01 2004.

[127] D. Rickard, "Chapter 4 - Aqueous Metal–Sulfide Chemistry: Complexes, Clusters And Nanoparticles," in *Developments in Sedimentology*, vol. 65, D. Rickard, Ed.: Elsevier, 2012, pp. 121-194.

[128] G. Liu *et al.*, "MoS2 monolayer catalyst doped with isolated Co atoms for the hydrodeoxygenation reaction," *Nature Chemistry,* vol. 9, no. 8, pp. 810-816, 2017/08/01 2017.

[129] T. Spalvins, "Frictional and morphological properties of Au□MoS2 films sputtered from a compact target," *Thin Solid Films,* vol. 118, no. 3, pp. 375-384, 1984/08/17/ 1984.

[130] J. S. Zabinski, M. S. Donley, S. D. Walck, T. R. Schneider, and N. T. McDevitt, "The Effects of Dopants on the Chemistry and Tribology of Sputter-Deposited MoS2 Films," *Tribology Transactions,* vol. 38, no. 4, pp. 894-904, 1995/01/01 1995.

[131] E. Roberts and W. Price, "Advances in molybdenum disulphide film technology for space applications," in *6th European Space Mechanisms and Tribology Symposium*, 1995, vol. 374, p. 273.

[132] N. M. Renevier, J. Hamphire, V. C. Fox, J. Witts, T. Allen, and D. G. Teer, "Advantages of using self-lubricating, hard, wear-resistant MoS2-based coatings," *Surface and Coatings Technology,* vol. 142-144, pp. 67-77, 2001/07/01/ 2001.

[133] N. M. Renevier, V. C. Fox, D. G. Teer, and J. Hampshire, "Coating characteristics and tribological properties of sputter-deposited MoS2/metal composite coatings deposited by closed field unbalanced magnetron sputter ion plating," *Surface and Coatings Technology,* vol. 127, no. 1, pp. 24-37, 2000/05/01/ 2000.

[134] N. M. Renevier *et al.*, "Performance and limitation of hybrid PECVD (hard coating)—PVD magnetron sputtering (MoS2/Ti composite) coated inserts tested for dry high speed milling of steel and grey cast iron," *Surface and Coatings Technology,* vol. 163-164, pp. 659-667, 2003/01/30/ 2003.

[135] N. M. Renevier *et al.*, "Performance and limitations of MoS2/Ti composite coated inserts," *Surface and Coatings Technology,* vol. 172, no. 1, pp. 13-23, 2003/07/15/ 2003.

[136] V. C. Fox, N. Renevier, D. G. Teer, J. Hampshire, and V. Rigato, "The structure of tribologically improved MoS2–

metal composite coatings and their industrial applications," *Surface and Coatings Technology,* vol. 116-119, pp. 492-497, 1999/09/01/ 1999.

[137] H. Li *et al.*, "From Bulk to Monolayer MoS2: Evolution of Raman Scattering," *Advanced Functional Materials,* vol. 22, pp. 1385-1390, 04/10 2012.

[138] J. M. Chen and C. S. Wang, "Second order Raman spectrum of MoS2," *Solid State Communications,* vol. 14, no. 9, pp. 857-860, 1974/05/01/ 1974.

[139] P. J. Potts, *A Handbook of Silicate Rock Analysis*. Cambridge University Press, 1992.

[140] K. Zhang *et al.*, "An Ångström-level d-spacing controlling synthetic route for MoS2 towards stable intercalation of sodium ions," *Journal of Materials Chemistry A,* 10.1039/C8TA09066A vol. 6, no. 45, pp. 22513-22518, 2018.

[141] G. Solferino and A. J. Anderson, "Thermal reduction of molybdite and hematite in water and hydrogen peroxide-bearing solutions: Insights on redox conditions in Hydrothermal Diamond Anvil Cell (HDAC) experiments," *Chemical Geology,* vol. 322-323, pp. 215-222, 2012/09/05/ 2012.

[142] (13/09). *Tugarinovite R100218*. Available: http://rruff.info/Tugarinovite

[143] P. A. Spevack and N. S. McIntyre, "Thermal reduction of molybdenum trioxide," *The Journal of Physical Chemistry,* vol. 96, no. 22, pp. 9029-9035, 1992/10/01 1992.

[144] L. Yang *et al.*, "Lattice strain effects on the optical properties of MoS2 nanosheets," *Scientific Reports,* vol. 4, no. 1, p. 5649, 2014/07/10 2014.

[145] K. Kato, "THE EFFECT OF NITROGEN ON FRICTION AND WEAR OF HARD MATERIALS," *World Tribology Congress III,* 2005.

[146] E. H. Smith and R. D. Arnell, "A New Approach to the Calculation of Flash Temperatures in Dry, Sliding Contacts," *Tribology Letters,* vol. 52, no. 3, pp. 407-414, 2013/12/01 2013.